Role of IRE1-XBP1 arm in transendothelial migration of TNBC brain metastatic cells

by

Maliha Nuzhat Munir

Thesis Submitted to the Faculty of Graduate studies of
The University of Manitoba
in Partial Fulfillment of the Requirements for the Degree of
MASTER OF SCIENCE

Department of Human Anatomy and Cell Science
University of Manitoba
Winnipeg, Manitoba

UNIVERSITY OF MANITOBA
2021

Abstract

Introduction: Breast cancer represents the second most frequent cause of brain metastasis. 30% of the patients suffering from Triple Negative Breast Cancer (TNBC) develop brain metastasis which confers poor prognosis to breast cancer patients. However, the mechanisms that facilitate brain metastasis are not fully understood. TNBC cells have high levels of endoplasmic reticulum (ER) stress and show activation of the IRE1 pathway of the Unfolded Protein Response (UPR). Our lab previously demonstrated that MDA-231/BR cells, the brain metastatic subline of MDA-MB-231, have high endogenous levels of IRE1 activity suggesting that UPR pathway supports cancer cell survival under ER stress. My research investigates the involvement of the UPR IRE1 arm in cell survival and transendothelial migration of MDA-231/BR.

Methods: Characterization of MDA-231/BR cells under different ER stress inducers and the IRE1α RNAse inhibitor MKC8866 was performed by Western blot experiments and viability assays. shXBP1 clones were established and assessed for successful downregulation of sXBP1 by Western blot detection. Cell migration was assessed by real time cell analysis and transendothelial Boyden-chamber migration assay. Cytokines secreted from MDA-231/BR under induced ER stress and MKC8866 were determined. Brain endothelial cells were subjected to MDA-231/BR conditioned media to determine changes in cell viability and differences in gene expression of tight junctional proteinsby qPCR. Preliminary *in vivo* analysis was performed to assess the effect of XBP1 silencing on MDA-231/BR brain metastasis.

Results: MDA-231/BR cells showed constitutive activation of the IRE1 RNase arm which wasfurther induced by serum starvation and thapsigargin. The IRE1 RNase inhibitor MKC8866 completely blocked basal and induced IRE1 RNAse activity. In contrast to serum starvation, Tg treatment activated the pro-apoptotic PERK pathway which was confirmed by reduced cell viability and increased caspase 3/7 activity. MDA-231/BR cell migration studies under treatment with MKC8866 have shown a reduction in cell migration through endothelial layers. Knockdown of XBP1 however, did not consistently reduce endothelila transmigration of MDA-231/BR cells. ER stress-induced-

MDA-231/BR cells show increased secretion of pro-metastatic cytokines IL-6, VEGF-A and thrombospondin-1. Brain endothelial cells exposed to MDA-231/BR conditioned media showed increased expression of tight junctional protein occludin under IRE1 RNase inhibition. *In vivo* data showed no significant difference in survival of mice in control versus doxycycline treated group.

Conclusion: This study showed that the study of ER stress is dependent on different types of stressors used. Induction of ER stress leads to secretion of pro-inflammatory cytokines which can indirectly affect the endothelial cells to become more permeable and allow migration of breast cancer cells.

Acknowledgements

I would like to thank my supervisor, Dr. Sabine Hombach-Klonisch, for giving me the opportunity to pursue the MSc program in her lab and for her unlimited guidance and support throughout the program. My sincere gratitude towards my committee members Dr. Yvonne Myal and Dr. Donald Miller for their valuable suggestions, encouragement and support which helped me throughout my graduate studies.

I would like to thank my wonderful lab members who made my journey through the graduate studies so memorable. I am grateful to Dr. Aleksandra Glogowska, for training me in lab from scratch and for her guidance and advice. I am thankful to Dr. Thatchawan Thanasupawat and Aditya Kanojia for their valuable support in solving technical problems I faced while performing different methods in the laboratory. I would like to thank Sai Nivedita Krishnan and Shahin Shabanipour for their support and being there with me through all the tough times and good times in the lab.

I would like to acknowledge the financial support provided by Research Manitoba, Cancer Research Society, University of Manitoba and Department of Human Anatomy and Cell Science for the funding and awards provided to me throughout the program.

Finally, I would like to thank my fiancé and my family for sticking by my side through thick and thin despite being miles apart.

Table of Contents

List of Tables

List of Figures

List of Acronyms

Ask1	Apoptosis signal-regulating kinase 1
ATF6	Activating transcription factor 6
ATF4	Activating transcription factor 4
BBB	Blood brain barrier
BC	Breast cancer
BL1	Basal-like 1
BL2	Basal-like 2
BRCP	Breast cancer resistance protein
BTB	Blood tumor barrier
CI	Cell index
CASP 2	Caspase 2
CNS	Central nervous system
COX-2	Cyclogenase-2
CTC	Circulating tumor cell
DC	Dendritic cell
DCIS	Ductal carcinoma *in situ*
DFS	Disease free survival
DOX	Doxycycline
EC	Endothelial cell
EMT	Epithelial mesenchymal transition
ER	Estrogen receptor
ER	Endoplasmic reticulum
ERAD	ER associated degradation
EGFR	Epidermal growth factor receptor
GADD153	Growth arrest and DNA damage inducible gene
GCN2	General control nonderepressible-2
HER2	Human epidermal growth receptor 2
HIFα	Hypoxia inducing factor α
HRI	Heme-regulated inhibitor

IHC	Immunohistochemistry
IM	Immunomodulatory subgroup
ITS	Insulin transferase selenium
IRE1	Inositol requiring enzyme 1
JAM	Junctional adhesion molecule
LAR	Luminal androgen receptor
LCIS	Lobular carcinoma *in situ*
LD	Luminal domain
LN	Lymph node
LIN	Lobular intraepithelial neoplasia
M	Mesenchymal
MAGI	Membrane associated guanylate kinase protein
MMP	Matrix metalloproteinase
MRP	Multi drug resistance protein
MOI	Multiplicity of infection
MSL	Mesenchymal stem-like
N-SBR	Nottingham/Scarff/Bloom/Richardson score
NVU	Neurovascular unit
OS	Overall survival
PARP	Poly (ADP-ribose) polymerase
PDGF	Platelet-derived growth factor
PERK	PKR like ER kinase
P-gp	P-glycoprotein
PR	Progesterone receptor
RIDD	Regulated IRE1-Dependent Decay
SERCA	Sarco/endoplasmic reticulum Ca^{2+} ATPase
S1PR3	Sphingosine1-phosphate receptor 3
SRS	Stereotactic radiosurgery
ST6GALNAC5	A-2,6-sialyltransferase 5
TAD	Transcriptional activating domain
Tg	Thapsigargin

TGFβ	Tumor growth factor β
TJ	Tight junction
TNBC	Triple negative breast cancer
TGFβ	Transforming growth factor β
TNFα	Tumor necrosis factor α
TNM	Tumor node metastasis
TXNIP	Thioredoxin-Interacting Protein
UPR	Unfolded protein response
VEGF	Vascular endothelial growth factor
WB	Western blot
WBRT	Whole brain radiation therapy
ZO1	Zonula occluding 1

Chapter 1. Introduction

1.1. Breast Cancer

According to Canadian Cancer Statistics, cancer is the number one cause of death in Canada and the number of new cancer cases are increasing as the population is aging (1, 2). Breast cancer is a heterogenous disease that starts with the transformation of epithelial cells of the normal breast tissue to tumors (3). In 2020 it was estimated that breast cancer will be detected in a total of 27700 people in Canada making it the second most diagnosed cancer with a mortality rate of 13% (2). Breast cancer incidence in men is a rare phenomenon accounting for <1% of all breast cancer diagnoses (4). Even though the prognosis for breast cancer is similar in males and females, males are seen to survive less due to diagnosis at older age with advanced stages at the time of detection (5).

1.1.1. Staging of Breast Cancer

The Tumor-Node-Metastasis (TNM) system, is a system to stage breast cancer, has been devised to understand the anatomical extent of cancer and clarify whether it is local, regional or metastatic to help clinicians diagnose and treat the patients (6, 7). The TNM system takes three parameters into consideration: (i) the size of the tumor (T), (ii) the number of lymph nodes that are involved (N) and (iii) if the cancer has metastasized (M). Based on these factors different stages (0-IV) have been appointed to determine the pathological characteristics of these stages as summarized in the table 1.1.(8, 9)

Table 1.1 Breast Cancer Stages

Stage 0	Tis, N0, M0	Ductal carcinoma in situ (DCIS) and Lobular carcinoma in situ (LCIS), it is a pre-cancer of the breast and earliest form of breast cancer. In this stage cancer cells have not invaded to lymph nodes, surrounding tissues or distant sites.
Stage IA	T1, N0, M0	T1: Tumor size ≤ 2cm N0: No lymph node M0: No metastasis
Stage IB	T0/T1, N1mi, M0	T0/T1: Tumor size ≤ 2cm

		N1mi: micrometastasis in 1 to 3 axillary lymph nodes (LN) M0: No metastasis
Stage II A	T0/T1, N1, M0	T0/T1: Tumor size ≤ 2cm N1: Cancer has spread to 1 to 3 axillary LN or tiny amounts of cancer are found in internal mammary LN on sentinel lymph node biopsy. M0: No metastasis
Stage II B	T2, N1, M0 T3, N0, M0	T2: 5cm >Tumor Size > 2cm N1: It has spread to 1 to 3 axillary lymph nodes M0: No distant metastasis T3: Tumor size ≥5cm N0: No lymph node M0: No metastasis
Stage III A	T0-T2, N2, M0 T3, N1/N2, M0	T0-T2: The tumor is not more than 5 cm or cannot be found N2: It has spread to 4 to 9 axillary lymph nodes M0: No distant metastasis T3: The tumor size is larger than 5 cm N0: No lymph nodes M0: No distant metastasis.
Stage III B	T4, N0-N2, M0	T4: Tumor spread to chest wall or skin (T4) N0: no lymph nodes N1: 1 to 3 axillary lymph nodes N2: 4 to 9 axillary lymph nodes M0: No distant metastasis
Stage II C	Any T, N3, M0	Any T: The tumor is any size (or can't be located) N3: 10 or more axillary lymph nodes N3: lymph nodes under the collar bone N3: lymph nodes above the collar bone M0: no distant metastasis
Stage IV	Ant T, any N, M1	Any T: The cancer can be any size Any N: may or may not have spread to nearby lymph nodes M1: It has spread to distant organs or to lymph nodes far from the breast.

1.1.2. Breast cancer grading

Breast cancers are graded using the Nottingham-Scarff / Bloom / Richardson score (N-SBR) according to the histopathological characteristics of breast cancer tissue (10). The grading is based on three characteristics: (i) tubule formation describing the

percentage of cells that contain tubule shaped structures, (ii) nuclear pleomorphism describing the variability in nuclear size, shape and number to the normal cell and (iii) mitotic count representing the dividing cells (10). Each of these features are assigned scores ranging from 1-3 resulting in three different grades having a total count ranging from 3 to 9 as described in the table 1.2 (10, 11).

Table 1.2 Breast Cancer Grades:

Grade	Score	Description
I	3-5	Low-grade (well-differentiated) tumors that do not appear to be growing quickly and are less likely to spread
II	6-7	Intermediate-grade (moderately differentiated) tumors that have features between grade 1 and 3
III	8-9	High-grade (poorly differentiated or undifferentiated) tumors that tend to grow faster and are more likely to spread

1.1.2.1 Histological Classification of breast cancer

Breast cancer is classified according to the histological appearance and its origin from the epithelium lining the ducts or lobules. The term *in situ* carcinoma is used to define tumor limited to the epithelial component of the breast whereas invasive carcinoma is defined as cancer that has spread past the epithelial basement membrane to the surrounding tissue and possibly beyond (12). *In situ* carcinoma is sub classified to ductal carcinoma *in situ* (DCIS) and lobular intraepithelial neoplasia (LIN). DCIS is characterized as heterogenous group of pre-malignant tumors with different levels of differentiation, size and distribution of the lesion. The lesions in LIN are characterized by a more uniformly appearing round cells that are accumulating in the lobules and in which mitosis and necrosis is absent (13). Similarly, invasive carcinoma can be categorized to several histological subtypes based on architectural features such as papillary, tubular, mucinous, medullary, micropapillary, ductal and lobular carcinoma, and based on the immunohistochemical profile, such as neuroendocrine carcinoma (12, 14).

1.1.3. Molecular Classification of breast cancer

Breast cancer has been divided to several subtypes due to its heterogeneity, morphological, biological, and clinical features (15). Subtyping different types of breast cancer depends on the genetic expression pattern and clinically relevant parameters such as histological appearance and TNM grading (16, 17). This allows clinicians a better prognosis of the disease and an opportunity to plan for suitable therapies for patients. Gene profiling, histological and molecular pathology of various breast tumors associated with patient survival has resulted into distinct molecular classifications of BC: Luminal A, Luminal B, Her 2 enriched, Basal-like and Claudin low (18). The Luminal subtypes include the cancers positive for one or more of the hormone receptors Estrogen receptor (ER) and Progesterone receptor (PR). The Her 2 enriched subtype is characterized by increased expression of the receptor of Human epidermal Growth Factor 2 (HER2). The basal like subtype consists of Triple Negative Breast cancer (TNBC) which is negative for estrogen, progesterone and HER2 receptor (19). Another subtype was recently discovered by Herschkowitz et al through an integrated analysis of human and murine mammary tumors which classified as Claudin-low breast cancer (20, 21).

1.1.3.1. Luminal A

Luminal A is the most common form of breast cancer comprising of 40% of all BC (22). It is characterized by high expression of ER and lower expression of PR, HER2 along with proliferative marker Ki67. As a result these tumors usually have a low histological grade of 1, low degree of nuclear pleomorphism and, low mitotic activity resulting in a good prognosis (23, 24). Since this subtype is hormone receptor positive, it is treated with endocrine therapy. Tamoxifen, is a common drug used as an adjuvant chemotherapy for treating hormone positive breast cancers such as DCIS and lobular carcinoma (25).

1.1.3.2. Luminal B

The Luminal B subtype comprises of ~20% of all breast cancers (24). It is characterized by higher expression of proliferation associated genes such as G2/mitotic-specific cyclin-(B1CCNB1) and proliferative marker Ki-67, and less than 20%

expression of PR. Due to the high expression of Ki67 and p53 genes Luminal B tumors have poor cellular differentiation and rate as higher grade cancers (26). As a result, this subtype has a poor prognosis and is classified as high risk cancer compared to the luminal A subtype (27, 28). BC of the Luminal B subtype, similar to the HER2+ BC subtype, has been shown to be insensitive against endocrine therapy (23, 29). Fortunately, it is sensitive towards neoadjuvant chemotherapy and complete response rates can be achieved (30).

1.1.3.3. HER2+ subtype

The human epidermal growth factor receptor 2 (HER2) subtype accounts for 20-30% of invasive breast cancers and is characterized by the expression of Erb2 gene and the HER2 protein (31). These tumors are highly proliferative with high histological and nuclear grading and have ~40% p53 gene mutations (32). The immunohistochemical (IHC) profile demonstrates HER2 subtype as ER-negative/ PR-negative/ lymph node positive (31). Women with this subtype of breast cancer have an increased risk of locoregional recurrence and an increased breast cancer mortality (33, 34). HER2 positive tumors have high early relapse rate and high rate of metastasis to brain, liver, bone and lung sites (35). The rate of metastasis to the brain by HER2 enriched subtype was stated to be as high as 28.7% (35). Trastazumab, is a targeted monoclonal antibody against juxtamembrane region of the extracellular domain of HER2 receptor. It has been identified to selectively block HER2-HER3 dimerization and cause proteolytic cleavage of HER2 extracellular domain resulting in a reduction of active form of HER2. This binding results in decreased cellular repair capacity due to reduced PI3K signaling and various mediators of cell cycle (36). Trastazumab causes increased apoptosis capacity when used in a combinational therapy with chemotherapy or radiotherapy (37). The administration of the drug trastazumab to meatastatic HER2 positive patients has improved the prognosis, median time to disease progression and survival (38, 39). However, a higher incidence of brain metastasis has been reported recently in HER2 positive patients treated with trastuzumab but the reasons for this occurrence is unclear (40). The combination of pertuzumab and trastuzumab have proved to be successful in women with metastatic HER2-positive breast cancer (41). Similar to Trastazumab,

Pertuzumab inhibits HER2 dimerization by binding to a different epitope of HER2 extracellular domain but does not require overexpression of HER2 to work (42). As a result combination therapy provides wider inhibition of HER2 signalling.

1.1.3.4. Claudin low subtype

Claudin low subtype is characterized by genetic expression of low expressing cell–cell adhesion genes and tight junction proteins claudin 3, 4 and 7 and E-cadherin, high expressing epithelial–mesenchymal transition (EMT) genes, and stem cell-like gene expressing patterns (43). Claudin-low breast tumors are reported to be mostly ER-negative, PR-negative, HER2-negative, triple negative and are associated with poor prognosis (20, 44). Reportedly these tumors are also genomically stable with reduced proliferation rate (45).

1.1.3.5. Triple Negative breast cancer/ Basal-like breast cancer

Triple negative breast cancer is defined as a basal type of breast cancer that lacks the IHC expression of ER, PR and HER2 receptor (46). It accounts for 15-20% of all breast cancer cases and is generally more common in younger women, as well as in the African American and Asian population (47). This subtype has a heterogenous population of tumors with poor prognosis and overall, much shorter survival time compared to other subtypes. It is highly invasive with ~46% of patients having distant metastasis, commonly to the brain (48). 75% of TNBC are basal-like breast cancer (47). Basal-like subtype tumors do not express ER and HER2 and are characterized by expression of basal/myoepithelial cells and luminal epithelia having high histological grade, high mitotic indices, central necrotic zones as well as metaplastic areas, similar to what is seen in TNBC tumors (49, 50).

1.1.3.5.1. TNBC clinical features

TNBC tumors are usually large (>2cm) with a 54% chances of node positivity (51). There is no correlation between tumor size and lymph node positivity, meaning that the small tumors in this subtype can also have a high rate of node positivity (52). It is characterized by pathological features such as expression of basal cytokeratin (CK5/6, CK17), P-cadherin, epidermal growth factor receptor (EGFR), and P53 in most cases

(53). They also rarely express androgen receptor, E-cadherin, cyclin D and highly express cyclin E and cell proliferation gene Ki67 (53, 54). Zhang li *et al*. demonstrated that TNBC patients have an overall survival (OS) and disease free survival (DFS) of approximately 5 years (53). A high percentage of these patients have disease recurrences involving distant metastasis to various organs such as lungs and the central nervous system (CNS) (55, 56). The average time taken for metastasis to occur is usually around 2.6 years compared to 5 years in the other subtypes and the survival time is around 9 months (48).

1.1.3.5.2. TNBC subtypes

Gene expression profiling by Lehhmann et al. classified TNBC into 7 molecular types: two basal-like subgroup- basal-like 1 (BL1) and basal-like (BL2), two mesenchymal-like subgroup- mesenchymal (M) and mesenchymal stem-like (MSL), one immunomodulatory subgroup (IM), lastly, one luminal androgen receptor group (LAR) (57). The same study demonstrated that TNBC do not only have similar gene expression as basal type of cancer but also with other subtypes such as luminal A (17%), normal breast-line (12%), luminal B (6%), HER2 (6%) thus, providing evidence that TNBC is a heterogenous group of tumors (57-59). The BL1 subtype is characterized by high cell cycle regulation and DNA repair related genes and is sensitive to poly (ADP-ribose) polymerase (PARP) inhibitors and cisplatin (57, 60). The BL2 subtype is characterized by activation of signaling pathways such as the EGFR, MET, NGF, Wnt/β-catenin, and IGF-1R pathways. They are potentially treated with mTOR inhibitors and growth factor inhibitors (lapatinib, gefitinib, and cetuximab) (57, 60). The M subtype is characterized by the pathways controlling cell migration and cell differentiation such as Wnt pathway, anaplastic lymphoma kinase pathway and transforming growth factor (TGF)-β signaling. The patients diagnosed with this subtype can be treated with mTOR inhibitors or drugs targeting EMT (57, 61). The MSL subtype represents the growth factor signaling pathways EGFR, platelet-drived growth factor (PDGF), calcium signaling and extracellular signal-regulated kinase 2 (ERK1/2) and can be treated using PI3K inhibitors, Src antagonists, or anti-angiogenic drugs(62). The cytokine and immune signal transduction pathways such as the Th1/Th2 pathway, NK cell pathway, B cell receptor

signaling pathway and dendritic cell (DC) pathway are active in IM subtype (57). The LAR subtype gene ontology shows activation of hormonal-related signaling pathways such as porphyrin metabolism, steroid synthesis and estrogen/androgen metabolism making anti-androgen receptor therapy suitable for patients with this subtype of tumors (57, 62).

1.2. Breast Cancer Brain Metastasis (BCBM)

1.2.1. Incidence

Several factors play role in the metastasis of breast cancer to distant organs. Such factors include (i) early diagnosis (ii) subtype of breast cancer (iii) lymph node status (≥4 positive nodes) d)tumor grade (tumor grade 3), (iv) pathologic tumor size(>2 cm) (63). Approximately 15-30% of patients with metastatic breast cancer develop brain metastasis making it the second most cause of brain metastasis after lung cancer (40, 64, 65). HER2+ and TNBC subtypes are mostly associated with a high incidence of brain metastasis compared to other subtypes of breast cancer (40). The study of 1256 patients with brain metastasis from breast cancer by Niikura *et al*. demonstrated that patients with luminal type of breast cancer had a mean OS of 9.3 months, in contrast to patients with HER2+ tumors which have an OS of 16.5 months and patients with TNBC with an OS of 4.9 months (40). The risk factors associated with brain metastasis are younger age, high grade tumors, hormone receptor negative status and four or more positive metastatic lymph nodes (40, 64). The incidence of brain metastasis is approximately 30-40% in HER2+ and TNBC+ BC while the frequency of it is approximately 8-15% in luminal cancer (40, 65). Despite an improvement in detection and primary treatment of BC, there has been a slow increase in metastasis over recent years. In a study by Heitz F et al. it was reported that patients with TNBC had the shortest latency span of 22 months for the development of metastasis to the brain while patients with HER2 positive BC on average take 30 months to develop brain metastasis (66).

1.2.2. Metastatic Process

Metastasis is a highly complex and multi-step process involving interactions between tumor and host cells (65, 67). It can be summarized in three steps: (i) invasion, (ii) intravasation and (iii) extravasation. Metastasis starts when cancer cells go through EMT which facilitates the process of invasion and allow the tumor cells to cross the basement membrane, to invade the stroma of the mammary tissue and to intravasate into the blood vessels. The cells achieve mesenchymal properties by loss of E-cadherin and upregulation of markers such as vimentin, N-cadherin and fibronectin (68, 69). These changes are a result of the activation of transcription factors such as Snail, Slug, Twist or growth factors such as epidermal growth factor (EGF) and TGFβ (70-73). The cadherin cytoplasmic domain bind with β-catenin which connects to α-catenin to form cadherin-catenin complex (74, 75). This complex in turn binds to occludins proteins to stabilize the adherens junction (75). Studies have shown that in breast cancer, the expression of Snail results in downregulation of E-cadherin and genes coding for claudins and occludins (70, 76).

The extracellular matrix is remodeled by the cancer cells by the expression of matrix-degrading metalloproteinases (MMPs, ADAMs), such as matrix metalloproteinase 9 (MMP 9), enabling them to invade the stroma and penetrate the blood vessels resulting in intravasation (77). Intravasated tumor cells are referred to as circulating tumor cells (CTCs). If CTCs survive in the circulation, they may attach to the endothelium of small blood vessels at a distant site and extravasate in distant organs to form the metastasis. The metastatic latency is the time taken by the cancer cells to go through this process and adapt to the microenvironment and achieve the ability to grow metastatic tumors (65, 71, 78).

Lorger *et al*. has performed *in vivo* studies of the brain microenvironment during the initial stages of breast cancer brain metastasis showing that after injection of MDA-MB-435 cells intracardially in mice, the cancer cells are found in the capillaries from day 2 after injection to day 7. The cells take this time to increase the expression of resident microglia and reactive astrocytes to help during these initial steps of extravasation (79).

Following extravasation, the BC cells in the perivascular niche adapt to the new environment through vascular co-option (79-81). Vessel co-option, is a non-angiogenic process where the tumors hijack pre-existing blood vessels to remain viable and proliferate along the vessels to form micrometastases (82).

1.2.3. Current Treatment

The current treatment for BCBM consists of whole brain radiation therapy (WBRT), surgical resection, stereotactic radiosurgery (SRS) and chemotherapy depending on the patient's performance status and the number, size and localization of brain lesions (83). Surgical resection is usually performed on patients having accessible single metastasis and which can also be combined with WBRT to improve the neurological and overall survival of patients. The median overall survival ranged from 8 to 13 months after surgery and from 8.5 to 12.1 months after stereotactic surgery (84, 85) (86) (87). SRS is a non-invasive way of removing single or multiple tumors with minimal damage to the normal surrounding brain tissues (40, 63). The major limitation for the systemic treatment of brain metastasis remains the insufficient penetration of most drugs due to the presence of the blood-brain-barrier (BBB).

1.2.4. Blood brain barrier (BBB)

BBB is a term used to define the microvasculature system of the CNS. It is responsible for controlling cerebral homeostasis and protecting the CNS from neurotoxins, pathogens, inflammation, injury and disease by tightly regulating the movement of molecules between the blood and the CNS (88). The BBB comprises of two cell types: (i) endothelial cells lining the blood vessels that are anchored to the basement membrane and the (ii) mural cells consisting of astrocytes, pericytes and glial cells (89).

1.2.4.1 Neurovascular Unit (NVU)

The neurovascular unit (NVU) is a single functioning unit comprising of neurons, perivascular astrocytes, microglia, pericytes, endothelial cells and basement membrane.

The components of NVU such as endothelial cells, astrocytes and pericytes are responsible for regulating blood flow and substrate permeability for BBB development, thereby providing an intact barrier for brain function. Studies have shown that astrocytes help maintain the BBB in healthy adult brain by maintaining astrocytic cell polarity and by secreting Wnt growth factors (90, 91). The Wnt/β-catenin pathway is an important pathway which is functional in endothelial cells for maintaining barrier function by downregulation of the expression of tight junctional proteins such as claudin 5 and upregulation of plasmalemma vehicle associated protein, which is associated with compromised barrier function (92, 93). In addition to astrocytes, pericytes help in barrier maintenance by inducing astrocyte polarization and attachment of astrocyte end-feet to blood vessels (93). A study showed that reduced pericyte coverage over endothelial cells lead to an elevated permeability (94). The crosstalk between these cells allow maintenance of NVU.

1.2.4.2. Endothelial Cell

The endothelial cells in the CNS are non-fenestrated and are tightly connected to each other via the presence of tight junctional (TJ) proteins which limits the transcellular and paracellular movement of molecules (95). Endothelial cells (EC) are highly polarized having a luminal surface and an abluminal surface that is anchored on the basement membrane. Transport of solutes from the blood to the brain occurs through special transporter proteins (96, 97). The efflux transporters such as P-glycoprotein (P-gp), Breast Cancer Resistance protein (BRCP) and multi-drug resistance-associated proteins-1 and 2 (MRP-1, -2) are located on the luminal surface and aid in the extrusion of lipophilic molecules such as drugs. The nutrient transporters regulate the transport of electrolytes, nucleosides, amino acids as well glucose into the CNS along and the removal of waste products from the CNS to the blood (98-100). The combination of physical barrier properties such as the TJ proteins, and specific transporters to deliver required nutrients, allows the ECs to tightly regulate CNS homeostasis (88).

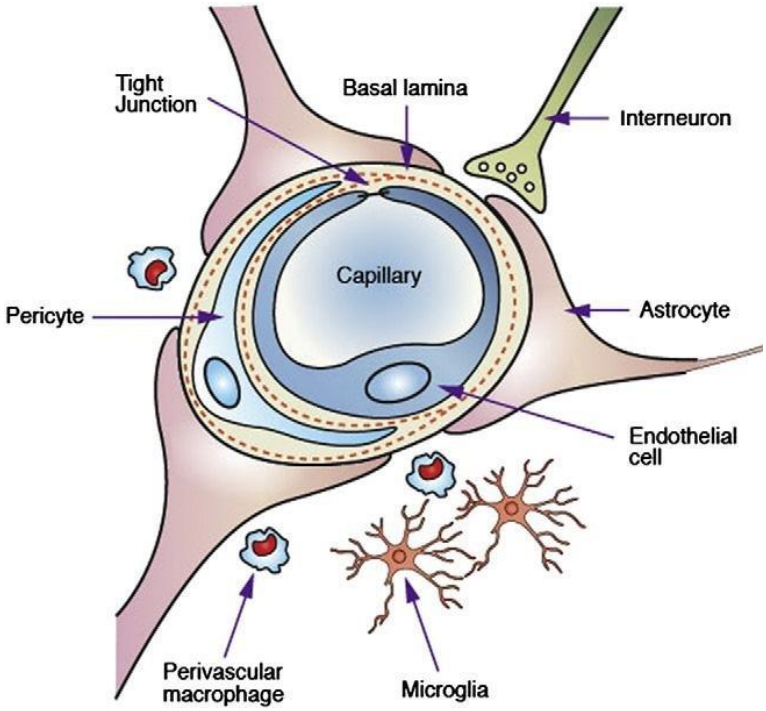

Figure 1.1 Blood brain barrier components
Parashar, Ashish & Kumar, Rajesh & Correspondence, Ashish & Parashar, Kumar. (2012). A Review on Novel Techniques for Drug Delivery to the Brain. Current Research in Pharmaceutical Sciences. 03. 134-141.

1.2.4.3. Tight Junctional Proteins

Despite being such a selective barrier for solute transport and the free movement of cellular elements between the systemic circulation and neuronal tissue, the tumor cells can breach this barrier by disrupting the tight junctional proteins and colonize in the brain niche resulting in metastasis (101, 102). The tight junction comprises of several transmembrane molecules such as claudins, occludin and junctional adhesion molecule (JAMs). The claudins play a vital role in formation of barrier permeability in the CNS, particularly claudin-5 has been shown to be the claudin expressed highest in brain endothelial cells compared to claudin 12 and 3 (103-105) (106, 107). Occludin is a regulatory protein, whose role is to increase impedance and decreased permeability between cells in the BBB (101, 108). JAMs are localized at the TJ and are members of the immunoglobin superfamily responsible for leukocyte migration (109). Naik *et al.* has shown that JAMs are inversely responsible for increasing the invasiveness of breast cancer cell by transient knockdown of the JAM protein in MDA-231 cells (110, 111). In

another study it was shown that there was a strong correlation between the expression of JAM-1 in the primary breast cancer tissue and survival of patients by analyzing tissue microarray of BC patients (112). This relation to enhanced invasiveness was explained by the decreased expression of β1-integrin (responsible for cell migration) along with a decrease in JAM-A expression in a siRNA-based approach where knockdown of JAM1 was performed (102, 112). JAM proteins are also involved in cellular signaling events and the modulation of the actin skeleton and modulation of cell polarity (102, 113). The transmembrane adhesion molecules such as JAMs are connected to cytoskeleton through a series of cytoplasmic scaffolding proteins such as Zonula occludin 1 (ZO-1), ZO-2, Cingulin, Jacop, Membrane-associated guanylate kinase protein (MAGIs), and Matrix Metalloproteinases (MPPs) (88, 114). TJP and cytoplasmic scaffolding proteins together form the functional junctional protein complex. Changes in the expression of these TJP in the endothelial cell result in breakdown of BBB resulting in transendothelial colonization.

1.2.4.4. Pericyte

Pericytes are key components in the stabilization of blood vessels, regulating capillary diameter and blood flow and controlling BBB integrity and neovascularization (115). PDGF is required for vessel maturation and the recruitment of pericytes to endothelial cells. Pericytes are important mural cells required by endothelial cells to maintain barrier function and expresses PDGF receptor beta (*Pdgfrb) (116). In vivo* study using *Pdgfb* or *Pdgfrb* null mutant mice showed that the permeability of the BBB was increased for a range of low molecular weight tracers (117, 118). The crosstalk between endothelial cells and pericytes results in an increase in tight junction formation within the EC and regulates the adhesion between the two cell types via the secretion of transforming growth factor-β (TGF-β) (119, 120). Furthermore, in an age-dependent study of mice it was found that the reduced expression of TJ and adherence proteins such as claudin 5, zonula occludens 1 and cadherin in pericyte-deficient mice led to paracellular leakage (118, 120).

1.2.4.5. Astrocyte

Astrocytic foot processes and their connection to the blood vessels play a crucial role in maintaining homeostasis within the brain and maintaining the barrier function by affecting the expression of tight junctional proteins in mature brain vasculature (121, 122). Astrocytes also have role in supporting immune defense in brain and protect the neurons from the waste by-products of homeostasis (123). Malignant tumor cells cause the activation of resident astrocytes to reactive astrocytes. These reactive astrocytes aid the tumor cells by upregulation of survival related genes like: BCL2-like1 (BCL2L1), TWIST related protein 1(TWIST1) and glutathione S transferase alpha 5 (GTSTA5) to redirect the protective effects of reactive astrocytes for their survival (79, 123, 124).

1.2.5. Molecular markers for breast cancer brain metastasis

Brain metastases are thought to originate in the blood. Interestingly, breast cancer metastasizes to almost all internal organs before metastasizing to the brain (125-127). Steven Paget proposed the 'seed and soil' theory that the metastatic spread of cancer is due to the interaction and cooperation between the cancer cells and compatible metastatic site (128). He described the tumor cells to be the 'seed' that selectively grow in microenvironment of different organs which is the 'soil' and metastases is only possible when the appropriate seed is implanted in suitable soil (129). Another hypothesis put forward is the role of circulatory route (vascular and lymphatic site) draining from the primary tumor. The tumor cells arrest non-specifically at the first organ following its route in the circulatory system (129). Both of these theories regarding metastasis are applicable depending on the type of tumor.

An important step in the breast cancer cells extravasation to the brain is the breach of the BBB. CTCs that originate from primary breast cancer, arrest in thin capillaries of the brain where they adhere to the endothelial cells and through their interaction successfully extravasate into the brain niche (79, 130).

The attachment of CTC to the brain endothelial is mediated by surface receptors and adhesion molecules like integrins, selectins and chemokines on both the BC cells as

well as the endothelial cells (131). Integrin called alpha v beta 3 ($\alpha_v\beta3$) has been shown to promote metastatic growth in the brain by increasing the expression of vascular endothelial growth factor (VEGF) to attract blood vessels. This was identified in an *in vivo* experiment where the metastatic growth in brain was compared between MDA-MB-435 cells with knockdown of $\alpha_v\beta3$ and parental cell having constant high activation of $\alpha_v\beta3$ (132). VEGF secreted by the BC cells promotes its survival and cause a partial disruption of both tight and adherens junctions in endothelial cells (133, 134). The secretion of MMP1 by brain metastasizing breast cancer cell line MDA-231 was shown to induce the migration of BC cells in both *in vitro* and *in vivo* conditions. This study proved that MMP1 induces metastasis by the degradation of junctional proteins claudin and occludin resulting in an increased permeability of the BBB (135).

Comparative genome-wide expression analysis of MDA-MB-231 cells and ER negative BC patient-derived tumor cells exhibited cyclogenase-2 (COX2), the epidermal growth factor receptor (EGFR) ligand HBEGF and α-2,6-sialyltransferase 5 (*ST6GALNAC5*) genes as selective mediators of breast cancer brain metastasis (136, 137). Interestingly, COX2 has been shown to upregulate the expression of MMP1 which affects the barrier permeability (135). Brain metastasizing BC cells have been shown to secrete VEGF in the microenvironment, which in turn affects the EC resulting in the release of Ang-2 . *In vivo* analysis showed that injection of 4T1 cells resulted in altered distribution of TJ protein ZO1 and claudin-5 within the EC(138).

1.2.6. Blood Tumor Barrier

Once the tumor proliferates, it creates a region of hypoxia which results in the tumor cells secreting vascular endothelial growth factor (VEGF) to develop new vasculature required to provide nutrients and oxygen to the growing lesion (139-141). This nascent neurovascular-tumor unit is termed the blood tumor barrier (BTB). The BTB is defined as a leakier version of the BBB with heterogenous permeability properties. In contrast to the BBB, the astrocytes, pericytes, and neurons within BTB are not close to the capillary (142, 143). The BTB lacks proper distribution of pericytes and is characterized by a reduction in the astrocytic feet processes as well as endothelial

junctional proteins resulting in a discontinuous endothelial layer (144). The BTB has different and varied expression of efflux transporters such as P-gp and BCRP (145, 146). The structural integrity and the permeability of the BTB varies among brain metastasis by different tumor types as well as within and between multiple brain metastatic tumors. This heterogeneity in the barrier function may cause highly variable drug penetration into the CNS lesions (40, 141). The BTB was shown to be associated with an altered subpopulation of pericytes characterized by high expression of desmin as well as a decrease in the astrocytic basement membrane component, laminin α2 (147).

Furthermore, the reactive astrocytes found in the vicinity of breast cancer brain metastatic lesions express sphingosine 1-phosphate receptor 3 (S1PR3) which results in the astrocytic IL-6 and CC-chemokine ligand 2 (CCL2) secretion which makes the BTB leaky (148, 149). The secretion of inflammatory cytokines such as TNFα, IL1, and IL6 by the astrocytes aid in tumor proliferation and survival while the downregulation of PTEN induce outgrowth and invasion of tumor cells within the brain (150, 151). Microglia attracted into the vicinity of the BTB also support tumor proliferation, invasion and angiogenesis by secreting TGFβ, TNFα, IL1, IL6, VEGF, EGF, and several metalloproteinases (152). Because the BTB heavily contributes to the tumor microenvironment and its progression, a significant effort is currently being made to develop chemotherapeutic drugs capable of penetrating the BTB to reach the metastatic lesions.

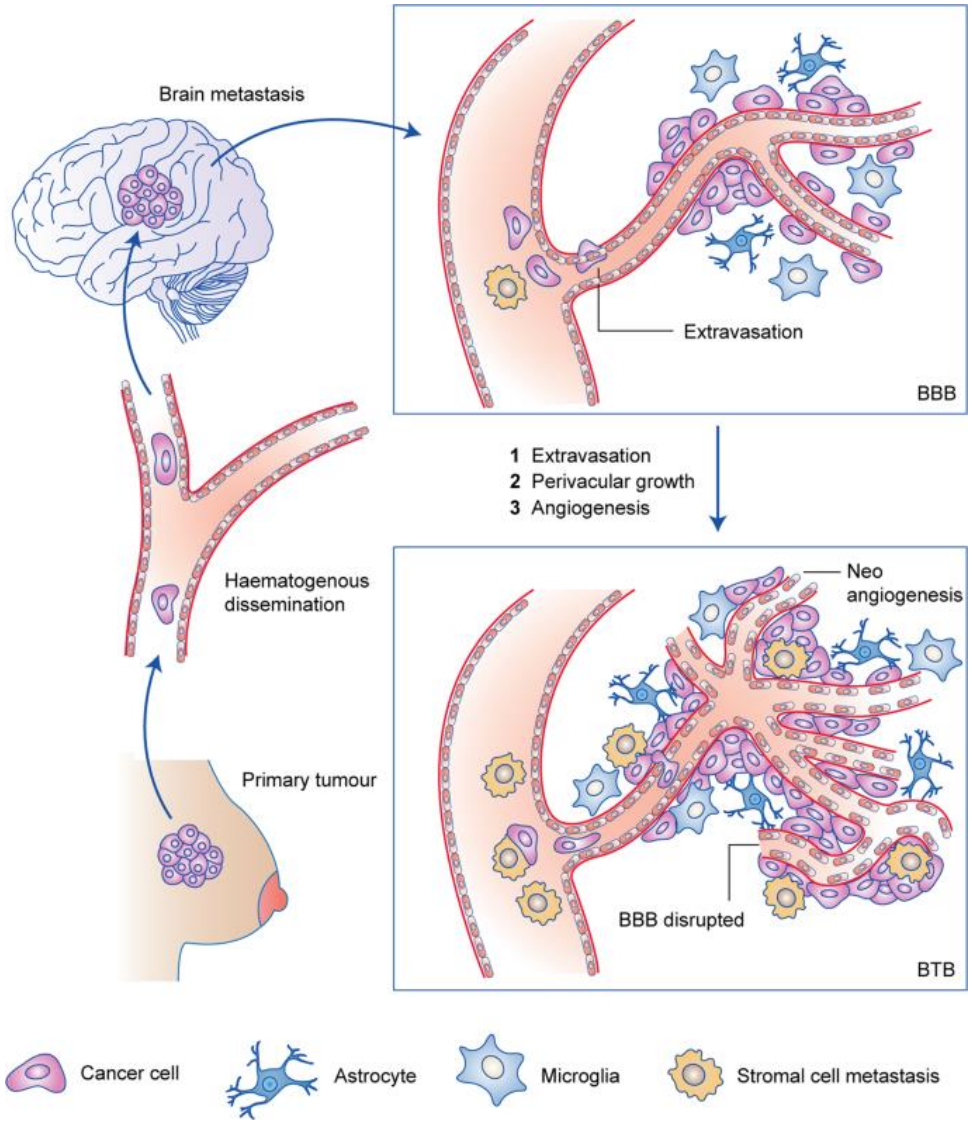

Figure 1.2 Blood tumor barrier
Circulating breast cancer cells extravasate to the brain by breaching the BBB and grow along the vessels in the brain by vascular co-option. When tumor grows in size, increased requirement to provide nutrients and oxygen to the cancer cells results in angiogenesis, which disrupts the BBB. The nascent leaky barrier with redistributed astrocytes, pericytes, junctional proteins of the BBB is referred to as BTB. Bailleux C, Eberst L, Bachelot T. Treatment strategies for breast cancer brain metastases. British Journal of Cancer. 2021 Jan;124(1):142-55.

1.3. Endoplasmic reticulum

1.3.1. Endoplasmic reticulum function and Stress

The endoplasmic reticulum (ER) is the largest organelle in the cell and the major biosynthetic site for proteins. It also regulates protein transport, protein posttranslational

modifications, protein folding and general protein homeostasis (153). Furthermore, it plays a vital role in synthesis and transport of lipids, general metabolism and Ca^{2+} storage (154-157). This diverse nature of the ER demonstrates the significance of the ER as an organelle that regulates metabolism and cell fate decisions (158).

Protein synthesis in the ER involves embedding of the mRNA:ribosome complex on the Endoplasmic Reticulum membrane (157). After a protein is synthesized, it is transported to the ER lumen where it is properly folded. Proper folding of proteins also require certain chaperone and folding enzyme-mediated post-translational modifications such as N-linked glycosylation and formation of disulfide bonds (155). After protein processing and folding in the ER, the functional proteins are secreted or incorporated into membranes. This protein processing process is subjected to a strictly regulated quality control system. When portions of the newly synthesized proteins don't reach final folding stage, they are terminated by degradation mediated by the proteosome via the Endoplasmic Reticulum Associated Degradation (ERAD) pathway (159). The high concentration of proteins present within the ER (100mg/mL) makes the environment of the organelle susceptible to protein aggregation (160, 161). Several intrinsic factors play a role in interfering with protein folding in the ER, causing accumulation of aberrant proteins and therefore, ER stress (160).

Several factors such as low glucose levels, hypoxia, redox stress or abnormal ER calcium content play a role in affecting protein maturation or protein folding in the ER (162). Moreover, the deficiencies in energy, increased protein synthesis, aberrant redox state or calcium levels can disturb protein folding and cause ER stress (163). Post translational modification involving N- linked glycosylation is affected due to rapid folding or oxidation of protein. Aberration in glycosylation results in the binding of misfolded peptide to ER Hsp 70 chaperones such as GRP78. The chaperones aid in the maturation of non-glycosylated polypeptide chain to prevent aggregation and proper post-translational modification and folding (155) (164). Misfolded proteins are harmful to the cell function. Thus, are tightly controlled even when the misfolding occurs continuously during adverse intrinsic and environmental conditions. The activation of the adaptive responses to overcome the stress caused by the misfolded proteins depend on the

condition and duration of the stress (158, 165). In response to the stress, the cells activate an adaptive signaling pathway called the Unfolded Protein Response (UPR) (160).

1.3.2. Unfolded Protein Response

The UPR is a homeostatic pathway that regulates proper protein folding under both physiological and pathological conditions. It is controlled by three major ER transmembrane sensors: inositol requiring enzyme 1 (IRE1), protein kinase RNA-activated (PKR)-like ER kinase (PERK) and activating transcription factor 6 (ATF6) (160). All three sensors comprise of 3 domains: an ER luminal domain (LD), a transmembrane domain and a cytoplasmic domain. The LD functions as sensor for ER stress and is normally bound by the ER resident chaperone heat shock protein A5/ glucose-regulated protein 78 (GRP78) and binding immunoglobulin protein (gene GRP78) (BiP) which regulates the activity of these ER sensors (158, 166). IRE1 and PERK cytoplasmic domains exhibit kinase activity and upon kinase activation are able to elicit downstream signaling pathways. Accumulation of unfolded proteins result in the dissociation of BiP from the three sensors, thereby activating the UPR system by promoting oligomerization of the IRE1 and PERK arms followed by trans-autophosphorylation. The dissociation of BiP from the ATF6 arm results in its trafficking to the Golgi apparatus where S1P and S2P proteases cleave the cytosolic and transmembrane domains releasing an ATF6f fragment (166-168). With the activation of these UPR arms the amount of unfolded proteins in the ER is reduced through several survival mechanisms such as the expansion of the ER membrane, the selective synthesis of crucial components of the protein folding and quality control machinery as well as the impediment of the stream of proteins into the ER through post-transcriptional regulation (169). However, after prolonged UPR activity when these methods are unable to mitigate stress and the homeostatic balance within the organelle, the cells are driven towards apoptosis (170).

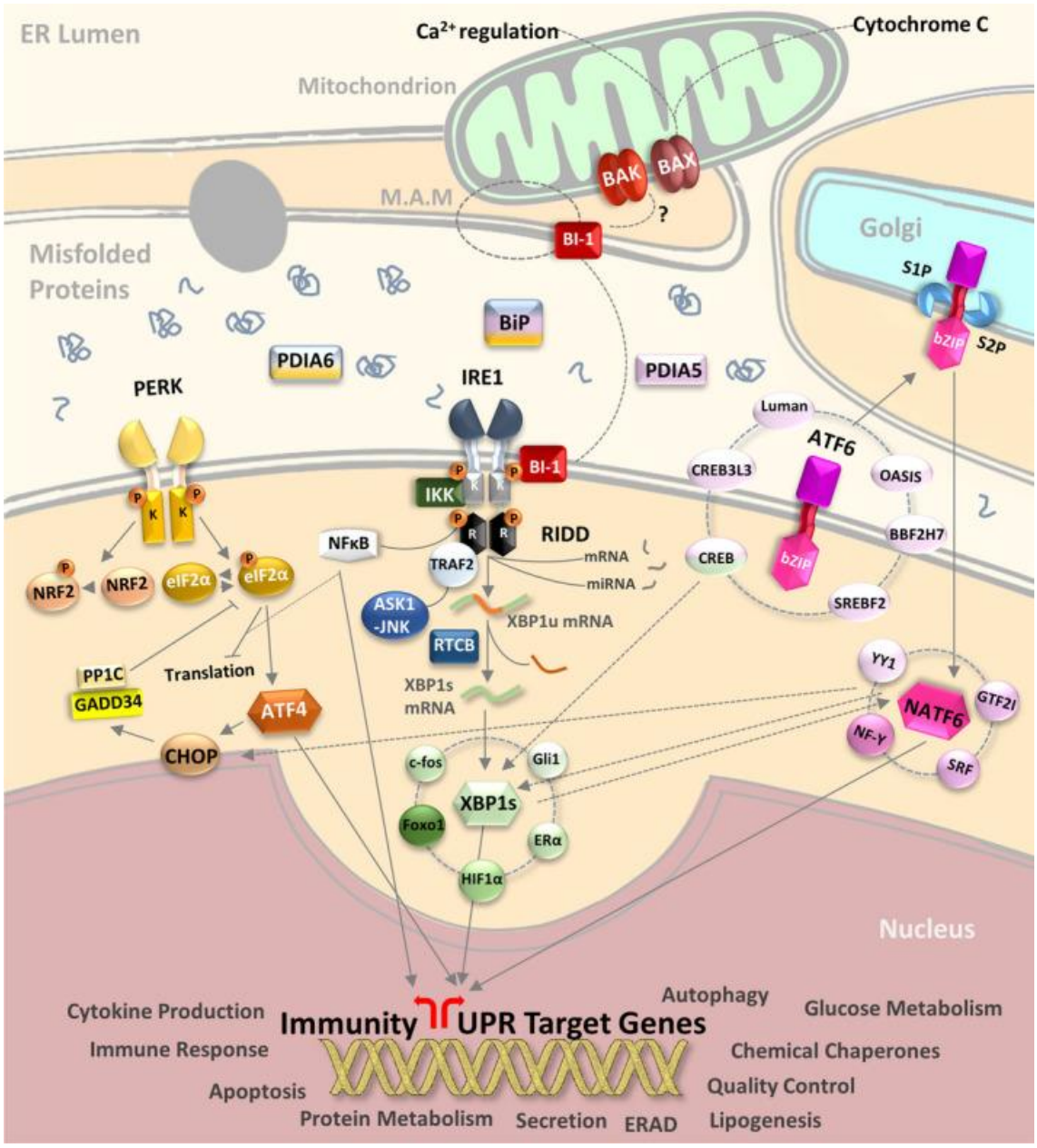

Figure 1.3 Unfolded Protein Response
Almanza A, Carlesso A, Chintha C, Creedican S, Doultsinos D, Leuzzi B, Luís A, McCarthy N, Montibeller L, More S, Papaioannou A. Endoplasmic reticulum stress signalling–from basic mechanisms to clinical applications. The FEBS journal. 2019 Jan;286(2):241-78.

1.3.2.1. PERK signaling

PERK is a type 1 ER transmembrane protein that detects the accumulation of misfolded protein by its luminal domain sensor (171, 172). BiP detachment from the ER luminal domain leads to oligomerization, trans-autophosphorylation and activation of the PERK arm, thereby activating its serine/ threonine kinase activity (173). Active PERK

results in the phosphorylation of eukaryotic initiating factor 2α (eif2α), which inhibits protein translation at ribosomes and thus reduces protein load in the ER to help alleviate accummulation of misfolded protein. This negative regulation pathway involves two components: (i) constitutive repressor of eif2α phosphorylation and (ii) growth arrest and DNA-damage inducible protein-34, acting as a fast response system to tackle ER stress resulting in temporary halt in global RNA translation (171). Meanwhile, the selective translation of transcript activating transcription factor 4 (ATF4) takes place. ATF translocates to the nucleus and stimulates the transcription of CHOP and GADD34 (171, 174, 175). ATF4 also stimulates the expression of adaptive genes responsible in amino acid transport and metabolism, protection from oxidative stress, protein homeostasis and autophagy resulting in loss of stress within the ER (158, 176). GADD34 promotes the assembly of a phosphatase complex which is responsible for dephosphorylation of eIF2α thus causing a negative feedback loop to terminate the repression of protein synthesis. But under prolonged ER stress GADD34 can switch the pro-survival mechanism to a proapoptotic mechanism (172).

In mammalian cells, the activation of eif2α is not restricted through PERK, rather three other individual kinases called PKR, general control nonderepressible-2 (GCN2) and heme-regulated inhibitor (HRI), which are activated by viral infection, amino acid starvation and heme depletion, respectively (177). Therefore, depending on the type of stressor, the duration of stress and the kinase activating the eif2α determines the cell fate (177). Following the ATF transcriptional activation of CHOP, the mechanism of apoptosis induced by CHOP involves the BCL-2 family members of proteins. It comprises of pro-apoptotic members the BH3 only proteins: BAX, BAK at the mitochondria which causes cytochrome c to be released, thereby activating the caspase cascade (178). CHOP also increases the expression of BIM, PUMA and NOXA to undergo apoptosis (179).

1.3.2.2. ATF6 signaling

ATF6 protein is expressed as two different homologues in the mammalian cell: ATF6α and ATF6β. Both of the homologues differ in their biochemical and, physiological characteristics and transcriptional activation domain (180). Under normal

cellular conditions ATF6 is a 90 kDa type II inactive transmembrane glycoprotein which encodes bZIP transcription factor domains in the cytosolic region of the protein (181, 182). Upon accumulation of misfolded proteins in the ER, BiP dissociates from ATF6, binding to the misfolded proteins, thereby activating the ATF6 pathway. Following activation, ATF6 translocates to the Golgi. In the Golgi, ATF6 is cleaved by site protease 1 then in an intramembrane region by site protease 2 by regulated intramembrane proteolysis into small fragments (183). The cytoplasmic fragment of the proteolytic cleavage called ATF6f is comprised of a transcriptional activation domain (TAD), a bZIP domain, DNA-binding domain and a localization signal to the nucleus (184). Inside the nucleus, ATF6f acts as a transcription factor to induce genes that encode chaperones (167). ATF6 has bifunctional role of being an adaptive response to mitigate stress, as well as causing apoptosis by controlling the regulation of DNA damage inducible protein GADD153 and growth arrest protein CHOP (160). Interestingly it was found that the active form of ATF6 is rapidly degraded in cell line models (185). This acts as a limitation in the study of the ATF6 arm in UPR.

1.3.2.3. Regulation of IRE1α activation and signaling

The IRE1 arm is the most evolutionarily conserved arm of the UPR (164). Mammalian genes encode for both isoforms of IRE1: (i) IRE1 α expressed most abundantly and ubiquitously, and (ii) IRE1 β, expressed in intestinal epithelial cells. While the knockout of expression of IRE1 α results in embryonic lethality in mice, the expression knockout of IRE1 β keeps the mice viable, which is why mammalian research on UPR is conducted on IRE1 α (186-188). IRE1 is a transmembrane protein with a N-terminal LD that can detect the degree of protein-folding within the ER, and a C-terminal cytoplasmic effector domain that possesses both protein serine/threonine kinase and RNase activities (189, 190).

The dissociation of BiP from the IRE1 arm due to the accumulation of misfolded proteins results in the oligomerization and activation of its cytosolic domain by enabling trans-autophosphorylation (191). This results in the activation of both cytosolic RNase and kinase domain of IRE1 arm. The IRE1 kinase and RNase activity are differentially regulated and dependent on the level and duration of ER stress. Activation of the RNAse

arm results in the unconventional excision of a small 26 nucleotide intron from the mRNA coding the transcriptional factor X-box binding protein 1 (XBP1) (191). The N-terminal region of unspliced isoform of XBP1 (XBP1u) contains a basic leucine zipper domain that induces XBP1 splicing by binding to the ER membrane (158, 192, 193). This is followed by ligation by the RNA ligase RTCB that leads to the generation of the spliced form of Xbp1 mRNA(155, 194-197). Its protein product sXBP1 is a basic leucine zipper (bZIP) transcription factor and sXBP1 translocate to the nucleus where it is responsible for the transcription of protein folding chaperones, foldases as well as components of ERAD pathway to aid in alleviating ER stress (198). In addition to that, XBP1s can also regulate lipid biosynthesis, glucose metabolism, DNA repair, cell survival and cell differentiation (199-203).

In addition to the splicing of XBP1, the RNAse activity also targets other transcripts through a process called Regulated IRE1-Dependent Decay (RIDD) (204). RIDD activity results in the degradation of mRNAs encoding for proteins related with signal peptide/transmembrane domains (164). In mammalian cells, RIDD is a conserved mechanism and the RIDD targets are enriched for mRNAs containing the consensus sequence CTGCAG (205, 206). The cleaved RNA fragments are then degraded by cellular exoribonucleases. In an interesting study it was shown that artificial dimerization of IRE1α in the absence of ER stress activated the XBP1 mRNA splicing but not mRNA decay demonstrating the role of RIDD in reducing the incoming protein load during stress and acting as an adaptive mechanism (204). However, in cases of extreme ER stress or when ER stress reaches a threshold, RIDD initiates apoptosis through repression of anti-apoptotic pre-microRNAs in caspase 2 (CASP2) dependent pathway (207). CASP2 is a proapoptotic protease essential for executing apoptosis (208). It has been identified that degradation of micro RNA 17, 34a, -96, and -125b, by the RNase domain of IRE1α stabilizes and promotes translation of Thioredoxin-Interacting Protein (*TXNIP)* and caspase-2 mRNAs (188). TXNIP promotes apoptosis through activation of caspase-1 and secretion of interleukin 1β (188, 207, 209). This shows that the IRE1 RNase arm is dynamic allowing it to switch between adaptation and apoptosis based on the level of stress present. The studies regarding RIDD activity is limited and difficult

due to the complex challenge of separating the RIDD activity from the XBP1 splicing activity of IRE1 (188).

The IRE1α is capable of regulating apoptosis, autophagy and ERAD independent of its RNAse activity through the kinase domain. The cytosolic domain of IRE1 interacts with adaptor protein TNF-receptor associated receptor 2 (TRAF2), an E3 ubiquitin ligase, leading to the activation of apoptosis signal regulating kinase 1 (ASK1), thereby activating the, JNK pathway (210). Phospohorylation of JNK activates proapoptotic members of the Bcl-2 family: BIM and BID leading to apoptosis under irreversible level of stress (158). This also mediates autophagy which might promote cell survival or result in cell death. The cytoplasmic domain of BCL 2 releases Beclin-1 which in turn leads to the formation of autophagosome by interacting with Ubiquitin Specific Protease 14 (USP14). (164, 211).

1.3.3. Chronic ER stress and pro apoptotic phase

The fate of a cell depends on the timing of the intensity of ER stress and how the signaling between IRE1α and PERK is coordinated to mitigate it. Upon accumulation of misfolded proteins and BiP dissociation form the LD, the IRE1 arm is activated causing Xbp1 mRNA to be spliced, allowing translation of sXBP1, an active transcription factor (191). This protein acts as a transcriptional factor for pro-survival genes- chaperones and ERAD to help rescue the cell from misfolded proteins (212-214). Similarly, activation of PERK signaling leads to phosphorylation of eIF2α that results in translational attenuation as a measure to protect the cells from accumulating newly synthesized proteins (214). ATF6 translocates to Golgi whereby it is cleaved, generating a fragmented ATF6, ATF6f, which can regulate genes involved in the ERAD and XBP1 pathways (165, 215, 216). Altogether, the expression of sXBP1, phosphorylation of eIf2α and ATF6f results in the adaptation of the cell to the accumulated stress as a survival mechanism.

In the presence of chronic stress, the cells shift from a pro-survival stage to a pro-apoptotic stage through a series of changes in the signaling pathways. Lin JH *et al* showed that splicing regulated by IRE1 is eventually impaired under prolonged ER stress suggesting that this change leads to cell death along with the components of the PERK

signaling pathway which are pro-apoptotic (217). However, considering the potential late pro-apoptotic IRE1 signaling outputs, this attenuation may indicate towards cyto-protective activity (214). In contrast to the attenuation of IRE1α signaling, the PERK signaling is sustained under ER stress and favors the upregulation of many proapoptotic components (218). However, eIF2α phosphorylation was also shown to be diminished after extended ER stress, indicating that the fine-tuning of the UPR is dynamic and specific for different cell types (219, 220).

Under chronic ER stress, numerous pro and anti-apoptotic components of the BCL-2 family of proteins aid in the intrinsic pathway of apoptosis of cells (221). It involves the release of cytochrome c from the mitochondria by the BCL-2 family (BAX, BAK) to promote a cytosolic protein complex to activate caspase cascade (178). Upstream regulator of BAX and BAC comprise the BH3 domain which causes upregulation of the BH-3 only proteins, PUMA and NOXA at a transcriptional level, which function as apoptosis inducers (158, 178, 179). The PERK pathway is involved in apoptosis through the transcription of CHOP also called growth arrest and DNA damage inducible gene (GADD153) which causes the downregulation of BCL-2 and an increase in trancription of PUMA and GADD34 (165, 222, 223). The IRE1α arm activates the apoptosis signal-regulating kinase 1 (ASK1) by interacting with TRAF2 and JNK pathway through its kinase domain to induce apoptosis by regulating BCl-2 family proteins (158).

1.3.4. IRE1 and its role in breast cancer

The microenvironment of tumors contributes to tumor cell exposure to a wide variety of challenges like lack of nutrients, hypoxia and decreased vascularization. All these factors can lead to the formation of misfolded protein within the ER resulting in the activation of the UPR. Cancer cells adapt to the challenges in the microenvironment by activating UPR as survival strategy. UPR especially the IRE1-XBP1 pathway has been associated with tumor development, progression and post-therapy responses (224). Investigations into the role of IRE1 in TNBC has shown that the level of sXBP1 is higher in basal cancer cell lines than luminal cancer cells, where sXBP1 levels are commonly

used as a readout of IRE1 activity (225, 226). The regulation of kinase and RNase activity of the IRE1α arm are differentially regulated and dependent on the level and duration of ER stress present. Furthermore, sXBP1 was shown to increase the levels of CD44 ^{high} and CD24 ^{low} cancer cell population and enhanced mammosphere formation *in vitro* and is associated with cancer relapse in breast cancer patients (226-229). The expression of hypoxia inducing factor 1 α (HIF1α) is high in CD44 ^{high} and CD24 ^{low} MDA-MB-231 cells and results in corresponding increase to sXBP1 under hypoxia and glucose deprivation. HIF1 α targets: VEGFA, PDK1 ,GLUT1 and DDIT4 have been associated to increase tumorigenicity in TNBC (226). VEGF is an angiogenic factor which has been reported to induce proliferation and migration of endothelial cells as well as tumor growth, adhesion and vascularization in MDA-231 cells (230).

Tumor vascularization occurs more extensively in TNBC compared to other BC resulting in significantly shorter recurrence-free survival and OS with a shorter time from diagnosis to relapse and from relapse to death (231-233). It has been reported that IRE1α mediates the transcriptional regulation of vascular endothelial growth factor (VEGF-A) through XBP-1 splicing in mouse embryonic fibroblasts (234). In a recent study it was found that MYC, a proto-oncogene, is responsible for inducing sXBP1 transcriptional activity and binding to the promoter and enhancer region of IRE1, resulting in XBP1 splicing activity in TNBC cell lines (235, 236). Interestingly, a combinational treatment of IRE1 inhibition and docetaxel in tumor- bearing mice resulted in reduced proliferation and increased apoptosis thus, improving the disease-free survival of the mice (235).This concludes that IRE1-XBP1 can be used as a potential therapeutic target for cancer treatment. In a study by Logue et al. it was identified that the IRE1 arm is responsible for the production of pro-inflammatory factors such as IL-6, IL-8, GM-CSF, and CXCL1in RNase dependent manner in TNBC cells, MDA-MB-231. They also studied the cytokine secretion of MDA-MB-231 cells under a neo-adjuvant chemotherapeutic drug named paclitaxel to determine that, the secretion of pro-inflammatory factors is elevated under this treatment. However, *in vivo* analysis with a combinational treatment of paclitaxel and IRE1 RNase inhibitor showed a reduction in tumor volume (225). These studies identify the importance of IRE1 signaling in TNBC and utilizing it as a potential therapeutic target for TNBC treatment.

All of these different findings regarding role of IRE1-sXBP1 in BC has prompted the development of several small molecular inhibitors targeting the IRE1 RNase domain (237-240). The structure of IRE1 is as such that multiple sites could be targeted by small molecules: (i) the nucleotide-binding pocket, (ii) the dimer-interface hydrophobic pocket, and (iii) the RNase active site (238). MKC8866 is a small hydrophobic molecule with orthohydroxyl aryl aldehyde moiety that attaches to the hydrophobic moeity of the RNAse domain for selective inhibition (241). Moreover, it qualifies as pre-clinical agent due to its acceptable pharmacokinetic and toxicity profile. Animal studies have shown that the administration of the MKC inhibitor in conjunction with chemotherapeutic agents like Paclitaxel results in tumor suppression and delayed tumor relapse in TNBC xenograft mouse models (225, 241).

1.4. Rationale and Hypothesis

Literature has shown that BC cells exploit the IRE1-XBP1 arm of the UPR for cell survival and progression. It has been established that TNBC cells have highly activated XBP1, which plays an important role in its tumorigenicity. Even though the IRE1 arm has been identified as a potential therapeutic target, the exact mechanism of how TNBC cells survive and migrate.

The hypothesis of the study is that IRE RNase activity promotes cancer cell survival under conditions of ER stress in brain metastasizing TNBC cells. Inhibition of IRE1 RNase activity or XBP1 silencing will attenuate transmigration of TNBC cells through endothelial cell barriers.

1.5. Objectives

- Identify the effect of ER stress induction on UPR activity in MDA-BR cells.
- Determine the effect of IRE1-XBP1 modulation on MDA-BR cell survival and migration.
- Determine if modulation of the IRE1-XBP1 pathway prevents passage of MDA-BR cells through EC barriers.

Chapter 2. Materials and Method

2.1. Cell culture

The breast cancer cell line MDA-MB-231-BR (brain metastasizing derivative of MDA-MB-231; in this document referred to as MDA-BR) was cultured in DME/F-12 medium [Hyclone, Thermo Scientific, Waltham, USA] with 5% Fetal Bovine Serum (FBS) [Gibco, Thermo Scientific]. The patient-derived breast cancer brain metastatic cell isolate PBS-94 was cultured in DMEM/F-12 medium with 10% FBS. The human immortalized endothelial cell line hCMEC/D3 was cultured in EGM-2 endothelial cell growth basal medium [Lonza], supplemented with 5%FBS, HEPES [Gibco], Lipid [Gibco], ascorbic acid [Sigma], hydrocortisone [Sigma], in a 5% CO_2 incubator with humidified air. Mouse brain derived bEnd3 cells was cultured in DME/F-12 medium [Hyclone, Thermo Scientific, Waltham, USA] with 10% FBS [Gibco, Thermo Scientific]. Stress was induced within the cells using two different stressors: serum starvation and thapsigargin. For serum-starvation treatment of MDA-BR cells and PBS94 cells, serum free media containing 1% insulin transferrin selenium (ITS) [Gibco] was used for 24 – 72 hours. The chemical inducer of ER stress, thapsigargin (Tg) [Sigma], was used at 5nM concentration. The IRE1 RNase inhibitor MKC8866 was provided by Fosun Orinove and used at a concentration of 10µM. The PERK kinase inhibitor AMG44 [Tocris, 5517] was used at concentration of 2µM.

Table 2.1 List of Inhibitors and ER stressors used:

Inhibitor	Working Conc.	ER stressor
MKC8866	10µM	Thapsigargin
AMG44	2µM	0% FBS media

2.2. Stable transduction in cultured cells

2.2.1. Plasmid constructs

Plasmid constructs for the Doxycycline-inducible expression of XBP1 shRNA with three different target sequences were synthesized by Dharmacon. They encoded for

ampicillin and puromycin resistance and red fluorescent protein. The plasmids were purchased in glycerol stocks and were streaked on selective ampicillin plates. Isolated colonies collected from the plate were grown in LB broth in a shaker at 300 rpm, 37˚C overnight and plasmids were extracted using the QIAprep Spin Miniprep Kit [Qiagen].

The plasmids were sent for lentiviral packaging using College of Medicine lentiviral core facility.

Table 2.2 List of the plasmids and their sequences

Plasmid	**Source**
shXBP1	Dharmacon V3SH11255-09EG7494
Plasmid Sequences	
V3SH11252-225143005 TAAGCATCCAGTAGGCAGG (targets 3'UTR and ORF)	
V3SH11252-226678330 TTCTGGAGGGGTGACAACT (targets ORF)	
V3SH11252-228775480 CTCTCGTAAAAGCTGATTT (targets ORF)	

2.2.2. Transduction and selection of stable clones

MDA-BR cells were transduced with shXBP1 lentivirus particles at multiplicity of infection (MOI) 5. Forty-eight hours after transduction cells were exposed to selective media using 3µg/ml of puromycin over the course of 2 weeks. Establishing clones were then picked and expanded. Successful XBP1 downregulation was tested by Western blot after treating the cells 5 days with Doxycylcine [Sigma D9891] (2 µg/ml) with daily change of Doxycycline (DOX) containing media. Stable shXBP1-expressing clones were verified by reduction of detectable sXBP1.

2.3. Protein isolation, Western blot Analysis

The cellular proteins were extracted using two different methods: 1X Laemmli buffer (Hibberd & Leedale, 1970) and M-PER (Mammalian Protein Extraction Reagent) [ThermoScientific 0078503] lysis buffer. Protease inhibitor (ThermoScientific) was added at concentration of 1:100 dilution to the collected lysate. The lysates were briefly sonicated and boiled at 90˚C for 5 minutes. For secreted protein samples, the supernatant

was collected and concentrated using SpeedVac concentrator. The dried samples were then resuspended in 100µl of ddH_2O and lysed with 5X Laemmli buffer, which concentrated the samples by 10-fold. The samples were then loaded into 7.5%, 10% or 12% stain free polyacrylamide gels for SDS-PAGE. After the protein separation, it was transferred to nitrocellulose membrane (0.2 µm) (Cytiva, Vancouver, Canada) using the BioRad semi dry auto transfer set at 25 V for 10 minutes. The non-specific proteins were blocked using 5% milk in TBST (7.6 pH). The blots were washed using the TBST (7.6 pH) washing buffer. TBST buffer composes of: sodium chloride (Sigma), Tris (Sigma) and Tween-20 (Sigma). The blots were incubated with the given dilution of primary antibodies in blocking buffer overnight at 4˚C. After the overnight incubation, the blots are washed 3 times for 5 minutes and then incubated with the appropriate secondary antibody (goat anti-mouse/ rabbit antibody conjugated to HRP (horseradish peroxidase). Specific bands were vizualized using ECL developer solutions (BioRad, Hercules, USA). β-actin was used as loading control.

Table 2.3 List of primary antibodies used for Western blot

Protein	**Host Species**	**Company and Catalog Number**	**Diluent**	**Dilution used**	**Expected Molecular weight (kDa)**
sXBP1	Rabbit	CST D2C1F	5% milk in 1xTBST (pH 7.6)	1:1000	60
BiP	Rabbit	CST C50B12	5% milk in 1xTBST (pH 7.6)	1:1000	78
IRE1	Rabbit	CST 14C10	5% milk in 1xTBST (pH 7.6)	1:1000	130
P-JNK	Rabbit	CST 9251S	5% milk in 1xTBST (pH 7.6)	1:1000	42, 50
T-JNK	Rabbit	CST 9252S	5% milk in 1xTBST (pH 7.6)	1:1000	42, 50

PERK	Rabbit	CST DIIA8	5% milk in 1xTBST (pH 7.6)	1:1000	140
Phospho-eif2 alpha	Rabbit	CST 9721	5% BSA in 1xTBST (pH 7.6)	1:1000	37
T-eif2 alpha	Rabbit	CST 5324	5% BSA in 1xTBST (pH 7.6)	1:1000	37
ATF4	Rabbit	Abcam 1849909 CSTD4B8	5% milk in 1xTBST (pH 7.6)	1:1000	50
CHOP	Mouse	CST 2895	5% milk in 1xTBST (pH 7.6)	1:1000	27
Beta actin	Mouse	Santa Cruz (sc-47778)	5% milk in 1xTBST (pH 7.6)	1:10,000	42
Thrombospondin-1	Rabbit	Abcam 85762	5% milk in 1xTBST (pH 7.6)	1:1000	150

Table 2.4 List of secondary antibodies utilized

Antibody	**Host species**	**Company and catalog number**	**Diluent**	**Dilution used**
Goat anti rabbit - HRP	Goat	Cell Signaling Technology (7076s)	5% milk in 1xTBST (pH 7.6)	1:2000;
Goat anti mouse-HRP	Goat	Cell Signaling Technology (7074s)	5% milk in 1xTBST (pH 7.6)	1:2000;

2.4. RNA isolation, cDNA preparation and Polymerase chain reaction (PCR)

RNA was isolated from hCMEC/D3 cell line 24 hours after treatment with conditioned media (48 hours) from MDABR cells using Trizol reagent (Thermo Scientific) following the manufacturer's protocol. The concentration and purity of RNA was assessed by measuring the absorbance of RNA at 260 and 280 nm using an UV

spectrophotometer. cDNA was prepared using 1µg of RNA and qScript cDNA master mix (Quanta Biosciences, Beverly, USA). The composition of the working solution and thermocycling conditions for cDNA synthesis was as follows (Table 2.5, 2.6):

Table 2.5 Composition of cDNA working solution

Component	**Volume**
RNA	Variable (1µg)
cDNA master mix	4 µL
Double distilled water	variable
Total	20µL

Table 2.6 Thermocycling conditions for cDNA synthesis

Temperature (in ºC)	**Time (in minutes)**
25ºC	5 minutes
42ºC	30 minutes
85ºC	5 minutes
4ºC	Hold

The cDNA prepared was then used to analyze gene expression using quantitative Polymerase Chain Reaction (PCR). The primers used and the PCR master mix compositions are described in Table 2.7 and 2.8, respectively. The thermocycling conditions are elucidated in Table 2.7.

Table 2.7 Primer sequence and number of cycles run for the qPCR

Gene	**Primer location**	**Sequence**	**Amplicon size (base pairs)**	**Tm**	**Number of cycles**
Claudin 5	Reverse	5’-AAC TCG CGG ACG ACA ATG TT-3’	20	63	40
Claudin 5	Forward	5’-AAG CGT GCT CTA CCT GTT TTG-3’	21	62	40
Claudin 3	Reverse	5’-CGT AGT CCT TGC GGT CGT AG-3’	20	61	40
Claudin 3	Forward	5’-GCC ACC AAG GTC GTC TAC TC-3’	20	60	40
Occludin	Reverse	5’-TCA GGA ACC GGC GTG GAT TT-3’	20	67	40

Occludin	Forward	5’-TGC CTT CAC CCC CAT CTG AC-3’	20	66	40

Table 2.8 qPCR master mix

Component	**Volume (in µL)**
Double distilled water	7.2
SYBR green	10
Forward primer	0.4
Reverse primer	0.4
cDNA	2
Total	20

2.5. Supernatant Analysis

Supernatant was collected from MDA-BR and PBS-94 cells after treatments with thapsigargin (5 nM) and serum starvation +/- MKC8866 (10 µM) for 48 and 72 hours, respecively. The supernatant was spun at 2500 rpm for 5 minutes to pellet floating cells. 1 ml of the conditioned media was aliquoted to be kept in -80˚C overnight. The frozen samples were loaded in speed vac machine for 4 h. The desiccated samples were resuspended in 100 µl of double destilled water and protease inhibitor. Prior to loading the samples for SDS-PAGE, the Laemmli buffer was added to the samples and they were heated at 90˚C in the water bath for 5 minutes.

2.5.1. Cytokine Analysis

MDA-BR cells were cultured for 48 h with 5 nM thapsigargin and 10 µM MKC8866 in 2% FBS media condition and for serum starvation in 0% FBS media condition for 72 hours. shXBP1-BR clone 02 and 03 cells were treated daily with or without doxycycline (2µg/ml) for 5 days. The conditioned media from the cells were collected and spun down at 2500 rpm for 5 minutes to remove floating cells from the supernatant. The cell free supernatant was then concentrated and purified using Amicon Ultra 2ml Centrifugal filters (Millipore, UFC 200324). The corresponding protein lysates were collected from the cells using M-PER lysis buffer. The samples’ protein concentration was quantified using BCA protein quantification kit and 15 µg of protein

was loaded for the SDS-PAGE to detect ER stress targets and confirm whether the treatments were effective. The supernatant protein concentrates were measured using the BCA protein measuring kit. The samples were sent for analysis to Eve Technologies (multiplex HD48 Cytokine/chemokine array) after equalizing the protein concentration in all the samples to a concentration of 1.5mg/ml.

2.6. Cell viability

2.6.1. WST Assay

MDA-BR cells were seeded at a density of 2000 cells/well in DMEM/F12 1:1 in 96 well plates for 24 hours. After 24 hours, cells were treated with 10 µM MKC8866 under 5% and 0% FBS media composition for 24 hours, 48 hours and 72 hours. DMSO was used as solvent control. The cells were also treated with thapsigargin (5 nM), MKC8866 (10 µM) and DMSO in 5% FBS media for 8 hours, 24 hours and 48 hours. WST reagent was added to the cells and incubated in 5% CO_2, at 37˚C for 4 hours. The WST reagent contains Tetrazolium compound that changes to soluble yellow colour which is quantified at 450 nm using an ELISA plate reader (Perkin Elmer, Boston, USA).This assay is based on the NAD(P)H-dependent cleavage of the tetrazolium salt WST-1 to formazan by cellular mitochondrial dehydrogenases. The amount of formazan dye formed in this reaction is directly proportional to the activity of mitochondrial dehydrogensases and thus, it depends on viable cells

Seeding of hCMEC/D3 cells was performed at a density of 4000 cells per well in complete endothelial media in 96 well plate and incubated overnight in 5% CO_2 at 37˚C. Conditioned media from MDA-BR cells were collected and added to the seeded endothelial cells in 100% and 50% dilution. Prior to adding, the cells were removed by spinning the supernatant for 5 minutes at 2500 rpm. The cells were incubated with the conditioned media for 24 hour, 48 hour and 72 hours. WST reagent was applied to the cells and incubated in 5% CO_2, at 37˚C for 4 hours. The reading was taken using 450nm absorbance in the ELISA plate reader.

2.6.2. Real Time Cell Analysis:

The cell viability measurement with the xCelligence system (ACEA Biosciences, Inc., San Diego, CA, USA) uses culture plates with gold micro electrode at the bottom of the plate (E-plate) to monitor cells in real-time. The system detects changes of cellular impedance across the electrodes and represents the data as cell index (CI) which is automatically calculated by the system. The CI value is influenced by cell number, cell size, and cell attachment. This system can determine real-time cell cytotoxicity, cell growth and cell death. The cellular impedance is recorded every 15 minutes using the RTCA software. The plate was equilibrated for 30 minutes in the incubator before MDA-BR cells were seeded in the E-plate at 20 000 cell/ml. The cells were treated with 5 nM thapsigargin with and without MKC8866 at 10 µM in 5% FBS media or they were exposed to serum-free free media with and without MKC8866 (10 µM) .

2.7. Caspase Assay

Human TNBC cells MDA BR were seeded at a density of $4x10^3$ cells/ well in DMEM/F12 1:1 and were cultured in 96 well plates for 24 hours after which, they were treated with ER stress inducers: 5 nM thapsigargin +/- MKC8888 (10 µM) and serum starvation +/- MKC8888 (10 µM) and incubated for 8 hours, 24 hours and 48 hours. Luminescent caspase substrate was added to cells for 4 hours while shaking at 350 rpm at RT. The relative luminescence was measured in the ELISA plate reader (Perkin Elmer, Boston, USA) and presented compared to untreated controls.

2.8. Migration assay

2.8.1. Real time migration assay

Real-time measurements of MDA-BR cell migration was performed by using the xCelligence system where 50,000 cells were seeded per well in CIM-Plates. Before seeding the cells, the chamber was equilibrated at 37˚C incubator for 30 minutes. The cells were treated with 5 nM thapsigargin with and without MKC8866 at 10 µM in 5% FBS media or they were exposed to serum-free free media with and without MKC8866

(10 µM) over a period of 48 hours. Data was collected and analyzed using the RTCA software.

2.8.2. *In vitro* transendothelial migration assay

It is a filter-based-2-chamber migration assay performed using two cell models: MDA-BR and mouse brain endothelial cells bEnd3. The bEnd3 cells were seeded on rat-tail collagen (150µg/ml) (Corning) coated 8µm fluoroblok inserts (Corning) at density of 14,000 cell/ml and allowed to grow to a monolayer under treatment with complete endothelial media for five days. MDA-BR cells were added on top of the endothelial monolayer at a density of 50,000 cells per insert and incubated for 24 hours with and without 10µM MKC8866. MDA-BR cells stably express GFP and the GFP fluorescence can be detected with in the FITC channel from the bottom of the fluoroblok filter without interference from GFP signals from the filter top. The fluorescence readings were taken using Synergy HT plate reader.

The MDA-BR/shXBP1 clone 02 and 03 were seeded on confluent bEnd3 cell monolayers seeded on top of collagen coated 0.8µM fluoroblok inserts as described above. The shXBP1 clones 2 and 3 were treated with and without DOX for 5 days prior to seeding endothelial migration assay. The upper chamber contained 0% FBS media with and without DOX while the lower chamber contained 5% FBS media with and without DOX. The cells were incubated for 24- and 48- hours following which the GFP signal was detected using the same method as described above.

2.9. *In vivo* study with shXBP1 MDA-BR clones

75,000 shXBP1-BR clones were injected into the left ventricular (LV) chamber of 8-12-week-old female mice using ultrasound-guided intracardial xenografting. The injection was done under anesthesia with isofluorane. The anesthetized mice were shaved at the anterior chest wall and placed on a warmed mouse platform of an ultrasound system for small animals (VisualSonics Vevo 2100 High-Frequency Imaging System (SOP #P107). For intracardial injections of the tumor cells, the skin of the anterior chest wall was disinfected using iodine solution. A thick layer of ultrasound gel was applied

over the disinfected area of the chest wall. An ultrasound transducer was positioned on the chest wall till the whole heart was within the field of view. 100µL of the cell suspension containing 75,000 cancer cells were filled into a 1mL syringe. A 3/4-inch-long 27-gauge needle was fitted onto the syringe, which was then and secured onto a syringe holder. The syringe was slowly forwarded towards the chest wall until the needle tip was well within the imaging field of view aiming directly at the LV chamber. The syringe needle was slowly advanced through the skin and skeletal muscle at an intercostal space, ultimately into the LV chamber. Placement of the needle within the LV chamber was readily confirmed by a quick pulse of red blood in the syringe. Then, 100 µL of cancer cell suspension was injected into the LV chamber in a 20-µL increment over a time period of 30-40 seconds (242-244). Following injections, the syringe was withdrawn.

Afterwards, the mice were administered meloxicam (2 mg/Kg bw) subcutaneously once per day for 3 post-operative days. Doxycycline was added to the mouse diet in two different ways: drinking water for mice injected with shXBP1 clone 03 and chow for mice injected with shXBP1 clone 02. Doxycycline chow was purchased from Harlan Laboratories (Madison, WI, USA). Because mice consume 4-5 g/d of doxycycline, the diet was tailored to deliver a daily dose of 2-3 mg. DOX was administered via drinking water at a concentration of 2 mg/ml ad libitum.

The initial weight of the mouse was measured, and the humane endpoint weight was calculated as 20% reduction of the of the initial weight. The mice were closely monitored for physical signs, body conditions, behaviors and weight. The parameters are described in the table below:

Table 2.9 Mouse monitoring chart

Physical signs	Normal	Ruffled	Hunched	Closed Eyes	Sunken Eyes
	Fast respiration	Slow respiration	Bloody feces	Skin wound	
Body conditions	Emaciated	Well-conditioned	Under conditioned	Over conditioned	Obese

Behavior	Normal	Not moving	Depressed	Isolated	Hyperactive
Weight	Starting weight in g	Endpoint weight: reduction by 20% in g			

Symptoms such as hind limb paralysis, weight loss, ruffled fur, hunched back were indications of the mouse reaching endpoint. The mice were euthanized when signs of metastatic disease were observed, such as hind limb paralysis, weight loss to 20 % reduced initial body weight, heavy breathing, ruffled fur or reduced activity. The euthanization was performed by an overdose or isofluorane followed by cervical dislocation. The brain was collected immediately for harvesting cells and fixation in neutral buffered formalin.

2.10. Statistical Analysis

The Western blot densitometry was performed using the Biorad image lab software and graphical presentation was done using GraphPad Prism 8 statistical software. These independent experiments were performed at different times, using different passage number of cells and the Western blots were developed with different exposure times leading to generation of values that were not directly comparable for statistical analysis. Thus, the quantification was shown separately for each experiment. The survival plot for the shXBP1-MDA-BR *in vivo* xenograft studies were made using Kaplan-Meier survival curve to determine if the difference in survival in the treatment group is more than expected based on chance. The quantification for WST analysis and qPCR experiments from three independent experiments were calculated using GraphPad Prism 8, two-way ANOVA, Tukey's multiple comparisons statistical tests. P values less than 0.05 were considered as significant. The level of significance was defined as *$p<0.05$, **$p<0.01$, ***$p<0.001$.

Chapter 3. Results

3.1. IRE1α RNase activity is strongly induced by serum starvation and thapsigargin

Two different types of cellular stress conditions were used to treat MDA-BR cells to determine its effect on the ER stress response pathway. The chemical inducer thapsigargin (Tg) and serum starvation as a milder stressor were used. Tg is an inhibitor of the sarco/endoplasmic reticulum Ca^{2+} ATPase (SERCA) pump, which prevents transport of Ca^{2+} into the ER. Calcium homeostasis in the ER is required for proper functioning of the chaperones to aid in protein folding (245). Depletion of calcium from the ER by thapsigargin thus prevents the folding and maturation of proteins causing ER stress (246). Serum starvation is a physiological stressor that stresses cells due to the lack of nutrients in the media and causes stress over longer durations. IRE1α RNase inhibitor MKC8866 was used to selectively inhibit the activity of the RNase domain.

MDA-BR cells were treated under serum starvation (0% FBS) over a period of 24, 48 and 72 hours with and without the RNase inhibitor MKC8866 (10μM). The lysates were collected, and cellular proteins were separated on SDS-PAGE for the detection of sXBP1 (Figure 3.1). The results showed that under normal media condition of 5% FBS media, MDA-BR cells have a basal level of ER stress that increased over the time as shown by increasing levels of sXBP1. The basal IRE1α activation was further induced upon treatment with 0% FBS media. The inhibitor successfully inhibited the IRE1α splicing activity in the serum starved cells at all time points (Figure 3.1).

MDA-BR cells were treated with Tg (5nM) only and Tg plus MKC8866 (10μM) for 2, 4, 8, 24 and 48 hours. Western blot (WB) analysis for the detection of sXBP1 using the total protein lysates (Figure 3.2) showed that Tg strongly induced IRE1α activity during all the time points tested and the IRE1α splicing activity was successfully inhibited by the inhibitor MKC8866 (Figure 3.2). The strong induction of sXBP1 resulted in a shorter developing time for each blot. As a result, a very faint band of basal sXBP1 was detected in the early time points of incubation for the controls. These experiments

showed that the MDA-BR cells have a basal level of ER stress which can be further induced using both chemical and physiological inducers of ER stress. The IRE1α RNase inhibitor MKC8866 was able to inhibit both, the basal and induced IRE1α splicing activity.

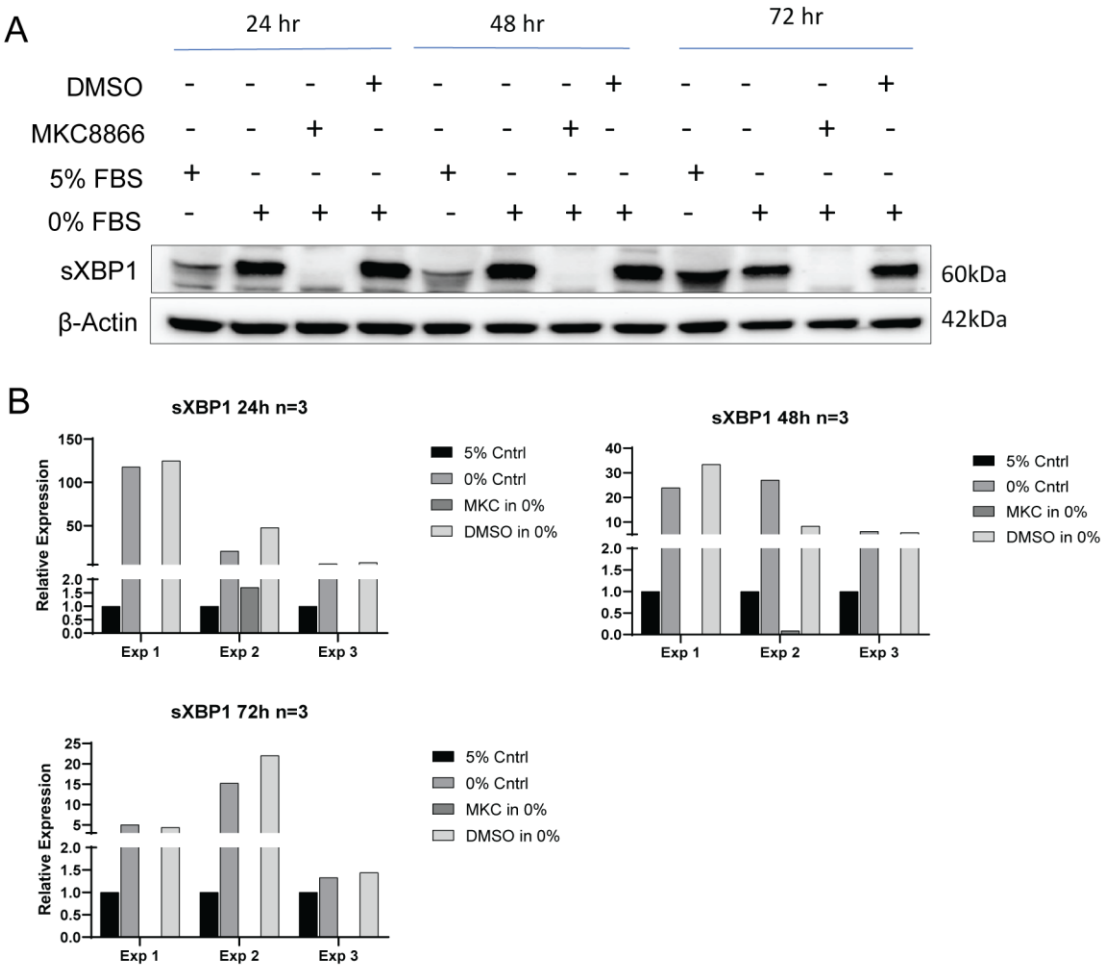

Figure 3.1 Serum starvation induced IRE1α RNase activation in MDA-BR cells
MDA-BR cells were treated in 0% FBS media, +/- MKC8866 (10μM) for a period of 24h, 48h and 72h. DMSO served a solvent control and 5% FBS as complete media control The lysates were collected and loaded for SDS-PAGE for sXBP1 detected. (A) Qualitative representation of sXBP1 expression showing an induction under serum starvation stress and it is inhibited by MKC8866. (B) Quantitative protein expression of 3 separate experiments was determined by densitometry using β-actin as reference.

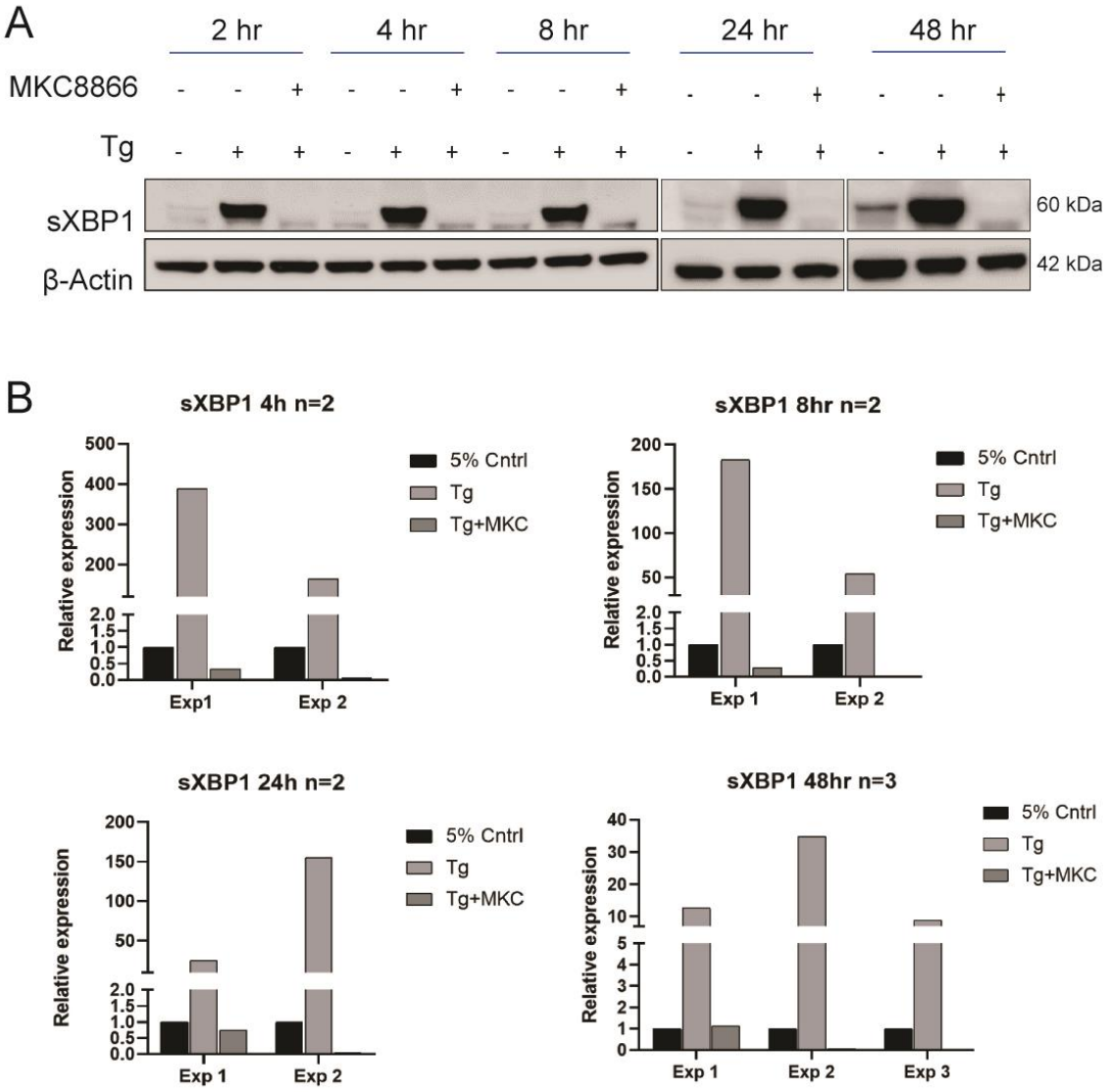

Figure 3.2 IRE1 RNase activation is strongly induced by thapsigargin in MDA-BR cells

MDA-BR cells were treated with thapsigargin (Tg) (5nM), +/- MKC8866 (10μM) in 5% FBS media for the time points of 2h, 4h, 8h, 24h and 48h. The lysates were collected and loaded for SDS-PAGE for the detection of sXBP1. (A) Qualitative representation of sXBP1 expression showing an induction under Tg treatment and it is inhibited by MKC8866. (B) Quantitative protein expression of separate experiments was determined by densitometry using β-actin as reference.

3.2. Regulation of PERK activity under ER stress induced by serum starvation and thapsigargin

MDA-BR cells were treated with 5% FBS media, 0% FBS media, Tg and MKC8866 to determine how these treatments affected the PERK downstream protein of the UPR pathway. The lysates containing cellular proteins were collected and separated on SDS-PAGE to detect the downstream signaling proteins of IRE1α and PERK arms.

Under serum starvation induced stress, expression of sXBP1 was increased compared to the 5% FBS media control and MKC8866 treatment resulted in the inhibition of sXBP1 under stress (Figure 3.3A). We did not detect changes in the expression of P-JNK under serum starvation–induced ER stress or with MKC8866 treatment. P-JNK is expected to be activated by the IRE1 kinase activity under high ER stress conditions. We investigated the activity of the PERK arm of UPR in MDA-BR cells under both stress-inducing culture conditions. The PERK downstream effector protein eIF2α showed increased phosphorylation under serum starvation as detected with an antibody specific for P-eIF2α (Figure 3.3B, C). PERK kinase activity increased over time with serum starvation. Interestingly, the expression of P-eIF2α was further induced upon the inhibition of the IRE1α RNase arm for all the 3 time points observed. However, serum starvation consistently did not increase the protein expression of the selective translational target ATF4 and the ATF4 transcriptional target CHOP, which are both downstream executioners of the PERK-P-eIF2α pathway. It is worth mentioning that we consistently found basal protein levels for CHOP in MDA-BR cells cultured under normal media and serum-free media conditions (Figure 3.3 B, E).

In contrast to the results seen under serum starvation, a strong activation of the PERK arm was detected under treatment with Tg (Figure 3.4 A, B). Under short term Tg treatment for 2, 4 and 8 hours an upward shift in the molecular weight for PERK protein was observed that possibly reflects phosphorylation of PERK under Tg-induced ER stress. Tg treatment strongly induced the PERK downstream effectors ATF4 and CHOP and this was seen as early as 2 hours after Tg exposure. The simultaneous exposure to MKC8866 completely blocked IRE1 activity but did not influence PERK signaling as

shown by unaltered ATF4 and CHOP protein levels compared to respective Tg alone exposures (Figure 3.4 A, B). The IRE1α kinase activity was not activated as P-JNK protein levels remained unchanged at all time points measured (Figure 3.4 A). The PERK downstream mediators P-eIF2α, ATF4 and CHOP showed a marked increase in cellular levels under the induction of thapsigargin. This induction was not affected by MKC8866 treatment. Thus, Tg-induced ER stress strongly activated the PERK arm of UPR in MDA-BR cells.

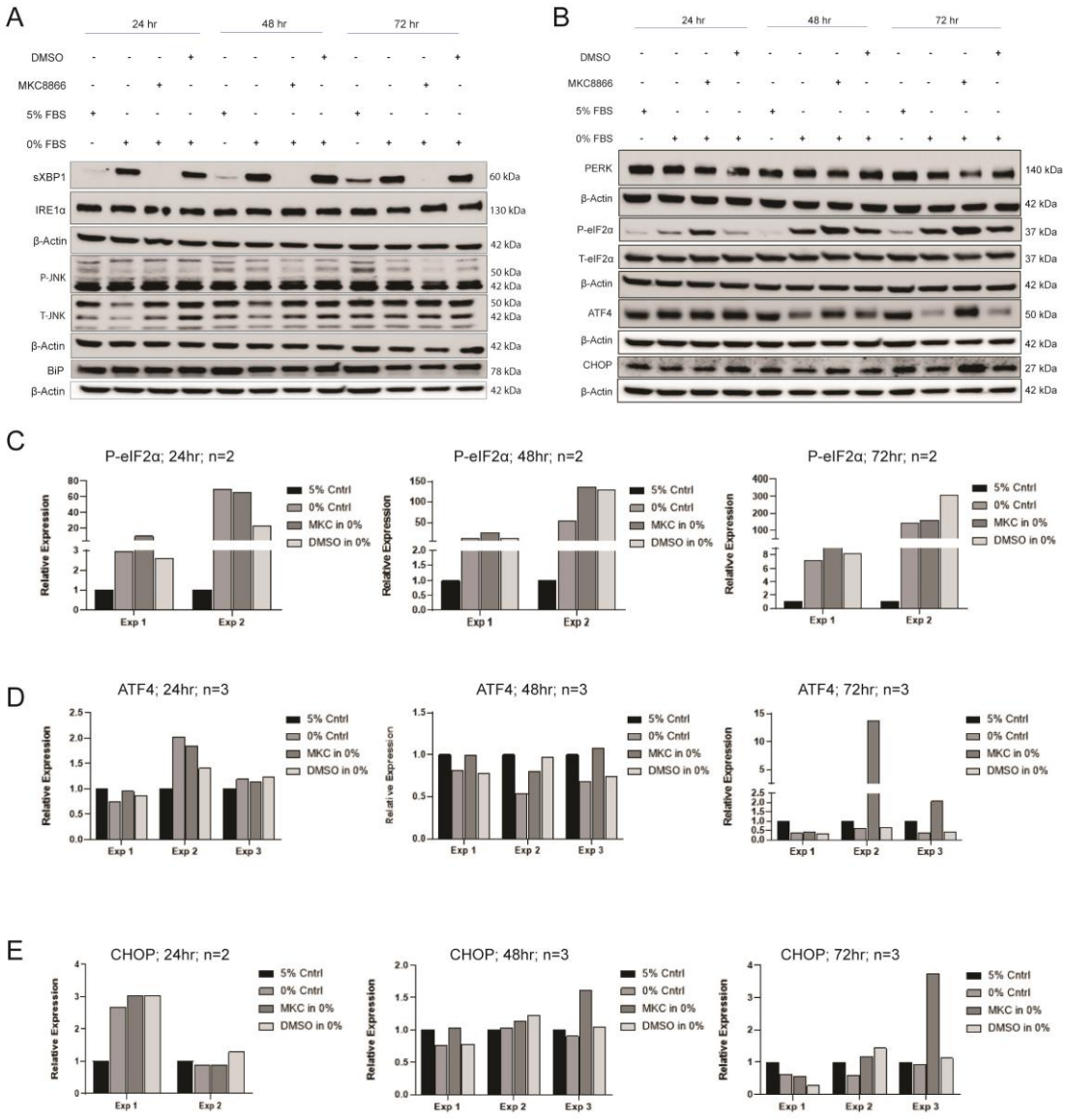

Figure 3.3 Serum starvation does not increase PERK activity or IREα kinase activity

MDA-BR cells were treated in 0% FBS media, +/- MKC8866 (10μM) for a period of 24h, 48h and 72h. DMSO serves as solvent control and 5% FBS as complete media control The lysates were collected and loaded for SDS-PAGE. IRE1 downstream proteins: IRE1α, P-JNK, T-JNK and PERK downstream proteins: P-eIF2α, T- eIF2α, ATF4 and CHOP were detected by Western blot. (A) Qualitative representation of the IRE1α kinase target protein. (B) Representative Western blot of the PERK downstream proteins. (C, D, E) Quantitative protein expression for P-eIF2α, ATF4 and CHOP from separate experiments was determined by densitometry using beta-actin as reference.

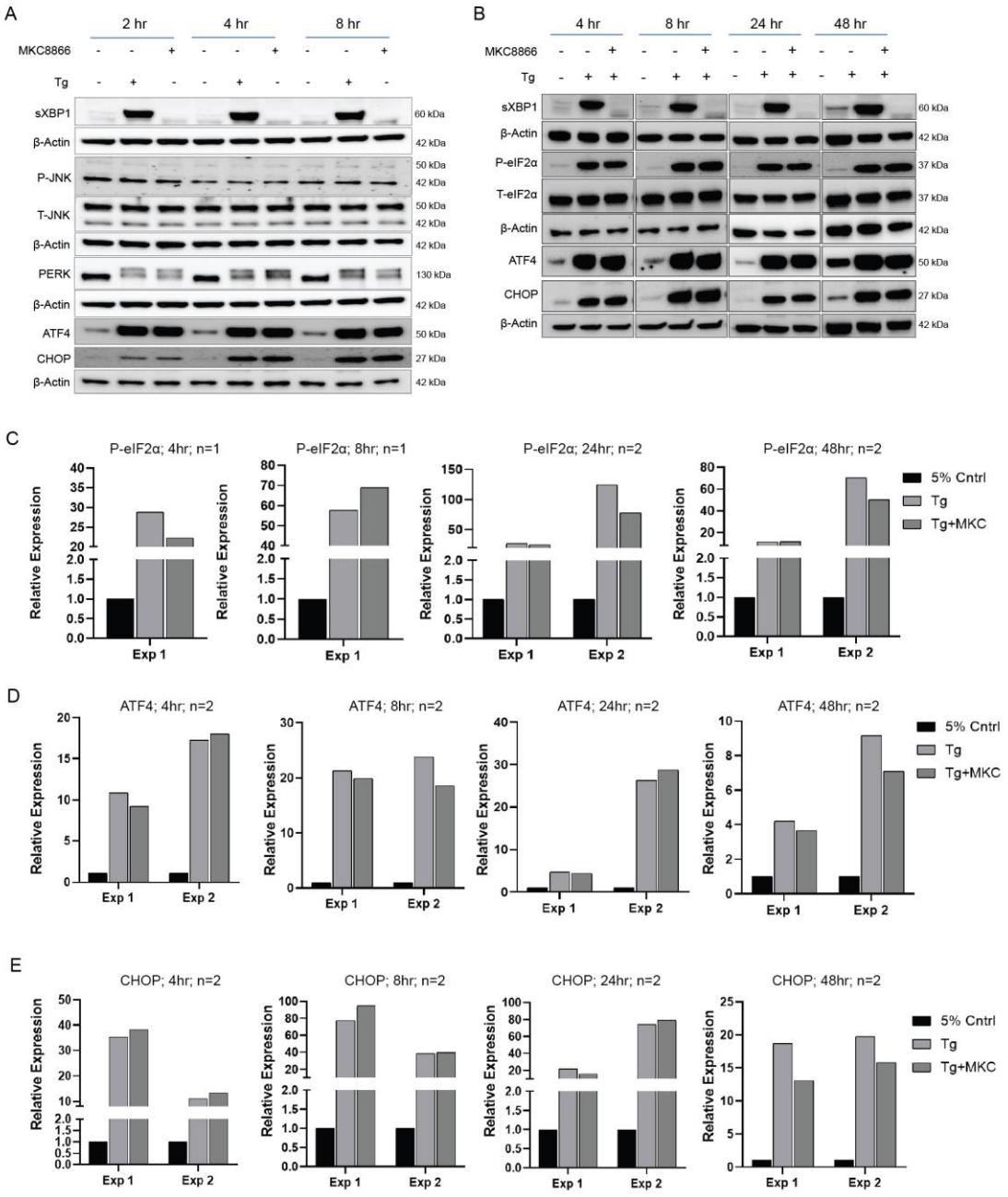

Figure 3.4 Thapsigargin treatment activates the PERK arm but not the IRE1α kinase

MDA-BR cells were treated with thapsigargin (5nM) +/- MKC8866 (10μM) for the time periods of 2h, 4h, 8h, 24h and 48h with 5% FBS as media control. The lysates were collected and loaded for SDS-PAGE. PERK downstream proteins P-eIf2α, T-eIF2 α, ATF4 and CHOP showed an induction under treatment with Tg which was unaffected by RNAse inhibition. (A, B) Representative Western blot of P-JNK, T-JNK, P-eIF2α, ATF4 and CHOP expression. (C, D, E) Quantitative protein expression of the P-eIf2α, ATF4 and CHOP proteins.

3.3. ER stress induction differentially affects viability of MDA-BR cells

Cell viability experiments on MDA-BRs cell was carried out to determine the cytotoxic effect of the different stress conditions and inhibitor treatments. The WST assay for cell viability is based on the NAD(P)H-dependent cleavage of the tetrazolium salt WST-1 to formazan by cellular mitochondrial dehydrogenases. The amount of formazan dye formed in this reaction is directly proportional to the activity of mitochondrial dehydrogensases and thus, it depends on viable cells.

The measurements in the treated samples were compared to the respective controls. Serum starvation alone did not reduce MDA-BR cell viability over 24, 48 and 72 hours. Although not consistently detected, the addition of MKC8866 at 10 µM reduced mitochondrial dehydrogenase activity at 48 and 72 hours under serum starvation-induced ER stress compared to the respective control (Figure 3.5 A). In contrast, under induction of ER stress by Tg treatment, a decrease in cell viability was observed under Tg treatment alone after 48 hours compared to the 5% FBS medium contrtrols and DMSO solvent control samples. The simultaneous treatment of Tg and MKC8866 showed a significant reduction in cell viability at 24 and 48 hours (Figure 3.6 A). This indicated that the cells were struggling to remain viable or to survive.

To further assess the viability of MDA-BR cells under the different treatments, real time cell analysis was performed using the xCelligence system. Changes in the electrical impedance were measured and reported as cell index on the Y-axis of the graph. The cell index decreased rapidly to almost 0 after the addition of Tg treatment at 20 hours. This indicated that the cells were either dying due to stress or getting detached from the chamber resulting in the decrease in impedance (Figure 3.7) In contrast, the cells treated with serum starvation steadily increased the cell index values. Treatment of MKC8866 neither reduced the cell index in MDA-BR cells under serum starvation, nor did it prevent the decline in cell index upon Tg exposure. Thus, inhibition of IRE1α did not influence the cell index measurements.

The reduced viability and cell index value of MDA-BR cells under Tg treatment indicated that the cells may experience apoptosis. In addition to this, the WB data (Figure 3.4) also showed that pro-apoptotic marker CHOP was also induced under Tg treatment. The caspase 3/7 assay was performed on the cells under Tg treatment (Figure 3.8 A) to determine whether the treatment was inducing apoptosis. The results indicated that there was a significant decrease in caspase activity at 24 hours under the treatment of both Tg and MKC8866 compared to the respective control. However, an increase was observed at 48 hours after normalizing the caspase 3/7 readout to the total cell count (Figure 3.8 A). Under the treatment of serum starvation, a loss of caspase activity was observed at 48 hours under the inhibition of MKC8866 (Figure 3.8 B). These results confirmed that under higher time incubation with Tg, the cells become pro-apoptotic in contrast to serum starved conditions.

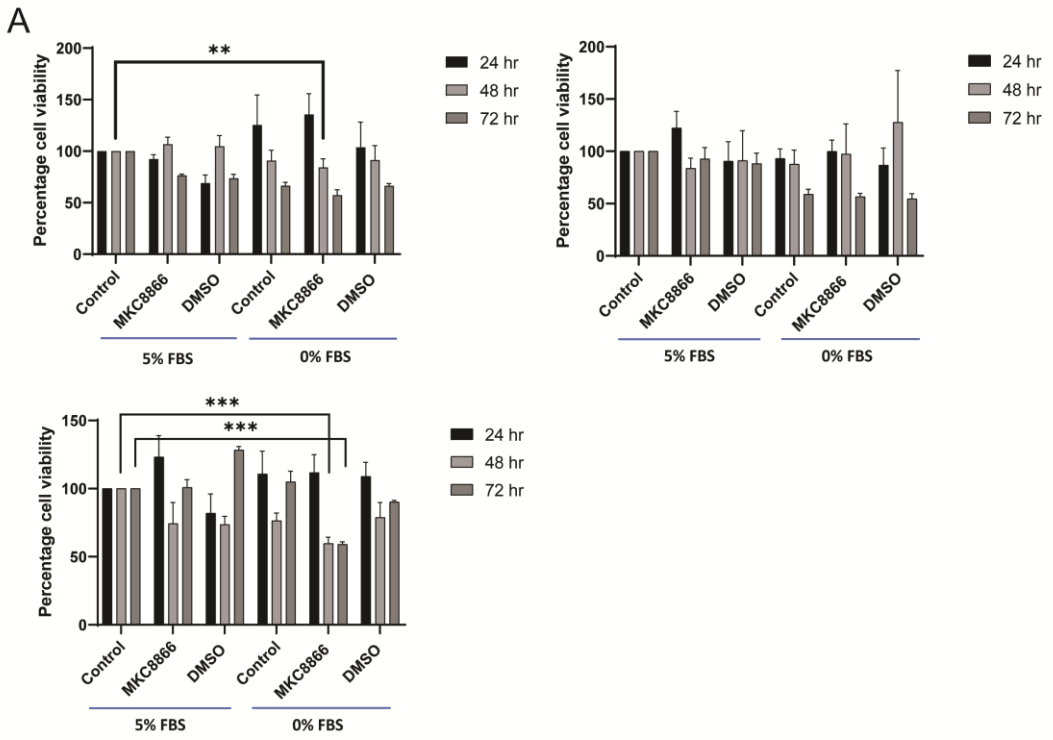

Figure 3.5 Serum starvation does not affect viability of MDA BR cells
MDA-BR cells were treated with 5% FBS and 0% FBS media, +/- MKC8866 and DMSO control for time periods of 24h, 48h and 72h. (A) Quantitative representation of 3 independent experiments showing that viability loss is significant for treatment of MKC8866 under serum starvation after 72 h. Statistical analysis was done with two-way ANOVA, multiple comparison, p**<0.01, p***<0.001. The comparison was made to the 5% FBS control of each time point. The 5% FBS control was set to 100 % for each time point.

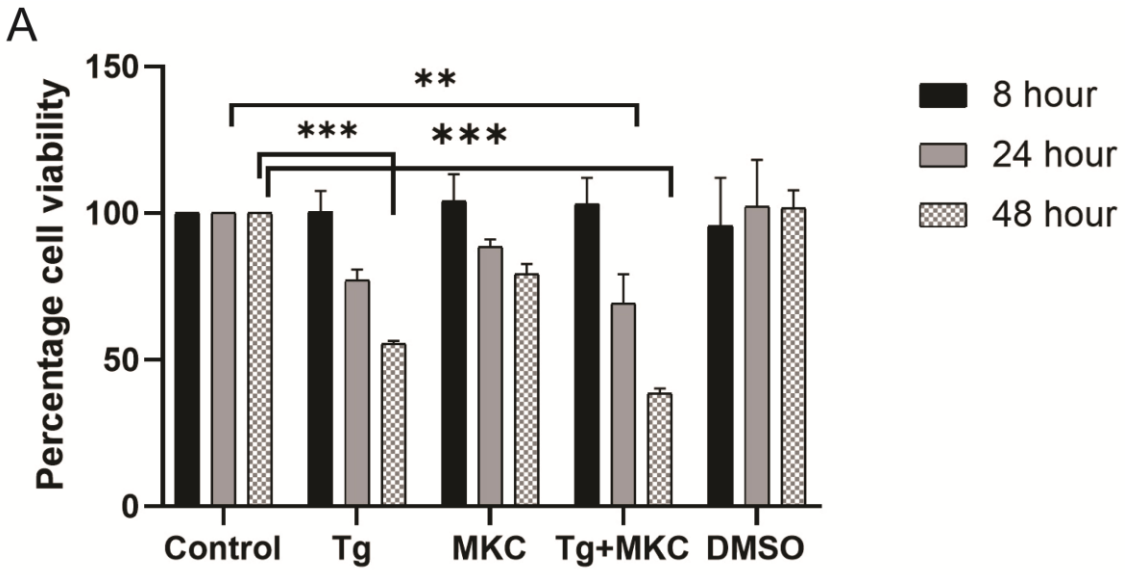

Figure 3.6 Thapsigargin induced ER stress reduces viability of MDA-BR cells
MDA-BR cells were treated with 5% FBS media, thapsigargin (5nM), +/- MKC8866 for time periods of 8h, 24h and 48h. (A) Quantitative representation of cell viability under thapsigargin induced stress condition showing that viability of cells under thapsigargin and thapsigargin +MKC8866 decrease at 24h and 48h time points. Statistical analysis was done using two-way Anova, multiple comparisons p**<0.01, p***<0.001. The comparison was made to the respective control of each time point.

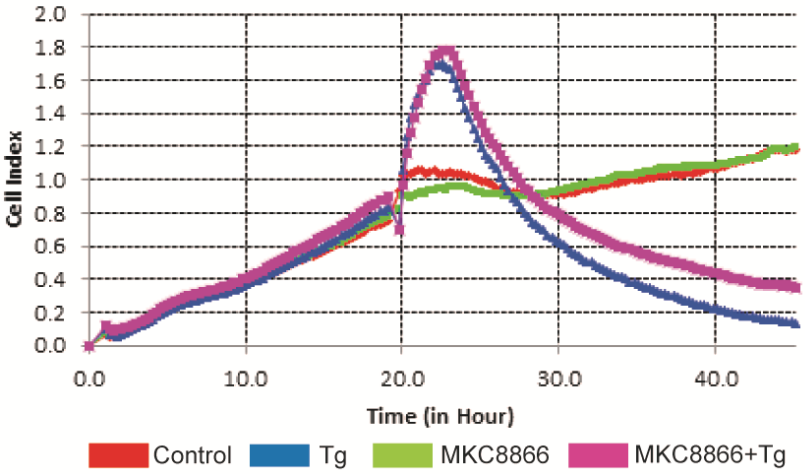

Figure 3.7 Impedance measurements confirm differential response to both ER stress inducing conditions
MDA-BR cells were seeded in E-plate and the impedance was measured to determine the viability of cells under treatment with 5% FBS, thapsigargin (2nM) +/- MKC8866 and 0% FBS +/- MKC8866. The cells were observed within a period of 48h. Treatment with thapsigargin alone and thapsigargin +MKC8866 shows reduced viability after 20h whereas the cells under 0% FBS treatment maintain their viability for 48h. Analysis was performed using the Xcelligence software. This experiment was performed in collaboration with Dr. Glogowska.

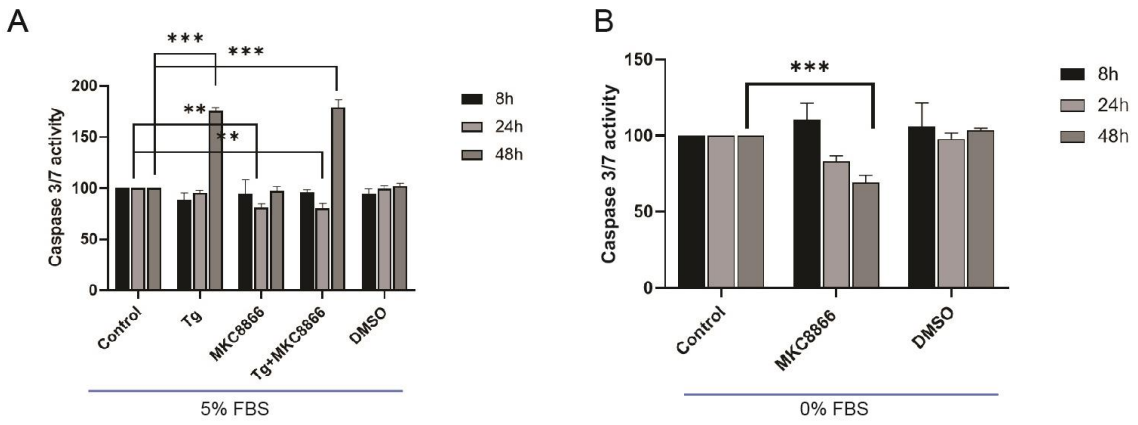

Figure 3.8 Induction of ER stress by thapsigargin induces apoptosis
A caspase-3/7 activity assay was performed to determine cell apoptosis. MDA-BR cells were seeded in 96 well plate and allowed to attach overnight. The following day treatments were added: (A) 5% FBS media containing 5nM Tg +/-MKC8866, media control and (B) 0% FBS media +/- MKC8866 for a period of 8h, 24h and 48h. The luminescence was measured in the plate reader to determine the caspase-3/7 activity. Each treatment had n=3 repeats, the statistical analysis was done using two-way ANOVA, multiple comparison p**<0.01, p***<0.001.

3.4. XBP1 knockdown in MDA-BR cells increases P-eIf2α

To provide an alternative mechanism to investigate the IRE1-sXBP1 pathway, stable MDA-BR cell clones were established in which XBP1 can be silenced by doxycyclin-induced XBP1 shRNA induction. The MDA-BR cells were transduced with shXBP1 lentiviral particles and selected with the antibiotic puromycin (3 µg/ml) (Figure 3.9) Viable and proliferating clones were isolated after two weeks of selective pressure in puromycin containing media. The selected clones were treated with and without doxycycline (2 µg/ml) for 5 days and lysates were collected. Successful silencing of XBP1 was confirmed by the lack of sXBP1 detection in Western blot. Selected clones showed knockdown of sXBP1 under doxycycline treatment (Figure 3.10A). The expression of P-eIf2α under knockdown of XBP1 was detected. Similar to the result under inhibition of RNase arm using MKC8866, the shRNA-induced XBP1 knockdown also showed an increase in the expression of P-eIf2α for all of the selected clones (Figure 3.10A). shXBP1 clones 02 and 03 were tested for the downstream proteins of PERK under doxycycline induced XBP1 silencing (Figure 3.10B). The results showed that under XBP1 knockdown an increase in P-eIf2α was noticed however, the expression of

ATF4 and CHOP which are downstream of P-eIf2α did not show any change. This result is similar to unaltered protein levels for ATF4 and CHOP under serum starvation in MDA-BR cells. This suggested that downregulation of XBP1 alone leads to increased phosphorylation of eIf2α, but does not increase the PERK downstream cascade.

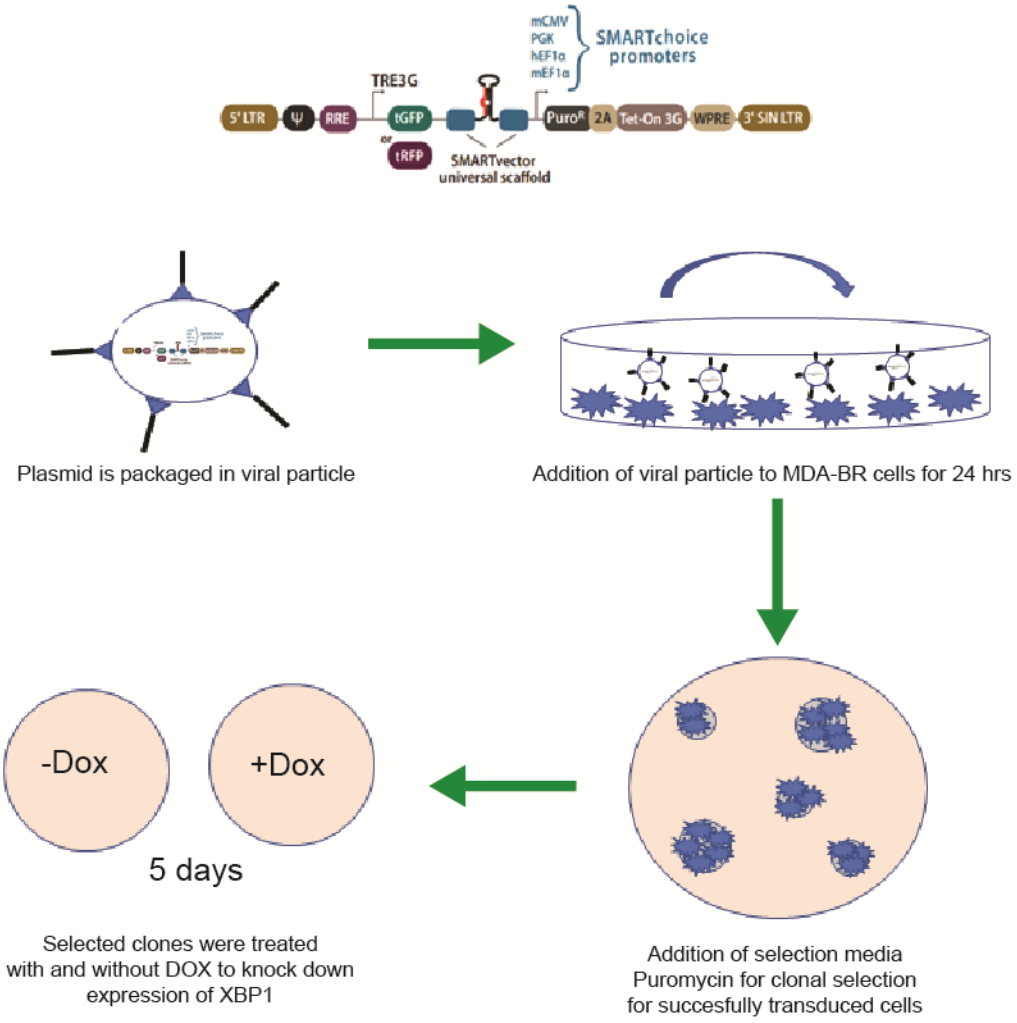

Figure 3.9 Establishing stable clones of MDA-BR with inducible shRNA for XBP1

The plasmid construct encodes for a doxycycline-inducible XBP1 shRNA. It encodes for the resistance to puromycin and upon DOX induction expresses RFP. The plasmid was packaged in lentiviral particles used to transduce the MDA-BR cells for 24h. Following transduction, puromycin (3µg/ml) selective media was added to the cells to select the cells with successful transduction. The clones were picked and tested for shXBP induction by treatment with DOX (2µg/ml) for 5 days.

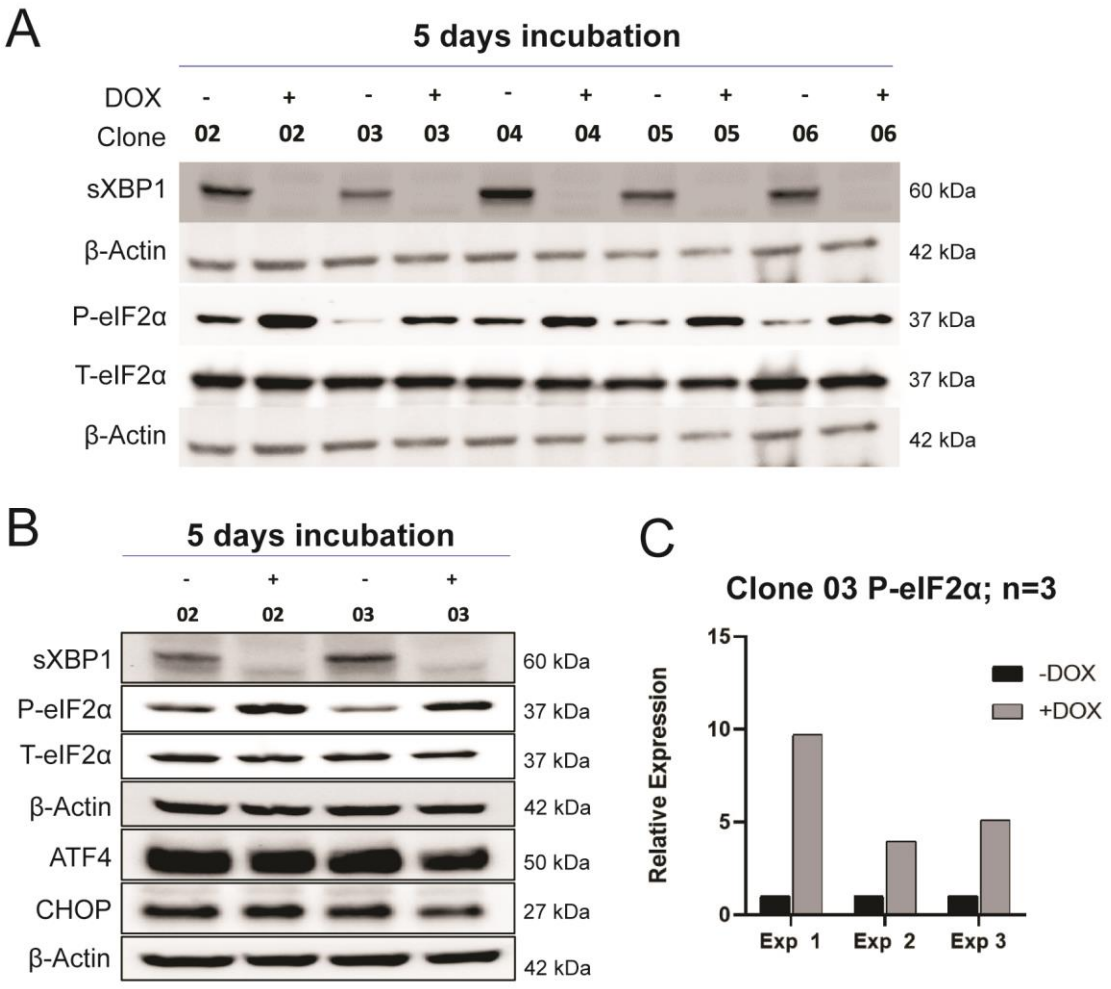

Figure 3.10 Doxycycline downregulates sXBP1 protein and induces P-eIf2α in MDA-BR clones

MDA-BR/shXBP1 clones were treated +/- DOX (2µg/ml) for 5 days. The lysates were collected and loaded for SDS-PAGE. sXBP1 and P-eIF2α were detected. (A) Representative Western blot of six different MDA-BR/shXBP1 clones showed that Dox treatment abolished sXBP protein. Levels of P-eIF2α were elevated with Dox treatment (B) The increase in P-eIF2α was not accompanied by changes in ATF4 and CHOP under DOX treatment (C) Quantitative protein expression for P-eIF2α from 3 independent experiments was determined by densitometry using beta-actin as reference.

3.5. The effect of IRE1α RNase on the migration of MDA-BR cells

To determine whether the inhibition of IRE1α RNase activity affects the migration of MDA-BR cells through brain endothelial monolayers a filter-based 2-chamber migration assay was performed using two cell models: MDA-BR and immortalized mouse brain endothelial cell line, bEnd3 cells which is often used for BBB

studies (247). The bEnd3 cells were seeded at a density of 14,000 cells/ml on rat-tail collagen coated 0.8µM fluoroblok inserts and cultured in complete endothelial media to grow to a confluent monolayer (247) (Figure 3.11). MDA-BR cells were seeded at a density of 50,000 cells per insert onto the endothelial layer in the top chamber and incubated for 24 hours with and without 10µM MKC8866. MDA-BR cells stably express GFP and the GFP fluorescence can be detected within the FITC channel from the bottom of the fluoroblok filter without interference from GFP signals from the filter top. The results showed that under IRE1α RNase inhibition, the migration of MDA-BR cells was significantly reduced compared to the migration in the solvent control (Figure 3.11).

To understand whether the inhibitor treatment was having an effect on the migratory abilities of the MDA-BR cells, real time cell migration assays were performed using the xCelligence RTCA system and CIM migration plates (Figure 3.12). The CIM plate represents an electronic Boyden chamber where the cells are seeded in upper chamber on top of microporous membrane, through which the cells pass to the lower chamber and deposit on gold impedance electrodes. The electrodes are responsible for producing sensitive and reproducible continuous readout of cell migration. The MDA-BR cells were treated with and without 10 µM MKC8866 and allowed to migrate through the membrane. Cell migration was measured by detection of impedance changes over a time period of 20 hours following inhibitor treatments. The measured impedance data points showed that the IRE1α inhibitor did not affect the migration ability of the MDA-BR cells.

To investigate if the inhibitor-mediated blocking of the IRE1α splicing activity contributed to the reduced MDA-BR transendothelial migration, the shXBP1 clones were used to perform the transmigration assay using bEnd3 cell monolayers and collagen coated 0.8µM fluoroblok inserts as described above (Figure 3.13A). The shXBP1 clones 2 and 3 were treated with and without DOX for 5 days before they were seeded on top of the endothelial cells at density of 14,000 cells/ml. The media on the upper chamber of the insert contained 0% FBS media with and without DOX while the bottom chamber contained 5% FBS media with and without DOX. The cells were incubated for 24- and 48- hours. Corresponding Western blot analysis was performed with cellular lysates from parallel cultures to confirm the downregulation of sXBP1 in the Dox-treated clones

(Figure 3.13B). Although clone 03 showed a trend for reduced transendothelial MDA-BR migration under DOX treatment for the two time points 24 h and 48 h, this was not a significant and consistent finding as the trend for reduction in DOX-treated MDA-BR migration was observed only for the 24 hour time period in subsequent experiments. Despite the successful DOX-mediated downregulation of sXBP1 in MDA-BR clone 02, this clone did not show any change in transendothelial migration (Figure 3.13A). Therefore, the transendothelial migration experiments with the XBP1 silencing model did not consistently confirm the results obtained with the IRE1 RNase inhibitor.

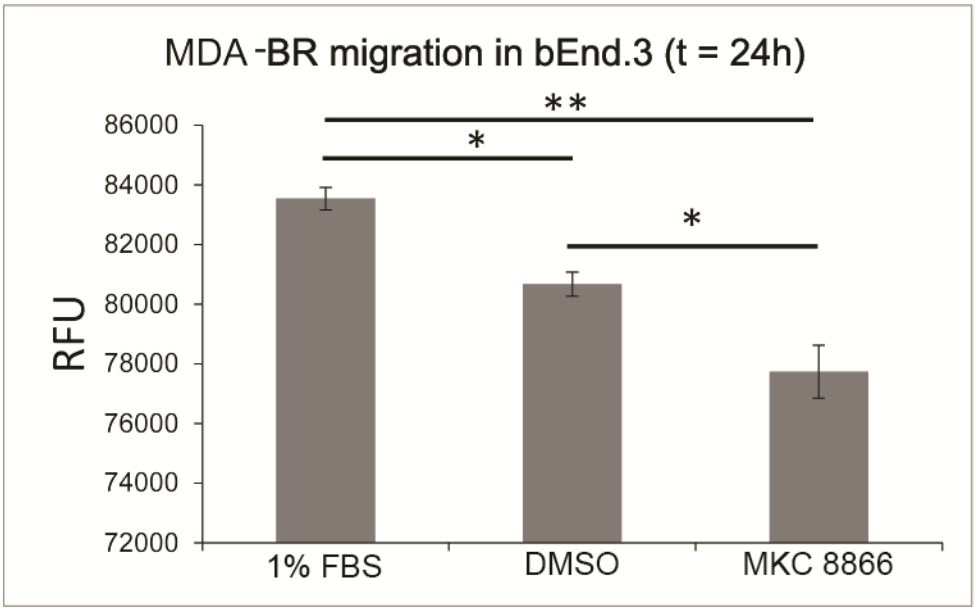

Figure 3.11 Inhibition of IRE1α RNase reduces transendothelial migration of MDA-BR through endothelial barriers

Endothelial bEnd3 cells were seeded on top of collagen coated 0.8µM fluoroblok filters in transwell plates and grown to full confluency for 5 days in complete endothelial media. MDA-BR cells were seeded on top of the endothelial cell at density of 50,000 cells per insert. The upper chamber contained 0% FBS media +/- MKC8866 while the lower chamber contained 1%FBS media +/- MKC8866. The cells were allowed to migrate for 24h. GFP +ve MDA-BR cells were detected on the lower side of the insert using a plate reader and the relative fluorescence unit (RFU) was measured. The statistical analysis was performed using one-way ANOVA with Tukey's multiple comparisons test. p*<0.05, p**<0.01. This experiment was performed in collaboration with Dr. Miller.

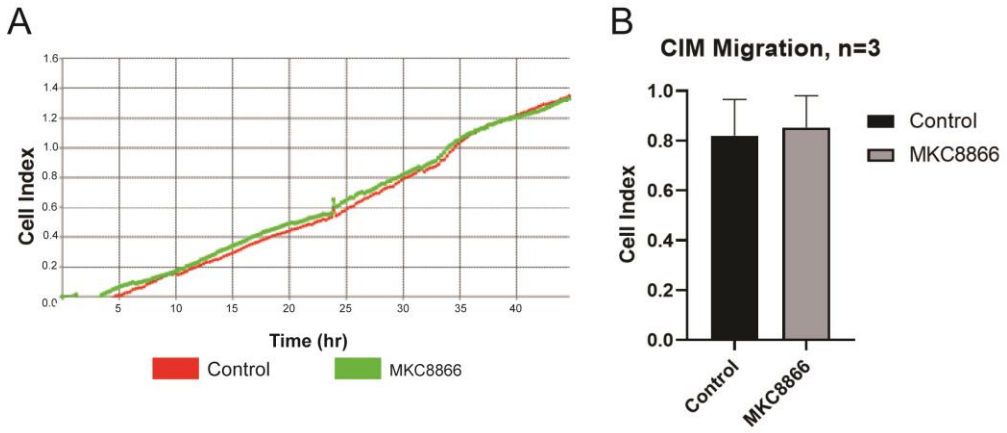

Figure 3.12 IRE1α inhibition alone does not affect the migration capability of MDA-BR cells

Cell migration was done in real time using the xCelligence system. MDA-BR cells were seeded on CIM plates and treated with and without MKC8866 (10µM) in 1% FBS media over a period of 48 hours. The data shows that the cell migration capability is not changed under the inhibition of IRE1α RNAse activity. Data acquisition and analysis were performed with the RTCA software. (A) A representative example of three independent experiments is shown are shown in the graphs for 24 h and 48 h. (B) Quantification analysis of 3 independent experiments performed. These experiments were performed in collaboration with Dr. Aleksandra Glogowska.

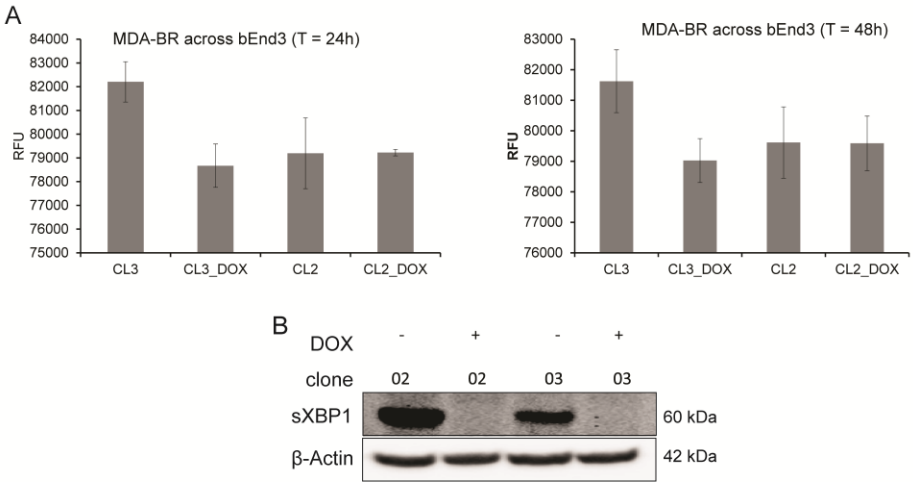

Figure 3.13 Silencing XBP1 in MDA-BR cells does not consistently reduce transendothelial migration

The bEnd3 endothelial cells were seeded on top of collagen coated FluoroBlok filter and grown to full confluency over 5 days in complete endothelial media. shXBP1-BR clone 02 and 03 were treated +/- DOX (2µg/ml) for 5 days. The clones were seeded at density of 50,000 cells on top of the endothelial monolayer in each insert. The upper chamber contained 0% FBS media +/- DOX and the bottom chamber contained 5% FBS media +/- DOX. The GFP+ve signal on the bottom side of insert was detected using plate reader at 24h and 48h. (A) Quantitative analysis of the relative fluorescence units (RFU) after subtraction of media background. Statistical analysis using one way ANOVA with Tukey's multiple comparisons test did not show any significance in the result. (B) Western blot detecting sXBP1 confirming the Dox-induced XBP1 silencing in the clones.

3.6. Effect of MDA-BR conditioned media on brain endothelial cells

Human immortalized brain endothelial cells hCMEC/D3 were used to determine how endothelial cells were affected by supernatants from MDA-BR cells. The viability of the endothelial cells under treatment with conditioned media (CM) from MDA-BR was determined to see if MDA-BR secreted factors could change endothelial cell viability as one potential cause for the MDA-BR transendothelial migration in our 2-chamber assays (Figure 3.14). MDA-BR cells were cultured with 0% FBS media with and without MKC8866 (10 μM) to induce IRE1α activity and block IRE1α RNAse for 48 hours. The CM was collected, centrifuged at 2.5 rpm for 5 minutes to remove any cells from the supernatant. The CM was added to the endothelial cells at100% and 50% for 24-hour, 48 hour and 72 hours and viability was quantified using WST assays. The viability of the hCMEC/D3 endothelial cells was not significantly affected by the CM from MDA-BR cells compared to media and solvent controls (Figure 3.14).

Brain endothelial cell tight junctional proteins are an important component of the barrier function. To assess if secreted factors from MDA-BR cells could affect the expression of major junctional protein in the brain endothelial cells we investigated the expression of claudin 5, claudin 3 and occludin in hCMEC/D3 cells following exposure to MDA-BR CM (Figure 3.15). Conditioned media from MDA-BR cells was collected as described above. The endothelial cells hCMEC/D3 were treated with the CM for 24 hours and the RNA was extracted using the Trizol extraction method. qPCR was performed to determine potential transcriptional changes of the junctional proteins. The results showed no significant changes for claudin 3 and claudin 5 gene expression upon exposure to CM from serum starved and MKC8866 treated MDA-BR cells. Interestingly, the occludin expression levels increased upon exposure of hCMEC/D3 cells to CM from serum-starved MDA-BR cells. CM from MKC8866 treated MDA-BR cells caused an increase in occluding expression and this increase was pronounced under exposure to CM from serum-starved MDA-BR (Figure 3.15).

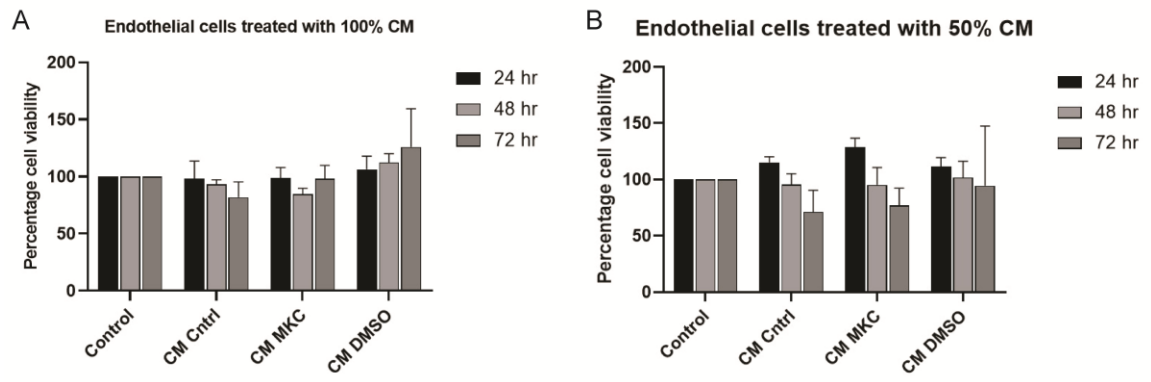

Figure 3.14 Viability of endothelial cells is not affected when treated with MDA-BR conditioned media

Endothelial cells, hCMEC/D3, were seeded in 96 well plate and exposed to conditioned media from MDA-BR cells for 24h, 48h and 72h. Conditioned media (CM) were collected from MDA-BR cells grown in serum-free media +/- MKC8866 (10 µM) and DMSO control for 48h. (A) WST cell viability assays were performed to assess cell viability and values from untreated controls were set to 100%. Quantitative analysis from 3 experiments shows that the viability is not affected by the treatment with conditioned media from MDA-BR cells.

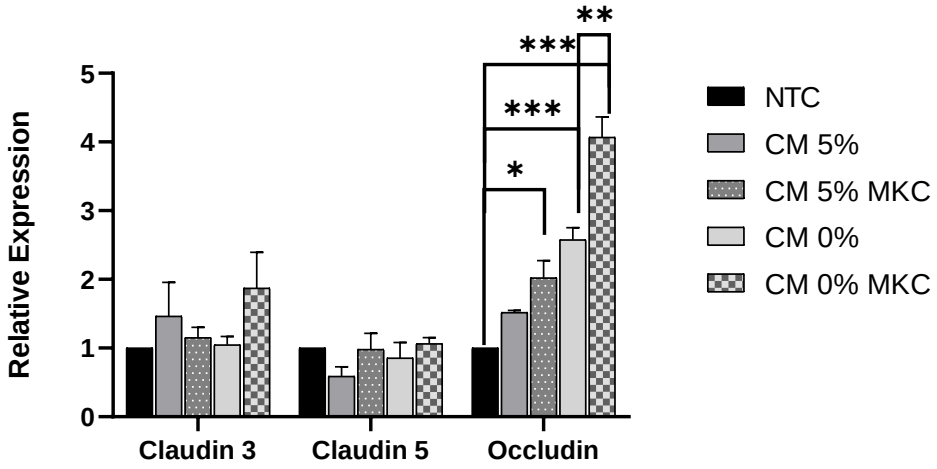

Figure 3.15 MDA-BR conditioned media differentially affect endothelilal cell junctional protein expression

MDA-BR cells were treated with 5% FBS media +/- MKC8866 (10 µM) and 0% FBS media +/- MKC8866 (10 µM) for 48 hours. hCMEC/d3 cells were grown to full confluency in complete endothelial media. MDA-BR conditioned media (CM) were added to hCMEC/D3 cells for 24h and changes in the gene expression levels for claudin 5, 3 and occluding were quantified by qPCR. The expression of occludin was induced under exposure to CM from serum-starved and MKC8866 treated MDA-BR cells. Statistical analysis two-way ANOVA, multiple comparisons was performed. p*<0.05, p**<0.01, p***<0.001.

3.7. ER stress conditions alter pro-angiogenic MDA-BR secreted cytokines

A cytokine analysis was performed to detect secreted chemokines/cytokines released by the MDA-BR cells when treated with different stress condition and MKC8866 inhibitor. For drug-induced ER stress, the cells were treated with Tg (5nM) and Tg (5nM) with MKC8866 (10μM) for 48 hours in 5% FBS containing media. For serum starvation-induced ER stress induction, MDA-BR cells were cultured in 0% FBS media with and without MKC8866 (10 μM) for 72 hours, after which the CM was collected. The culture supernatant was purified and concentrated using Amicon Ultra centrifuge filters and equal protein amounts for each sample were sent for cytokine array analysis by Eve technologies for the HD48 array. The results were reviewed and two cytokines were selected for this work based on the following criteria: (1) protein levels >50 pg/ml in the control sample and (2) having a known role in angiogenesis: VEGF-A and IL-6. VEGF plays an important role in stimulating angiogenesis by inducing proliferation and migration of endothelial cells but also signals in tumor cells (248). The analysis showed that for both experiments, the secretion of VEGF by MDA-BR cells was markedly higher in serum starvation treatment than in Tg-mediated ER stress induction (Figure 3.16 A). However, the ER stress-induced increased secretion of VEGF-A was not markedly changed upon MKC8866 inhibition.

IL-6 is a pro-inflammatory cytokine responsible for regulating proliferation, apoptosis, metabolism, survival, angiogenesis, and metastasis (249) Our analysis showed that secretion of IL-6 markedly increased under both Tg treatment and 0% FBS treatment (Figure 3.17 A). In contrast to the observed VEGF secretion, addition of MKC8866 lead to a reduction in the levels of secreted IL-6 under both, Tg-induced and serum starvation-induced ER stress indicating that the secretion of IL-6 might be IRE1α RNase dependent.

To assess if the reduced IL-6 secretion observed under MKC8866 treatment was related to the cellular levels of sXBP1 we used MDA-BR/shXBP1 clones 2 and 3 to determine secreted cytokines under treatment with and without DOX for 5 days to silence

XBP1 expression in MDA-BR cells. The cytokine analysis was performed on these culture supernatants (Figure 3.16 B, 3.17 B). The levels of secreted IL-6 were similar for both clones and were not found regulated by DOX treatment of MDA-BR cells. Interestingly, the levels of secreted VEGF-A were six times higher in MDA-BR/shXBP1 clone 02 than in clone 03. DOX treatment did not make a difference for the secretion of VEGF-A and IL-6 in both clones. The secretion of IL-6 was found to be three times higher in MDA-BR/shXBP1 clone 3 compared to parental MDA-BR cells and the MDA-BR/shXBP1 clone 2.

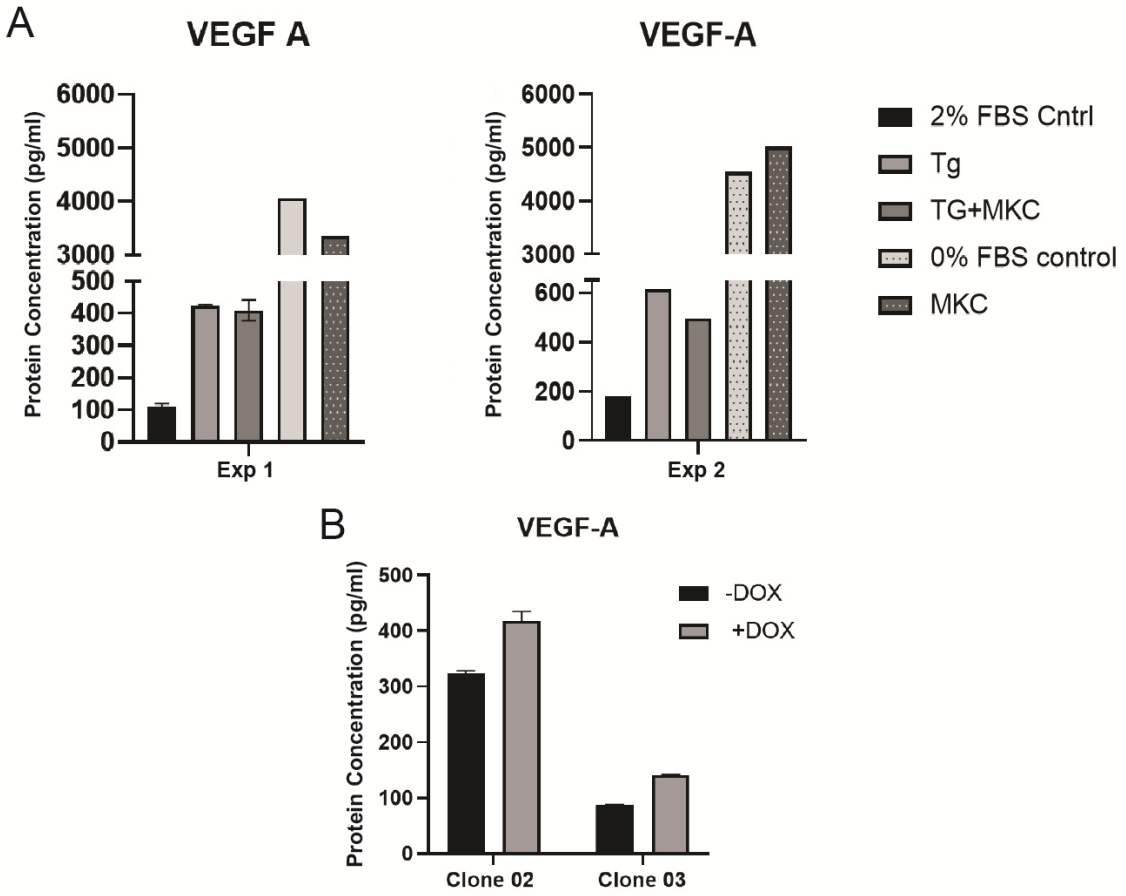

Figure 3.16 Secretion of VEGF-A
MDA-BR cells were treated with 5% FBS media containing thapsigargin (5 nM) , thapsigargin and MKC8866 (10 µM) for 48h and 0% FBS media +/- MKC8866 (10 µM) for 72h. shXBP1 clone 02 and 03 were treated with +/- DOX (2µg/ml) for 5 days. The supernatant was collected and concentrated using Amicon 2ml centrifuging column for cytokine analysis. (A) The concentration of VEGF-A secreted by MDA-BR cells are shown from 2 independent experiments. (B) The concentration Quantitative analysis of VEGF-A secreted by MDA-BR/shXBP-1 clones is shown.

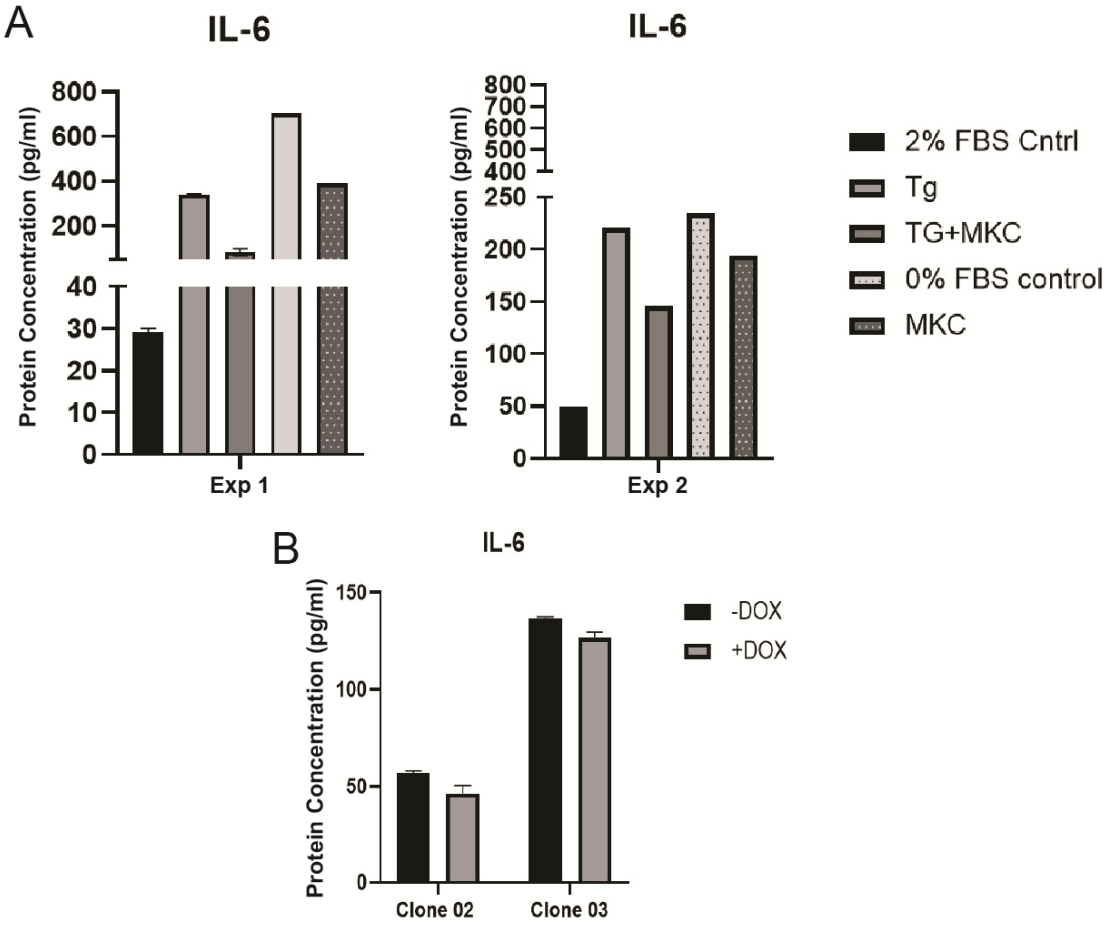

Figure 3.17 Secretion of IL-6
MDA-BR cells were treated with 5% FBS media containing thapsigargin (5 nM) , thapsigargin and MKC8866 (10 µM) for 48h and 0% FBS media +/- MKC8866 (10 µM) for 72h. shXBP1 clone 02 and 03 were treated with +/- DOX (2 µg/ml) for 5 days. The supernatant was collected and concentrated using Amicon 2ml centrifuging column for cytokine analysis. (A) The concentration of IL-6 secreted by MDA-BR cells are shown from 2 independent experiments. (B) The concentration Quantitative analysis of IL-6 secreted by MDA-BR/shXBP-1 clones is shown.

3.8. Thrombospondin-1 is regulated under ER stress in brain metastasizing breast cancer cells

Thrombospondin-1 has been associated with tumor invasion and migration, adhesion as well as proliferation. A previous aptamer-based proteomic (SomaLogic) analysis performed in the Hombach lab revealed that THSP1 is expressed in MDA-BR cells and it was found to be upregulated by treatment with thapsigargin. To validate these

proteomic results MDA-BR cells were cultured with 2% FBS medium +/- Tg treatment to induce ER stress and cell lysates and culture supernatants were probed for THSP-1 expression by Western blot (WB). Protein expression for THSP-1 in MDA-BR cells was confirmed by WB (Figure 3.18 A, B). We also confirmed the induction of cellular THSP-1 protein levels upon treatment with Tg for different time points (Figure 3.18A). Treatment with MKC8866 failed to reduce the Tg-induced THSP-1 indicating an IRE1α RNase independent ER stress pathway to upregulate THSP-1 expression. (Figure 3.18 A, B). Serum starvation-induced ER stress did not increase cellular levels of THSP-1 (Figure 3.18B). Corresponding culture supernatants from MDA-BR cells were collected and proteins were subjected to Western blot analysis to detect secreted thrombospondin-1(Figure 3.18B). Interestingly, the amounts of secreted thrombospondin-1 detected by WB was higher in serum starved MDA-BR cells compared to samples treated with Tg to induce ER stress. It was observed that the secreted THSP-1 under serum starvation had a slightly higher molecular weight than 150 kDa compared to the expression in Tg induced samples.

Since MKC8866 did not affect the protein expression of Tg-induced thrombospondin-1 in MDA-BR cells, we tested the effect of AMG-44, a PERK kinase inhibitor, on THSP-1 protein levels (Figure 3.18A). Although AMG-44 successfully reduced the PERK downstream intermediate P-eif2α it did not have an effect on THSP-1 levels. Thrombospondin-1 protein levels are increased under Tg-induced ER stress conditions, our data indicate that it is not regulated by IRE1α RNase or PERK arm of UPR.

A second cell model of brain metastatic breast cancer, PBS-94, was utilized to assess thrombospondin-1 expression. (Figure 3.19) PBS-94 are patient-derived cells initially isolated from the breast cancer brain metastasis of a patient diagnosed with HER2+ BC. Thrombospondin-1 was detected in both, cellular protein lysate of PBS-94 cells and the culture supernatant. ER stress induction by Tg and serum starvation was assessed by WB through increased sXBP1 protein levels. Similar to MDA-BR cells, PBS-94 cells responded to Tg-induced ER stress with a strong increase in thrombospondin-1 protein levels. MKC8866 treatment did not change Tg-induced THSP-

1 increase, similar to the results observed in MDA-BR cells. Secreted THSP-1 was also detected in the culture supernatants of serum starved PBS94 cells.

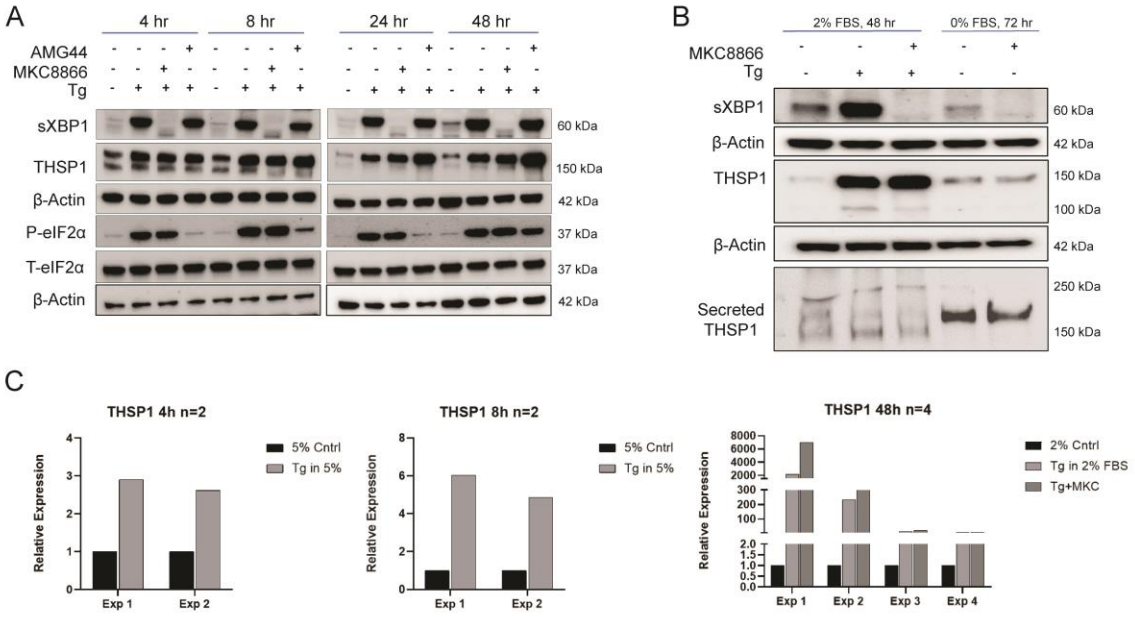

Figure 3.18 ER stress induction regulated thrombospondin-1 in MDA-BR cells
MDA-BR cells were treated with 5% FBS media containing thapsigargin (5 nM), thapsigargin and MKC8866 (10 µM) for 4h, 8h, 48h and 0% FBS media +/- MKC8866 (10 µM) for 72h. The supernatant and cell lysates were collected and loaded for SDS-PAGE. The expression of sXBP1 and **thrombospondin-1 (**THSP-1) was detected. (A) Thapsigargin increased the expression of THSP-1 protein, inhibition of RNase pr PERK activity does not affect the level of THSP-1. (B) Secreted THSP-1 was found at higher levels in serum starved conditions. Inhibition of RNase activity does not affect the level of THSP-1. (C) Quantitative protein expression for THSP-1 from separate experiments was determined by densitometry using beta-actin as reference.

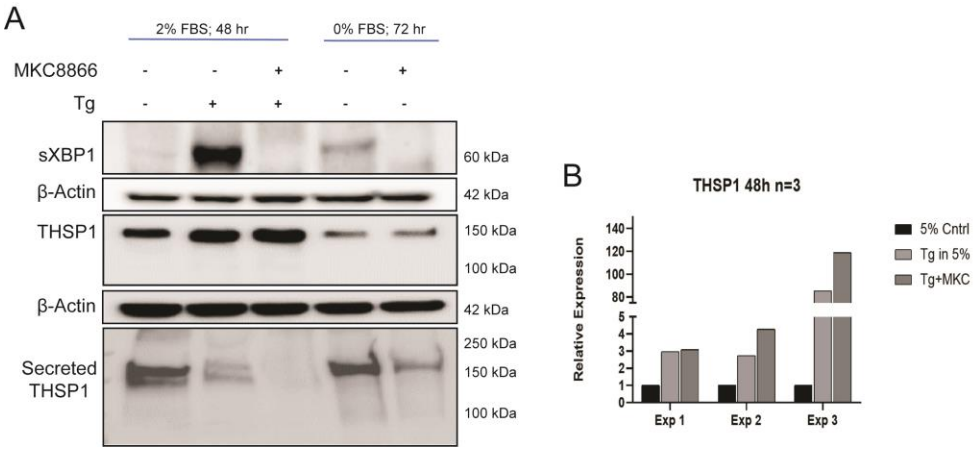

Figure 3.19 ER stress induction regulated thrombospondin-1 in PBS-94 cells
PBS-94 cells were treated with 5% FBS media containing thapsigargin (5 nM), thapsigargin and MKC8866 (10 µM) for 48h and 0% FBS media +/- MKC8866 (10 µM) for 72h. The supernatant

and cell lysates were collected and loaded for SDS-PAGE. The expression of sXBP1 and thrombospondin-1 **(**THSP-1) was detected. (A) Thapsigargin, increased the cellular levels of THSP-1 protein bot not its secretion. Secreted THSP-1 was found at high levels in serum starved conditions. Inhibition of RNase activity does not affect the level of cellular THSP-1. (B) Quantitative protein expression for THSP-1 from separate experiments was determined by densitometry using beta-actin as reference.

3.9. *In vivo* pilot study of XBP1 silencing in MDA-BR on survival of mice

A pilot *in vivo* study was performed using the DOX inducible MDA-BR/shXBP1clone 3 and 2 in two separate experiments. The aim of these *in vivo* pilot experiments was to get an initial assessment of the effect of XBP-1 silencing on the ability of MDA-BR cells to form brain metastasis. The following experiments were performed:

Experiment 1: Mice intracardially injected with MDA-BR/shXBP-1 clone 3 cells were administered DOX through drinking water at a concentration of 2 mg/ml ad libitum. Mice were monitored 3 times per week or daily if signed of illness appeared, such as weight loss, ruffled fur, decreased activity or limb paralysis. The endpoint chart showed that the mice reached humane endpoint within 2 weeks after xenografting (Figure 3.20 A) and there was no difference in survival of mice between the control and DOX treated groups.(Figure 3.20 C) Western blot detection of sXBP1 confirmed that clone 3 upon treatment with DOX *in vitro* prior to xenografting showed knockdown of sXBP1. (Figure 3.20 B)

Experiment 2: Prior to intracardial xenografting of MDA-BR/shXBP-1 clone 2, the cells were treated with DOX for 5 days prior to the intracardial injection. The DOX was administered to the mice in the form of chow. The concentration of DOX in the chow was designed to deliver a daily dose of 2-3 mg based on consumption of 4-5g/day by a mouse. Mice were monitored for humane endpoints as described. The endpoint chart for mice xenografted with MDA-BR/shXBP1 clone 2 showed that the overall survival time was more than two weeks (Figure 3.20 A) but the survival curve does not show any difference in survival between the DOX treated and non-treated mice (Figure 3.20 C). The western blot for sXBP1 confirmed that the cells injected in the mice had

successful knockdown of XBP1 when it was injected in the mice. (Figure 3.20 B) The H&E stain of mouse brain sections do not show any gross histological difference between DOX treated and non-treated mouse.

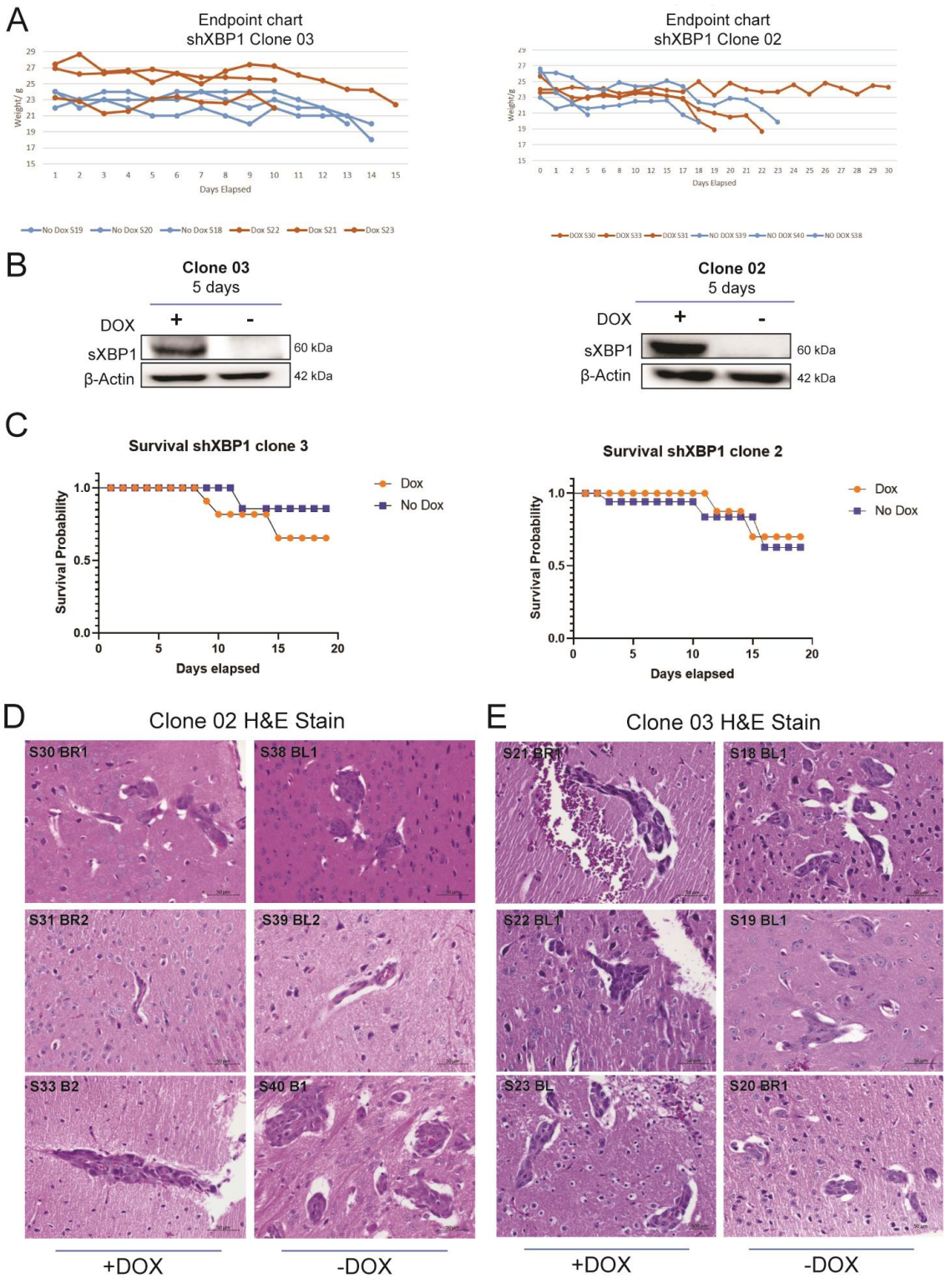

Figure 3.20 ***In vivo*** **pilot study of XBP1 silencing in MDA-BR on survival of mice**
MDA-BR/shXBP1 clones 03 and 02 were intracardially xenografted in mice and mice were treated with DOX to knockdown the expression of XBP1 in the MDA-BR breast cancer cells. The mouse weight and physical signs were monitored. (A) The weight chart of mice injected with

MDA-BR/shXBP1 clone 03 and treated with DOX in drinking water until humane endpoints were reached. The mice injected with clone 3 and treated with DOX were S21, 22, 23 and control mice were S18, 19, 20. The weight chart of mice injected with MDA-BR/shXBP1 clone 02 and treated with DOX in chow until humane endpoints were reached. The mice injected with clone 02 and treated with DOX were S30, 31, 33 and control mice were S38, 39, 40. (B) Qualitative expression of sXBP1 to show that the cells knockdown sXBP1 after treatment with DOX *in vitro* for clone 03 and clone 02 (C) Survival chart of mice injected with clone 02 pre-treated with DOX prior to injection and treated with DOX in chow after injection and survival chart of mice injected with clone 03 and treated with DOX in drinking water (D and E) H&E staining of metastatic lesions in mice brain collected from mice after euthanization shows no difference in histology among the DOX treated versus non treated mice brain tissues.

Chapter 4. Discussion

4.1. ER stressors differentially affect MDA-BR cells

The study of how ER stress and UPR affects signaling within a cell *in vitro* requires the use of various types of stressors. Such studies help understand disease progression due to ER stress. It has recently been demonstrated that TNBC cell lines in culture have a high expression of basal ER stress present compared to other types of BC (225). This makes the study of identifying the role of UPR in TNBC important as a potential therapeutic target. In this study two different stressors were employed to understand how the UPR regulates signaling upon induction of ER stress: (i) the chemical inducer Thapsigargin and (ii) Serum starvation, which acted as a physiological stressor for cells. Thapsigargin is a chemical inhibitor of SERCA pumps. The function of SERCA pumps is to transport Ca^{2+} ions from the cytoplasm to the lumen of the ER. Inhibition of SERCA pumps by Thapsigargin leads to an increase in Ca^{2+} in the cytoplasm and depletion of Ca^{2+} in the ER, which disrupts the function of chaperones to properly fold proteins resulting in ER stress and stress-induced apoptosis depending on the level of stress (250). However, in the tumor microenvironment, stress is induced from microenvironmental conditions such as nutrient deprivation, hypoxia, low pH or cell intrinsic metabolic alterations such as accumulation of reactive oxygen species (251). In order to mimic the stress present in tumor microenvironment, serum starvation was used as a physiological stressor by treating the cells with 0% FBS media leading to nutrient deprivation in cells. As serum starvation is a milder stress compared to thapsigargin treatment, this allowed us to observe the cells for longer incubation periods compared to that of thapsigargin. The activation of UPR by the different stress inducers was investigated first. The results indicated that serum starvation and thapsigargin treated cells exhibit different responses with respect to the timing and the extend of involvement of the two UPR pathways we investigated: IRE1α and PERK.

Various studies have shown that IRE1 arm is an important pro-survival arm of the UPR which is linked to tumor development and survival (225, 226). The level of stress present in the cell is indicated by the expression of IRE1 downstream protein sXBP1

which acts as a transcription factor in the nucleus to help with proper folding of proteins by promoting transcription of ER chaperones. In BC cells, sXBP1 also cooperate with other transcription factors such as HIF1a and regulate gene transcription in a cell-type specific manner. In this study RNase specific inhibitor called MKC8866 was used to selectively inhibit the RNase activity of IRE1 arm to prevent splicing of XBP1 and detect whether this leads to a change in BC cell migration. Both the stressors caused IRE1 activation as determined by sXBP1 expression. The basal sXBP1 levels were already increasing over time potentially due to nutrient reduction or signals from cells due to increasing confluency indicating that brain metastasizing BC cells readily activate the IRE1-XBP1 pathway. MKC8866 successfully and completely inhibited the basal and induced IRE1 RNase activity. To assess if the changes seen under the inhibition of MKC8866 was a result of splicing of XBP1, stable MDA-BR cell clones were generated for inducible silencing of XBP1 by shRNA.

Under serum starvation-mediated ER stress, the expression of sXBP1 was induced. Interestingly, it was identified that this treatment also induced the activation of PERK downstream protein P-eIF2α. Upon treatment of serum starved cells with an RNase inhibitor, MKC8866, sXBP1 levels were inhibited but P-eIF2α level was further induced. Since MKC8866 was inhibiting both splicing of XBP1 and the RIDD activity of the RNase arm, it might be possible that the induction of P-eIF2α was caused by the inhibition of RIDD activity since the knockdown of XBP1 in shXBP1 clones also showed similar activation of P-eIF2α.

The expression of P-eIF2α downstream proteins, ATF4 and pro-apoptotic marker CHOP remained constant for the treatments. In fact, when XBP1 was knocked down in MDA-BR/shXBP1 clones, P-eIF2α expression was significantly induced while ATF4 and CHOP expression remained unaffected. Integrated stress response (ISR) is an evolutionary conserved signaling pathway which aids the cells to adapt to various environmental and pathological conditions such as proteostasis defect, nutrient deprivation, oxidative stress, hypoxia etc. by activating four kinases: PERK, GCN2, PKR and HRI (252). These four kinases converge together during stress to phosphorylate eIF2α to prevent translational initiation and upregulation of transcription factors which

aid in restoring homeostatic balance in ER. Hence, it is possible that the increase in P-eIF2α stemmed from the activation of PKR, GCN2 or HRI, which caused a translational halt to prevent entry of new peptides, thereby, allowing proper folding of the proteins within the ER to help the cells survive (252).

On the other hand, the stress induced by thapsigargin was much stronger compared to that of serum starvation and resulted in complete activation of the PERK arm downstream mediators beyond eIf2a: ATF4 and CHOP. Although, changes in PERK phosphorylation was not studied, but a double band with higher molecular weight in PERK WB was detected suggesting its activation. Contrary to what was observed in serum starved cells, MKC8866 did not significantly affect the expression of these proteins and the stress ultimately reduced cell viability, as seen by viability assays. Viability assays confirmed that cells remained viable under serum starvation, indicating that cells still survive under mild ER stress. On the other hand, an increase in CHOP expression and the reduced viability under Tg treatment indicated that Tg induced pro-apoptotic mechanisms in MDA-BR cells. To confirm this, the caspase 3/7 assay was performed on the cells under Tg treatment. The results indicated that at higher time point of 48 hours, MDA-BR cells exhibited high caspase 3/7 readout when normalized to the cell count in the same treatment. It was observed that the cells under Tg treatment had a morphological change where they rounded up and the cell count with trypan blue showed that the total number of cells was significantly less, compared to the control. The number of dead cells in the treated samples was not significant suggesting that the stress prevented proliferation of MDA-BR cells. This discrepancy in total cell number compared to control indicated that under Tg induced stress, MDA-BR cells have high caspase activity.

4.2. The IRE1-sXBP1 activity in MDA-BR migration

Recent studies suggest an emerging role of IRE1 RNase activity in modulating tumor cell growth and survival (225). However, the exact role played by IRE1 RNase activity in tumor cell transendothelial migration remains unknown. It was hypothesized that IRE1 influences migration of breast cancer cells through the brain endothelial layer

and identifying this role will make IRE1 a potential target towards breast cancer-brain metastasis treatment. Migration assays were performed using MDA-BR cells and endothelial cells in transwell assay to determine the effect of IRE1 RNase inhibition on migration of BC cells through the endothelial monolayer. The assay involved seeding the endothelial cells on collagen coated 8µm fluoroblock inserts and growing them in complete media until a monolayer was formed. Although endothelial barrier functionality has been demonstrated for this assay (253), the limitation of using this model was the lack of astrocytes and pericytes to enhance the barrier capability of endothelial cells (254). MDA-BR cells (GFP+ve) were added on top of the endothelial monolayer and the GFP signal on the lower side of the insert was detected using a plate reader. Upon MKC8866 treatment, there was a decrease in transendothelial migration of BC cells through the endothelial monolayer. In order to assess if the reduction in migration was an effect of IRE1-sXBP1 signaling, transendothelial migration assay using the shXBP1-BR clones was performed. Interestingly, the knockdown of XBP1 did not show a consistent decrease in migration compared to the control. This indicated that the decrease in migration of the MDA-BR cells might not be solely dependent on splicing of XBP1. It is important to note that MKC8866 inhibits the whole RNase arm which includes both the RIDD activity and splicing of XBP1. However, in our clone model, addition of DOX was only knocking down XBP1 expression leaving RIDD activity unchanged. This suggested that the inhibitor might be affecting the migration of cells through RIDD activity or through a combination of sXBP1 reduction and inhibition of RIDD activity. Migration study using real time Cell-Xcelligence assay was performed to understand whether MKC8866 is affecting the migration capability of the MDA-BR cells. However, MDA-BR cells retained migration capability regardless of MKC8866 treatment indicating that MKC8866 did not directly affect MDA-BR migration ability. Hence, to identify why transendothelial migration of BC cells through the endothelial monolayer decreased upon MKC8866 treatment, the expression of TJ proteins in endothelial cells was studied. This was because, the permeability of BBB is primarily determined by the tight junctional complexes between the brain endothelial cells which comprises of claudin, occludin, and JAM (255). Claudin 5 is highly expressed and although claudin 3 is expressed at a lower level, it is constitutively expressed in brain EC (256) Occludin is responsible for

interaction with claudins and actin cytoskeleton, and regulating adhesion between cells (255). It was identified that when endothelial cells were treated with conditioned media from MDA-BR cells treated with MKC8866 and serum starvation, they exhibited a significant induction of the TJ protein Occludin transcriptional activity. The results indicated that, CM from MDA-BR cells treated with MKC8866 were influencing endothelial cells which might be due to the residual activity of MKC8866 in the CM. Data using the inhibitor on endothelial cell cultures suggested that there may be a direct effect on occludin gene expression by MKC8866. However, preliminary data showed that EC do not express basal level of stress nor was stress induced in the cells by treatment with CM treatment containing MKC8866 by WB detection. As a result it cannot be concluded whether MKC8866 has an off-target effect on the EC. Overall, these results indicated that while inhibition of IRE1 RNase activity by MKC8866 did not directly affect the migration of MDA-BR cells, the observed increased expression of Occludin under inhibition of IRE1 RNase activity may indicate that either EC were affected directly by MKC8866 or MKC8866 treatment changed secreted factors in MDA-BR cells that influenced endothelial barrier functions.

4.3. Secretion of inflammatory proteins by MDA-BR cells

Viability assays conducted on endothelial cells treated with conditioned media from MKC8866-treated MDA-BR cells revealed that viability in EC is not affected by CM exposure. Although RNase inhibition did not directly affect MDA-BR cell migration, there were a lot of potential factors that could contribute to their transendothelial migration. These factors included secreted proteins such as inflammatory cytokines which prompted us to perform a cytokine analysis of MDA-BR cell culture supernatants.

The culture supernatants of the MDA-BR cells treated with MKC8866 and the two ER stressors were analyzed to detect possible secreted products which might potentially affect the endothelial cells. The initial step of metastasis for BC cell, is arrest in thin capillaries where these cells reside for 3-7 days prior to which the cells extravasate through the vessel to the perivascular niche (79). Cancer cell survival within the capillaries is a very critical step that limits rate of brain metastasis. BC cells survive this

by adapting to the environment and activating signaling that protects them from immune system. After successful extravasation is complete, the key step for metastasis is the development of blood vessels to provide nutrients and oxygen for the developing tumor cells. MDA-BR cells grow by vascular co-option so that they are in constant contact with existing EC. Indicating that, not much additional angiogenesis in the early stage of brain metastasis is caused by these cells. The analysis of CM from MDA-BR cells showed increased levels of the proteins VEGF-A and IL-6. They can contribute to progression of BC through survival, proliferation and angiogenesis (257). TNBC expresses significantly high levels of VEGF in large tumors, metastatic lesions as well as in plasma of BC patients (258). The expression of VEGF correlates with poor prognosis and OS of patients (259). In a study using retinal cells, it was shown that expression of secreted VEGF was increased in cells under serum starved stress condition (260). Similarly, in our study it can be can see that the secretion of VEGF-A was induced under ER stressors Tg and serum serum starvation. However, the secretion was not regulated in an IRE1 RNase dependent manner. This was because MKC8866 treatment of MDA-BR cells did not change levels of secreted VEGF-A. Solid tumors secrete VEGF that binds to the VEGF receptor on the endothelial cell such as VEGFR1/VEGFR2 to induce formation of blood vessels and support the growing tumor by providing nutrients and oxygen (259). High expression of VEGF-A by the MDA-BR cells under serum starvation compared to thapsigargin treatment may indicate that the physiological stressor of serum starvation has a more profound impact on the ability to secrete VEGF and initiate angiogenesis. Due to the discrepancies in the secretion because of different stress induced treatments, it is important to design experiments under physiological stress conditions which mimic the tumor microenvironment. Hypoxia is another such stressor which can be tested and it is known to induce VEGF in TNBC (226). The cytokine analysis from MDA-BR shXBP1 clones showed that the basal levels of secreted VEGF-A did not show any change under DOX induced XBP1 silencing suggesting that sXBP1 was not essential for VEGF secretion.

THSP-1 is another protein with a known role in angiogenesis and metastasis that was upregulated in both BC cells: MDA-BR and PBS 94 due to ER stress. Its expression has previously been detected in MDA-MB-231 cells where it played an important role in

breast cancer invasion and metastasis (261). Fontana *et al.*, showed that THSP-1 dynamically regulated angiogenesis in MDA-231 cells (262). In this study, the expression of THSP-1 was induced under Tg treatment but did not increase the secreted protein in these cells. It has previously been established that different cellular THSP-1 levels resulted in stimulation of integrin α6 which in turn increased adhesion and migration properties of BC cells (263). This result is important for our study as it indicated that the high level of intercellular THSP-1 under Tg induction might affect cellular expression of proteins which can indirectly help BC cells to adhere to endothelial cells and migrate. After treating the MDA-BR cells with both IRE1 RNase inhibitor and PERK arm inhibitor it was observed that the regulation of THSP-1 was not dependent on either of these arms. Lynch *et al.* identified that THSP-1 has adaptive ER stress response through ATF6α regulation in rat cardiomyocytes (264) suggesting that the ATF6 arm might modulate the expression of THSP-1 in BC cells. In contrast to drug induced ER stress, serum starvation stress resulted in an increased secretion of THSP-1 further demonstrating that ER stressors differentially affect the cells. Secreted THSP-1 act as substrate for various cell surface receptors in the tumor microenvironment such as: CD36, CD47, calrecticulin which could be linked to its role in modulating brain EC phenotypes and may contribute to TEM.

THSP-1 also promotes tumor invasion by upregulating the formation of the enzyme plasmin that degrades the extracellular matrix and promotes tumor cells adhesion (265). Prolonged expression of THSP-1 by fibroblasts resulted in an increase in VEGF expression from tumor cells stimulating angiogenesis (262, 265). This shows that THSP-1 is an important modulator of angiogenesis, tumor growth and metastasis (266).

IL-6 is a critical regulator of pro-metastatic processes including cell invasion, cell migration and epithelial-to-mesenchymal transition (267, 268). The increased expression of IL-6 is an important cytokine in breast cancer metastasis as clinical studies of breast cancer patients had revealed an increase in circulating levels of IL-6 and increased chances of metastasis (269-271). Furthermore, in a study done on murine astrocyte it was shown that ER stress increased the level of IL-6 in a PERK dependent manner (272). By conducting cytokine analysis, it was detected that IL-6 was induced under both serum

starvation and thapsigargin which was subsequently reduced upon MKC8866 treatment, indicating that the secretion of IL-6 might be dependent on IRE1 RNase activity. This confirmed previously published data on the MDA-MB-231 parental cells by *Logue et al.* (225). In fact, when cytokine analysis was performed on shXBP1-BR clones, a similar trend was observed. This would indicate that RNase activity positively regulates IL-6 secretion in MDA-BR cells, potentially influencing cell migration.

4.4. *In vivo* experiment to determine the effect of downregulation of XBP1 on survival

To investigate whether the IRE1-XBP1 ER stress signaling affected brain metastasis, MDA-BR/shXBP1 clones, were injected to perform preliminary *in vivo* analysis. Two different pilot studies were designed: in the first study, shXBP1 clone 3 was injected into mice, after which, they were fed water containing DOX that knocked down XBP1. In the second study, shXBP1 clone 2 was DOX-treated for 5 days *in vitro* prior to injection in mice and the mice were fed with DOX-containing chow. During injection of shXBP1 clone 03, the cells were not pre-treated with DOX. Since the downregulation of XBP1 requires time under DOX treatment post injection, it provided the cancer cells enough time to migrate to the brain before XBP1 was knocked down. Therefore, clone 02 was pre-treated with DOX to ensure reduced sXBP1 before the cells get in contact with brain capillary endothelium upon injection. Despite these differences in technique, both the experiments showed no significant difference in the time for metastasis to become symptomatic. The micro-metastatic lesions in the brain also did not show any histological differences. This would suggest that XBP1 did not play a role in brain metastasis. However, there were several limitations to the pilot studies. Although the successful silencing of XBP1 under dox treatment was shown *in vitro* prior to xenografting, the reduction in sXBP1 after xenografting was not demonstrated. It is known that BC cells reside in brain capillaries for up to seven days before migrating through the endothelial layer (79). Thus, it is likely that strong ER stress induction and sub-optimal DOX concentrations may have resulted in increased sXBP1 levels *in vivo.* BiP was found to be increased in MDA-BR brain metastatic tissue lesions indicating ER stress to be present in TNBC cell. This indicated that the lack of sXBP1 detection in the

brain lesions most likely is related to lack of suitable antibody for FFPE tissues. Alternatively, an assay for the in-situ detection of sXBP1 mRNA by in-situ hybridization might be developed which will help to ensure the presence of sXBP1 in the brain metastatic lesions.

4.5. Conclusion and Significance

This study identified that both serum starvation and thapsigargin induced stress to modulate different responses in the MDA-BR cells which was inhibited by MKC8866. This showed that the nature of the ER stress inducing condition is critical for the investigation of the role of ER stress. Upon induction of ER stress the secretion of VEGF-A, IL-6 and THSP-1 were elevated. These proteins have the potential to indirectly affect the EC and increase TEM of BC cells. Finally, both *in vivo* survival data and *in vitro* data transendothelial migration data suggested that only splicing of XBP1 was not directly regulating the migration of MDA-BR cells rather inhibition of IRE1 RNase activity successfully reduced transmigration of BC cells. This signified that further studies regarding the RIDD activity of RNase arm is required to understand the mechanism of migration of MDA-BR cells.

4.6. Limitations and Future Directions

It is important to study the effect of different stressors in various cell line because ER stress is dependent on kind of cell used and stressor used. This project lacked the data of how the two stressors affected other BC cell types such as the parental MDA-231 cells. Based on the results, the role of RIDD activity in RNase arm was inconclusive and it was only speculated that RIDD activity could cause induction of P-eIf2α under serum starvation stress and induce migration of MDA-BR cells through EC monolayer. This limitation can be solved by performing experiments where the shXBP1 clone is treated with both DOX and MKC8866 and only DOX for migration study or WB analysis.

Few other approaches can also be taken to understand the *in vivo* mechanism of metastasis by the MDA-BR cells. The use of MKC8866 is limited as the compound is

known to cross the BBB only insufficiently. Other MKC derivatives may be developed in the future with better brain penetration capability that are compatible with *in vivo* treatments. Alternatively, mouse experiments could be designed to temporarily open the BBB just prior to intravenous administration of MKC8866. This would be a proof of principle experiment to show the effect of IRE1 RNase inhibition on the growth of BC brain metastatic lesions.

References

1. Public Health Agency of C, Statistics C, Canadian Cancer S, provincial/territorial cancer r. Release notice - Canadian Cancer Statistics 2019. Health Promot Chronic Dis Prev Can. 2019;39(8-9):255.
2. Brenner DR, Weir HK, Demers AA, Ellison LF, Louzado C, Shaw A, et al. Projected estimates of cancer in Canada in 2020. CMAJ. 2020;192(9):E199-E205.
3. Elenbaas B, Spirio L, Koerner F, Fleming MD, Zimonjic DB, Donaher JL, et al. Human breast cancer cells generated by oncogenic transformation of primary mammary epithelial cells. Genes & development. 2001;15(1):50-65.
4. Korde LA, Zujewski JA, Kamin L, Giordano S, Domchek S, Anderson WF, et al. Multidisciplinary meeting on male breast cancer: summary and research recommendations. Journal of Clinical Oncology. 2010;28(12):2114.
5. Sánchez-Muñoz A, Vicioso L, Santonja A, Álvarez M, Plata-Fernández Y, Miramón J, et al. Male breast cancer: correlation between immunohistochemical subtyping and PAM50 intrinsic subtypes, and the subsequent clinical outcomes. Modern Pathology. 2018;31(2):299-306.
6. Benson JR, Weaver DL, Mittra I, Hayashi M. The TNM staging system and breast cancer. Lancet Oncol. 2003;4(1):56-60.
7. Cserni G, Chmielik E, Cserni B, Tot T. The new TNM-based staging of breast cancer. Virchows Arch. 2018;472(5):697-703.
8. Robin Smithuis JdB, Anneke Zeillemaker. Staging and Treatment of Breast Cancer 2016 [Available from: https://radiologyassistant.nl/breast/breast-cancer/staging-and-treatment-of-breast-cancer.
9. R G, F dB, V M, MC R, F V, B B, et al. PDGFRβ(+) cells in human and experimental neuro-vascular dysplasia and seizures. Neuroscience. 2015;306.
10. Christgen M, Langer F, Kreipe H. [Histological grading of breast cancer]. Pathologe. 2016;37(4):328-36.
11. Soceity CC. Grading breast cancer [Available from: https://www.cancer.ca/en/cancer-information/cancer-type/breast/grading/?region=on.
12. Makki J. Diversity of Breast Carcinoma: Histological Subtypes and Clinical Relevance. Clin Med Insights Pathol. 2015;8:23-31.
13. Fabbri AC, Maria Luisa ; Carbone, Antonino. Histological Classification of Breast Cancer.
14. Rosai J.

Rosai and Ackerman's surgical pathology e-book.
15. Tsang JYS, Tse GM. Molecular Classification of Breast Cancer. Adv Anat Pathol. 2020;27(1):27-35.
16. Sorlie T, Perou CM, Tibshirani R, Aas T, Geisler S, Johnsen H, et al. Gene expression patterns of breast carcinomas distinguish tumor subclasses with clinical implications. Proc Natl Acad Sci U S A. 2001;98(19):10869-74.
17. Perou CM, Sorlie T, Eisen MB, van de Rijn M, Jeffrey SS, Rees CA, et al. Molecular portraits of human breast tumours. Nature. 2000;406(6797):747-52.
18. Sims AH, Howell A, Howell SJ, Clarke RB. Origins of breast cancer subtypes and therapeutic implications. Nat Clin Pract Oncol. 2007;4(9):516-25.

19. da Silva JL, Nunes NCC, Izetti P, de Mesquita GG, de Melo AC. Triple negative breast cancer: A thorough review of biomarkers. Critical reviews in oncology/hematology. 2020;145:102855.
20. Fougner C, Bergholtz H, Norum JH, Sørlie T. Re-definition of claudin-low as a breast cancer phenotype. Nature communications. 2020;11(1):1-11.
21. Herschkowitz JI, Simin K, Weigman VJ, Mikaelian I, Usary J, Hu Z, et al. Identification of conserved gene expression features between murine mammary carcinoma models and human breast tumors. Genome biology. 2007;8(5):1-17.
22. Chikarmane S, Tirumani S, Howard S, Jagannathan J, DiPiro P. Metastatic patterns of breast cancer subtypes: what radiologists should know in the era of personalized cancer medicine. Clinical radiology. 2015;70(1):1-10.
23. Yersal O, Barutca S. Biological subtypes of breast cancer: Prognostic and therapeutic implications. World J Clin Oncol. 2014;5(3):412-24.
24. Johnson KS, Conant EF, Soo MS. Molecular Subtypes of Breast Cancer: A Review for Breast Radiologists. Journal of Breast Imaging. 2020;3(1):12-24.
25. Sparano JA, Gray RJ, Makower DF, Pritchard KI, Albain KS, Hayes DF, et al. Adjuvant Chemotherapy Guided by a 21-Gene Expression Assay in Breast Cancer. N Engl J Med. 2018;379(2):111-21.
26. Vuong D, Simpson PT, Green B, Cummings MC, Lakhani SR. Molecular classification of breast cancer. Virchows Arch. 2014;465(1):1-14.
27. Sorlie T. Molecular portraits of breast cancer: tumour subtypes as distinct disease entities. Eur J Cancer. 2004;40(18):2667-75.
28. Loi S. Molecular analysis of hormone receptor positive (luminal) breast cancers: what have we learnt? Eur J Cancer. 2008;44(18):2813-8.
29. Rouzier R, Perou CM, Symmans WF, Ibrahim N, Cristofanilli M, Anderson K, et al. Breast cancer molecular subtypes respond differently to preoperative chemotherapy. Clinical cancer research. 2005;11(16):5678-85.
30. Bhargava R, Beriwal S, Dabbs DJ, Ozbek U, Soran A, Johnson RR, et al. Immunohistochemical surrogate markers of breast cancer molecular classes predicts response to neoadjuvant chemotherapy: a single institutional experience with 359 cases. Cancer: Interdisciplinary International Journal of the American Cancer Society. 2010;116(6):1431-9.
31. Ozlem Yersal SB. Biological subtypes of breast cancer: Prognostic and therapeutic implications. World Journal of Clinical Oncology. 2014 Aug 10.
32. Tsutsui S, Ohno S, Murakami S, Kataoka A, Kinoshita J, Hachitanda Y. Prognostic significance of the coexpression of p53 protein and c-erbB2 in breast cancer. Am J Surg. 2003;185(2):165-7.
33. Panoff J, Hurley J, Takita C, Reis I, Zhao W, Sujoy V, et al. Risk of locoregional recurrence by receptor status in breast cancer patients receiving modern systemic therapy and post-mastectomy radiation. Breast cancer research and treatment. 2011;128(3):899-906.
34. Gabos Z, Thoms J, Ghosh S, Hanson J, Deschênes J, Sabri S, et al. The association between biological subtype and locoregional recurrence in newly diagnosed breast cancer. Breast cancer research and treatment. 2010;124(1):187-94.

35. Kennecke H, Yerushalmi R, Woods R, Cheang MCU, Voduc D, Speers CH, et al. Metastatic behavior of breast cancer subtypes. Journal of clinical oncology. 2010;28(20):3271-7.
36. Gajria D, Chandarlapaty S. HER2-amplified breast cancer: mechanisms of trastuzumab resistance and novel targeted therapies. Expert review of anticancer therapy. 2011;11(2):263-75.
37. Carlsson J, Nordgren H, Sjöström J, Wester K, Villman K, Bengtsson NO, et al. HER2 expression in breast cancer primary tumours and corresponding metastases. Original data and literature review. British journal of cancer. 2004;90(12):2344-8.
38. Increased Rate of Brain Metastasis with Trastuzumab Therapy Not Associated with Impaired Survival. Clinical Breast Cancer. 2003;4(2):114-9.
39. Pernas S, Tolaney SM. HER2-positive breast cancer: new therapeutic frontiers and overcoming resistance. Therapeutic advances in medical oncology. 2019;11:1758835919833519.
40. Witzel I, Oliveira-Ferrer L, Pantel K, Muller V, Wikman H. Breast cancer brain metastases: biology and new clinical perspectives. Breast Cancer Res. 2016;18(1):8.
41. Mortimer JE, Kruper L, Cianfrocca M, Lavasani S, Liu S, Tank-Patel N, et al. Use of HER2-Directed Therapy in Metastatic Breast Cancer and How Community Physicians Collaborate to Improve Care. Journal of Clinical Medicine. 2020;9(6):1984.
42. Sims A, Zweemer AJ, Nagumo Y, Faratian D, Muir M, Dodds M, et al. Defining the molecular response to trastuzumab, pertuzumab and combination therapy in ovarian cancer. British journal of cancer. 2012;106(11):1779-89.
43. Prat A, Parker JS, Karginova O, Fan C, Livasy C, Herschkowitz JI, et al. Phenotypic and molecular characterization of the claudin-low intrinsic subtype of breast cancer. Breast cancer research. 2010;12(5):1-18.
44. Prat A, Adamo B, Cheang MC, Anders CK, Carey LA, Perou CM. Molecular characterization of basal-like and non-basal-like triple-negative breast cancer. The oncologist. 2013;18(2):123.
45. Pommier RM, Sanlaville A, Tonon L, Kielbassa J, Thomas E, Ferrari A, et al. Comprehensive characterization of claudin-low breast tumors reflects the impact of the cell-of-origin on cancer evolution. Nature communications. 2020;11(1):1-12.
46. Perou CM, Sørlie T, Eisen MB, Van De Rijn M, Jeffrey SS, Rees CA, et al. Molecular portraits of human breast tumours. nature. 2000;406(6797):747-52.
47. Ismail-Khan R, Bui MM. A review of triple-negative breast cancer. Cancer Control. 2010;17(3):173-6.
48. Dent R, Trudeau M, Pritchard KI, Hanna WM, Kahn HK, Sawka CA, et al. Triple-negative breast cancer: clinical features and patterns of recurrence. Clinical cancer research. 2007;13(15):4429-34.
49. Rakha EA, Reis-Filho JS, Ellis IO. Basal-Like Breast Cancer: A Critical Review. Journal of Clinical Oncology. 2008;26(15):2568-81.
50. Weigelt B, Baehner FL, Reis-Filho JS. The contribution of gene expression profiling to breast cancer classification, prognostication and prediction: a retrospective of the last decade. J Pathol. 2010;220(2):263-80.
51. Pistelli M, Pagliacci A, Battelli N, Santinelli A, Biscotti T, Ballatore Z, et al. Prognostic factors in early-stage triple-negative breast cancer: lessons and limits from clinical practice. Anticancer research. 2013;33(6):2737-42.

52. Dent R, Trudeau M, Pritchard KI, Hanna WM, Kahn HK, Sawka CA, et al. Triple-negative breast cancer: clinical features and patterns of recurrence. Clin Cancer Res. 2007;13(15 Pt 1):4429-34.
53. Zhang L, Hao C, Dong G, Tong Z. Analysis of Clinical Features and Outcome of 356 Triple-Negative Breast Cancer Patients in China. Breast Care (Basel). 2012;7(1):13-7.
54. Bostrom P, Soderstrom M, Palokangas T, Vahlberg T, Collan Y, Carpen O, et al. Analysis of cyclins A, B1, D1 and E in breast cancer in relation to tumour grade and other prognostic factors. BMC Res Notes. 2009;2:140.
55. Minn AJ, Gupta GP, Padua D, Bos P, Nguyen DX, Nuyten D, et al. Lung metastasis genes couple breast tumor size and metastatic spread. Proceedings of the National Academy of Sciences. 2007;104(16):6740-5.
56. Lin NU, Claus E, Sohl J, Razzak AR, Arnaout A, Winer EP. Sites of distant recurrence and clinical outcomes in patients with metastatic triple-negative breast cancer: high incidence of central nervous system metastases. Cancer. 2008;113(10):2638-45.
57. Yin L, Duan JJ, Bian XW, Yu SC. Triple-negative breast cancer molecular subtyping and treatment progress. Breast Cancer Res. 2020;22(1):61.
58. Lehmann BD, Bauer JA, Chen X, Sanders ME, Chakravarthy AB, Shyr Y, et al. Identification of human triple-negative breast cancer subtypes and preclinical models for selection of targeted therapies. The Journal of clinical investigation. 2011;121(7):2750-67.
59. Bianchini G, Balko JM, Mayer IA, Sanders ME, Gianni L. Triple-negative breast cancer: challenges and opportunities of a heterogeneous disease. Nat Rev Clin Oncol. 2016;13(11):674-90.
60. Lehmann BD, Pietenpol JA. Identification and use of biomarkers in treatment strategies for triple-negative breast cancer subtypes. The Journal of pathology. 2014;232(2):142-50.
61. Gibson GR, Qian D, Ku JK, Lai LL. Metaplastic breast cancer: clinical features and outcomes. The American surgeon. 2005;71(9):725-30.
62. Diana A, Franzese E, Centonze S, Carlino F, Della Corte CM, Ventriglia J, et al. Triple-Negative Breast Cancers: Systematic Review of the Literature on Molecular and Clinical Features with a Focus on Treatment with Innovative Drugs. Curr Oncol Rep. 2018;20(10):76.
63. Cheng X, Hung MC. Breast cancer brain metastases. Cancer Metastasis Rev. 2007;26(3-4):635-43.
64. Tabouret E, Chinot O, Metellus P, Tallet A, Viens P, Goncalves A. Recent trends in epidemiology of brain metastases: an overview. Anticancer research. 2012;32(11):4655-62.
65. Custodio-Santos T, Videira M, Brito MA. Brain metastasization of breast cancer. Biochim Biophys Acta Rev Cancer. 2017;1868(1):132-47.
66. Heitz F, Harter P, Lueck H-J, Fissler-Eckhoff A, Lorenz-Salehi F, Scheil-Bertram S, et al. Triple-negative and HER2-overexpressing breast cancers exhibit an elevated risk and an earlier occurrence of cerebral metastases. European journal of cancer. 2009;45(16):2792-8.
67. Nguyen DX, Bos PD, Massagué J. Metastasis: from dissemination to organ-specific colonization. Nature Reviews Cancer. 2009;9(4):274-84.

68. Huber MA, Kraut N, Beug H. Molecular requirements for epithelial-mesenchymal transition during tumor progression. Curr Opin Cell Biol. 2005;17(5):548-58.
69. Trimboli AJ, Fukino K, de Bruin A, Wei G, Shen L, Tanner SM, et al. Direct evidence for epithelial-mesenchymal transitions in breast cancer. Cancer Res. 2008;68(3):937-45.
70. Ikenouchi J, Matsuda M, Furuse M, Tsukita S. Regulation of tight junctions during the epithelium-mesenchyme transition: direct repression of the gene expression of claudins/occludin by Snail. J Cell Sci. 2003;116(Pt 10):1959-67.
71. Martin TA, Ye L, Sanders AJ, Lane J, Jiang WG. Cancer invasion and metastasis: molecular and cellular perspective. Madame Curie Bioscience Database [Internet]: Landes Bioscience; 2013.
72. Cano A, Perez-Moreno MA, Rodrigo I, Locascio A, Blanco MJ, del Barrio MG, et al. The transcription factor snail controls epithelial-mesenchymal transitions by repressing E-cadherin expression. Nat Cell Biol. 2000;2(2):76-83.
73. Medici D, Hay ED, Olsen BR. Snail and Slug promote epithelial-mesenchymal transition through β-catenin–T-cell factor-4-dependent expression of transforming growth factor-β3. Molecular biology of the cell. 2008;19(11):4875-87.
74. Seddiki R, Narayana G, Strale PO, Balcioglu HE, Peyret G, Yao M, et al. Force-dependent binding of vinculin to alpha-catenin regulates cell-cell contact stability and collective cell behavior. Mol Biol Cell. 2018;29(4):380-8.
75. Loh C-Y, Chai JY, Tang TF, Wong WF, Sethi G, Shanmugam MK, et al. The E-cadherin and N-cadherin switch in epithelial-to-mesenchymal transition: signaling, therapeutic implications, and challenges. Cells. 2019;8(10):1118.
76. Blanco MJ, Moreno-Bueno G, Sarrio D, Locascio A, Cano A, Palacios J, et al. Correlation of Snail expression with histological grade and lymph node status in breast carcinomas. Oncogene. 2002;21(20):3241-6.
77. Wang X, Lu H, Urvalek AM, Li T, Yu L, Lamar J, et al. KLF8 promotes human breast cancer cell invasion and metastasis by transcriptional activation of MMP9. Oncogene. 2011;30(16):1901-11.
78. Kim K, Marquez-Palencia M, Malladi S. Metastatic Latency, a Veiled Threat. Front Immunol. 2019;10:1836.
79. Lorger M, Felding-Habermann B. Capturing changes in the brain microenvironment during initial steps of breast cancer brain metastasis. Am J Pathol. 2010;176(6):2958-71.
80. Kienast Y, Von Baumgarten L, Fuhrmann M, Klinkert WE, Goldbrunner R, Herms J, et al. Real-time imaging reveals the single steps of brain metastasis formation. Nature medicine. 2010;16(1):116-22.
81. Carbonell WS, Ansorge O, Sibson N, Muschel R. The vascular basement membrane as "soil" in brain metastasis. PloS one. 2009;4(6):e5857.
82. Garcia-Gomez P, Valiente M. Vascular co-option in brain metastasis. Angiogenesis. 2020;23(1):3-8.
83. Kodack DP, Askoxylakis V, Ferraro GB, Fukumura D, Jain RK. Emerging strategies for treating brain metastases from breast cancer. Cancer cell. 2015;27(2):163-75.

84. Andrews DW. Should surgery followed by whole-brain radiation therapy be the standard treatment for single brain metastasis? Nature Clinical Practice Oncology. 2008;5(10):572-3.
85. Andrews DW, editor Current neurosurgical management of brain metastases. Seminars in oncology; 2008: Elsevier.
86. Frazier JL, Batra S, Kapor S, Vellimana A, Gandhi R, Carson KA, et al. Stereotactic radiosurgery in the management of brain metastases: an institutional retrospective analysis of survival. International Journal of Radiation Oncology* Biology* Physics. 2010;76(5):1486-92.
87. Golden DW, Lamborn KR, McDermott MW, Kunwar S, Wara WM, Nakamura JL, et al. Prognostic factors and grading systems for overall survival in patients treated with radiosurgery for brain metastases: variation by primary site. Journal of neurosurgery. 2008;109(Supplement):77-86.
88. Daneman R, Prat A. The blood-brain barrier. Cold Spring Harb Perspect Biol. 2015;7(1):a020412.
89. Persidsky Y, Ramirez SH, Haorah J, Kanmogne GD. Blood-brain barrier: structural components and function under physiologic and pathologic conditions. J Neuroimmune Pharmacol. 2006;1(3):223-36.
90. Heithoff BP, George KK, Phares AN, Zuidhoek IA, Munoz-Ballester C, Robel S. Astrocytes are necessary for blood–brain barrier maintenance in the adult mouse brain. Glia. 2021;69(2):436-72.
91. Guérit S, Fidan E, Macas J, Czupalla CJ, Figueiredo R, Vijikumar A, et al. Astrocyte-derived Wnt growth factors are required for endothelial blood-brain barrier maintenance. Progress in Neurobiology. 2021;199:101937.
92. Wang Y, Rattner A, Zhou Y, Williams J, Smallwood PM, Nathans J. Norrin/Frizzled4 signaling in retinal vascular development and blood brain barrier plasticity. Cell. 2012;151(6):1332-44.
93. Engelhardt B, Liebner S. Novel insights into the development and maintenance of the blood–brain barrier. Cell and tissue research. 2014;355(3):687-99.
94. Armulik A, Genové G, Mäe M, Nisancioglu MH, Wallgard E, Niaudet C, et al. Pericytes regulate the blood–brain barrier. Nature. 2010;468(7323):557-61.
95. Reese TS, Karnovsky MJ. Fine structural localization of a blood-brain barrier to exogenous peroxidase. J Cell Biol. 1967;34(1):207-17.
96. Betz AL, Goldstein GW. Polarity of the blood-brain barrier: neutral amino acid transport into isolated brain capillaries. Science. 1978;202(4364):225-7.
97. Betz AL, Firth JA, Goldstein GW. Polarity of the blood-brain barrier: distribution of enzymes between the luminal and antiluminal membranes of brain capillary endothelial cells. Brain Res. 1980;192(1):17-28.
98. Mittapalli RK, Manda VK, Adkins CE, Geldenhuys WJ, Lockman PR. Exploiting nutrient transporters at the blood–brain barrier to improve brain distribution of small molecules. Therapeutic delivery. 2010;1(6):775-84.
99. Löscher W, Potschka H. Blood-brain barrier active efflux transporters: ATP-binding cassette gene family. NeuroRx. 2005;2(1):86-98.
100. Kooij G, Van Horssen J, Bandaru VVR, Haughey NJ, De Vries HE. The role of ATP-binding cassette transporters in neuro-inflammation: relevance for bioactive lipids. Frontiers in pharmacology. 2012;3:74.

101. Huber JD, Egleton RD, Davis TP. Molecular physiology and pathophysiology of tight junctions in the blood–brain barrier. Trends in neurosciences. 2001;24(12):719-25.
102. Jia W, Martin TA, Zhang G, Jiang WG. Junctional adhesion molecules in cerebral endothelial tight junction and brain metastasis. Anticancer Res. 2013;33(6):2353-9.
103. Amasheh S, Schmidt T, Mahn M, Florian P, Mankertz J, Tavalali S, et al. Contribution of claudin-5 to barrier properties in tight junctions of epithelial cells. Cell Tissue Res. 2005;321(1):89-96.
104. Nitta T, Hata M, Gotoh S, Seo Y, Sasaki H, Hashimoto N, et al. Size-selective loosening of the blood-brain barrier in claudin-5-deficient mice. J Cell Biol. 2003;161(3):653-60.
105. Morita K, Sasaki H, Furuse M, Tsukita S. Endothelial claudin: claudin-5/TMVCF constitutes tight junction strands in endothelial cells. J Cell Biol. 1999;147(1):185-94.
106. Daneman R, Zhou L, Agalliu D, Cahoy JD, Kaushal A, Barres BA. The mouse blood-brain barrier transcriptome: a new resource for understanding the development and function of brain endothelial cells. PLoS One. 2010;5(10):e13741.
107. Liebner S, Corada M, Bangsow T, Babbage J, Taddei A, Czupalla CJ, et al. Wnt/beta-catenin signaling controls development of the blood-brain barrier. J Cell Biol. 2008;183(3):409-17.
108. Hirase T, Staddon JM, Saitou M, Ando-Akatsuka Y, Itoh M, Furuse M, et al. Occludin as a possible determinant of tight junction permeability in endothelial cells. Journal of cell science. 1997;110(14):1603-13.
109. Martìn-Padura I, Lostaglio S, Schneemann M, Williams L, Romano M, Fruscella P, et al. Junctional adhesion molecule, a novel member of the immunoglobulin superfamily that distributes at intercellular junctions and modulates monocyte transmigration. The Journal of cell biology. 1998;142(1):117-27.
110. Naik MU, Naik TU, Suckow AT, Duncan MK, Naik UP. Attenuation of junctional adhesion molecule-A is a contributing factor for breast cancer cell invasion. Cancer research. 2008;68(7):2194-203.
111. McSherry EA, McGee SF, Jirstrom K, Doyle EM, Brennan DJ, Landberg G, et al. JAM-A expression positively correlates with poor prognosis in breast cancer patients. International journal of cancer. 2009;125(6):1343-51.
112. Mandell KJ, Babbin BA, Nusrat A, Parkos CA. Junctional adhesion molecule 1 regulates epithelial cell morphology through effects on β1 integrins and Rap1 activity. Journal of Biological Chemistry. 2005;280(12):11665-74.
113. Fanning AS, Ma TY, Anderson JM. Isolation and functional characterization of the actin-binding region in the tight junction protein ZO-1. The FASEB Journal. 2002;16(13):1-23.
114. Van Itallie CM, Anderson JM. Claudin interactions in and out of the tight junction. Tissue Barriers. 2013;1(3):e25247.
115. Obermeier B, Daneman R, Ransohoff RM. Development, maintenance and disruption of the blood-brain barrier. Nature medicine. 2013;19(12):1584.
116. Haug AV, Zehendner C, Werner A, Zeiher AM, Dimmeler S. Pericyte-Specific PDGF Receptor Beta Knockout Inhibits Angiogenesis and Vessel Maturation. Circulation. 2018;138(Suppl_1):A14818-A.
117. Armulik A, Genové G, Mäe M, Nisancioglu MH, Wallgard E, Niaudet C, et al. Pericytes regulate the blood–brain barrier. Nature. 2010;468(7323):557-61.

118. Bell RD, Winkler EA, Sagare AP, Singh I, Larue B, Deane R, et al. Pericytes Control Key Neurovascular Functions and Neuronal Phenotype in the Adult Brain and during Brain Aging. Neuron. 2010;68(3):409-27.
119. Daneman R, Zhou L, Kebede AA, Barres BA. Pericytes are required for blood–brain barrier integrity during embryogenesis. Nature. 2010;468(7323):562-6.
120. Winkler EA, Bell RD, Zlokovic BV. Central nervous system pericytes in health and disease. Nature neuroscience. 2011;14(11):1398.
121. Willis CL, Leach L, Clarke GJ, Nolan CC, Ray DE. Reversible disruption of tight junction complexes in the rat blood-brain barrier, following transitory focal astrocyte loss. Glia. 2004;48(1):1-13.
122. Liu C-Y, Yang Y, Ju W-N, Wang X, Zhang H-L. Emerging Roles of Astrocytes in Neuro-Vascular Unit and the Tripartite Synapse With Emphasis on Reactive Gliosis in the Context of Alzheimer's Disease. Frontiers in Cellular Neuroscience. 2018;12(193).
123. Kim SJ, Kim JS, Park ES, Lee JS, Lin Q, Langley RR, et al. Astrocytes upregulate survival genes in tumor cells and induce protection from chemotherapy. Neoplasia. 2011;13(3):286-98.
124. Kim SW, Choi HJ, Lee HJ, He J, Wu Q, Langley RR, et al. Role of the endothelin axis in astrocyte- and endothelial cell-mediated chemoprotection of cancer cells. Neuro Oncol. 2014;16(12):1585-98.
125. Palmieri D, Smith QR, Lockman PR, Bronder J, Gril B, Chambers AF, et al. Brain metastases of breast cancer. Breast Dis. 2006;26:139-47.
126. Weil RJ, Palmieri DC, Bronder JL, Stark AM, Steeg PS. Breast cancer metastasis to the central nervous system. Am J Pathol. 2005;167(4):913-20.
127. Fitzgerald DP, Palmieri D, Hua E, Hargrave E, Herring JM, Qian Y, et al. Reactive glia are recruited by highly proliferative brain metastases of breast cancer and promote tumor cell colonization. Clin Exp Metastasis. 2008;25(7):799-810.
128. Paget S. The distribution of secondary growths in cancer of the breast. 1889. Cancer Metastasis Rev. 1989;8(2):98-101.
129. Langley RR, Fidler IJ. The seed and soil hypothesis revisited—The role of tumor-stroma interactions in metastasis to different organs. International journal of cancer. 2011;128(11):2527-35.
130. Ramakrishna R, Rostomily R. Seed, soil, and beyond: The basic biology of brain metastasis. Surg Neurol Int. 2013;4(Suppl 4):S256-64.
131. Pedrosa R, Mustafa DA, Soffietti R, Kros JM. Breast cancer brain metastasis: molecular mechanisms and directions for treatment. Neuro Oncol. 2018;20(11):1439-49.
132. Lorger M, Krueger JS, O'Neal M, Staflin K, Felding-Habermann B. Activation of tumor cell integrin αvβ3 controls angiogenesis and metastatic growth in the brain. Proceedings of the National Academy of Sciences. 2009;106(26):10666-71.
133. Bachelder RE, Crago A, Chung J, Wendt MA, Shaw LM, Robinson G, et al. Vascular endothelial growth factor is an autocrine survival factor for neuropilin-expressing breast carcinoma cells. Cancer research. 2001;61(15):5736-40.
134. Fan J, Cai B, Zeng M, Hao Y, Giancotti FG, Fu BM. Integrin β4 signaling promotes mammary tumor cell adhesion to brain microvascular endothelium by inducing ErbB2-mediated secretion of VEGF. Annals of biomedical engineering. 2011;39(8):2223-41.

135. Wu K, Fukuda K, Xing F, Zhang Y, Sharma S, Liu Y, et al. Roles of the cyclooxygenase 2 matrix metalloproteinase 1 pathway in brain metastasis of breast cancer. Journal of Biological Chemistry. 2015;290(15):9842-54.
136. Bos PD, Zhang XH-F, Nadal C, Shu W, Gomis RR, Nguyen DX, et al. Genes that mediate breast cancer metastasis to the brain. Nature. 2009;459(7249):1005-9.
137. Wrobel JK, Toborek M. Blood-brain Barrier Remodeling during Brain Metastasis Formation. Mol Med. 2016;22:32-40.
138. Avraham HK, Jiang S, Fu Y, Nakshatri H, Ovadia H, Avraham S. Angiopoietin-2 mediates blood–brain barrier impairment and colonization of triple-negative breast cancer cells in brain. The Journal of pathology. 2014;232(3):369-81.
139. Plate KH, Scholz A, Dumont DJ. Tumor angiogenesis and anti-angiogenic therapy in malignant gliomas revisited. Acta neuropathologica. 2012;124(6):763-75.
140. Folkman J. Tumor angiogenesis: therapeutic implications. New england journal of medicine. 1971;285(21):1182-6.
141. Terrell-Hall TB, Ammer AG, Griffith JI, Lockman PR. Permeability across a novel microfluidic blood-tumor barrier model. Fluids Barriers CNS. 2017;14(1):3.
142. Lockman PR, Mittapalli RK, Taskar KS, Rudraraju V, Gril B, Bohn KA, et al. Heterogeneous blood–tumor barrier permeability determines drug efficacy in experimental brain metastases of breast cancer. Clinical cancer research. 2010;16(23):5664-78.
143. Shah N, Mohammad AS, Saralkar P, Sprowls SA, Vickers SD, John D, et al. Investigational chemotherapy and novel pharmacokinetic mechanisms for the treatment of breast cancer brain metastases. Pharmacol Res. 2018;132:47-68.
144. Watkins S, Robel S, Kimbrough IF, Robert SM, Ellis-Davies G, Sontheimer H. Disruption of astrocyte–vascular coupling and the blood–brain barrier by invading glioma cells. Nature communications. 2014;5(1):1-15.
145. Adkins CE, Mittapalli RK, Manda VK, Nounou MI, Mohammad AS, Terrell TB, et al. P-glycoprotein mediated efflux limits substrate and drug uptake in a preclinical brain metastases of breast cancer model. Frontiers in pharmacology. 2013;4:136.
146. Aryal M, Fischer K, Gentile C, Gitto S, Zhang Y-Z, McDannold N. Effects on P-glycoprotein expression after blood-brain barrier disruption using focused ultrasound and microbubbles. PLoS One. 2017;12(1):e0166061.
147. Lyle LT, Lockman PR, Adkins CE, Mohammad AS, Sechrest E, Hua E, et al. Alterations in Pericyte Subpopulations Are Associated with Elevated Blood-Tumor Barrier Permeability in Experimental Brain Metastasis of Breast Cancer. Clin Cancer Res. 2016;22(21):5287-99.
148. Gril B, Paranjape AN, Woditschka S, Hua E, Dolan EL, Hanson J, et al. Reactive astrocytic S1P3 signaling modulates the blood–tumor barrier in brain metastases. Nature communications. 2018;9(1):1-18.
149. Arvanitis CD, Ferraro GB, Jain RK. The blood–brain barrier and blood–tumour barrier in brain tumours and metastases. Nature Reviews Cancer. 2020;20(1):26-41.
150. Wasilewski D, Priego N, Fustero-Torre C, Valiente M. Reactive astrocytes in brain metastasis. Frontiers in oncology. 2017;7:298.
151. Zhang L, Zhang S, Yao J, Lowery FJ, Zhang Q, Huang W-C, et al. Microenvironment-induced PTEN loss by exosomal microRNA primes brain metastasis outgrowth. Nature. 2015;527(7576):100-4.

152. Wu S-Y, Watabe K. The roles of microglia/macrophages in tumor progression of brain cancer and metastatic disease. Frontiers in bioscience (Landmark edition). 2017;22:1805.
153. Hetz C, Zhang K, Kaufman RJ. Mechanisms, regulation and functions of the unfolded protein response. Nature Reviews Molecular Cell Biology. 2020;21(8):421-38.
154. Rapoport TA. Protein translocation across the eukaryotic endoplasmic reticulum and bacterial plasma membranes. Nature. 2007;450(7170):663-9.
155. Braakman I, Hebert DN. Protein folding in the endoplasmic reticulum. Cold Spring Harbor perspectives in biology. 2013;5(5):a013201.
156. Clapham DE. Calcium signaling. Cell. 2007;131(6):1047-58.
157. Schwarz DS, Blower MD. The endoplasmic reticulum: structure, function and response to cellular signaling. Cellular and Molecular Life Sciences. 2016;73(1):79-94.
158. Almanza A, Carlesso A, Chintha C, Creedican S, Doultsinos D, Leuzzi B, et al. Endoplasmic reticulum stress signalling - from basic mechanisms to clinical applications. FEBS J. 2019;286(2):241-78.
159. Bernasconi R, Molinari M. ERAD and ERAD tuning: disposal of cargo and of ERAD regulators from the mammalian ER. Current opinion in cell biology. 2011;23(2):176-83.
160. Hetz C, Martinon F, Rodriguez D, Glimcher LH. The unfolded protein response: integrating stress signals through the stress sensor IRE1α. Physiological reviews. 2011;91(4):1219-43.
161. Naidoo N. ER and aging—protein folding and the ER stress response. Ageing research reviews. 2009;8(3):150-9.
162. Marciniak SJ, Ron D. Endoplasmic reticulum stress signaling in disease. Physiological reviews. 2006;86(4):1133-49.
163. Moore KA, Hollien J. The unfolded protein response in secretory cell function. Annual review of genetics. 2012;46:165-83.
164. Coelho DS, Domingos PM. Physiological roles of regulated Ire1 dependent decay. Frontiers in genetics. 2014;5:76.
165. Hetz C. The unfolded protein response: controlling cell fate decisions under ER stress and beyond. Nature reviews Molecular cell biology. 2012;13(2):89-102.
166. Bertolotti A, Zhang Y, Hendershot LM, Harding HP, Ron D. Dynamic interaction of BiP and ER stress transducers in the unfolded-protein response. Nature cell biology. 2000;2(6):326-32.
167. Shen J, Chen X, Hendershot L, Prywes R. ER stress regulation of ATF6 localization by dissociation of BiP/GRP78 binding and unmasking of Golgi localization signals. Developmental cell. 2002;3(1):99-111.
168. Urra H, Dufey E, Lisbona F, Rojas-Rivera D, Hetz C. When ER stress reaches a dead end. Biochimica et Biophysica Acta (BBA)-Molecular Cell Research. 2013;1833(12):3507-17.
169. Gardner BM, Pincus D, Gotthardt K, Gallagher CM, Walter P. Endoplasmic reticulum stress sensing in the unfolded protein response. Cold Spring Harb Perspect Biol. 2013;5(3):a013169.
170. Tabas I, Ron D. Integrating the mechanisms of apoptosis induced by endoplasmic reticulum stress. Nat Cell Biol. 2011;13(3):184-90.

171. Kadowaki H, Nishitoh H. Signaling pathways from the endoplasmic reticulum and their roles in disease. Genes. 2013;4(3):306-33.
172. Li A, Song N-J, Riesenberg BP, Li Z. The emerging roles of endoplasmic reticulum stress in balancing immunity and tolerance in health and diseases: mechanisms and opportunities. Frontiers in immunology. 2020;10:3154.
173. McQuiston A, Diehl JA. Recent insights into PERK-dependent signaling from the stressed endoplasmic reticulum. F1000Research. 2017;6.
174. Schröder M, Kaufman RJ. The mammalian unfolded protein response. Annu Rev Biochem. 2005;74:739-89.
175. Ameri K, Harris AL. Activating transcription factor 4. The international journal of biochemistry & cell biology. 2008;40(1):14-21.
176. Quirós PM, Prado MA, Zamboni N, D'Amico D, Williams RW, Finley D, et al. Multi-omics analysis identifies ATF4 as a key regulator of the mitochondrial stress response in mammals. Journal of Cell Biology. 2017;216(7):2027-45.
177. Høyer-Hansen M, Jäättelä M. Connecting endoplasmic reticulum stress to autophagy by unfolded protein response and calcium. Cell Death & Differentiation. 2007;14(9):1576-82.
178. Youle RJ, Strasser A. The BCL-2 protein family: opposing activities that mediate cell death. Nature reviews Molecular cell biology. 2008;9(1):47-59.
179. Reimertz C, Kögel D, Rami A, Chittenden T, Prehn JH. Gene expression during ER stress–induced apoptosis in neurons: induction of the BH3-only protein Bbc3/PUMA and activation of the mitochondrial apoptosis pathway. The Journal of cell biology. 2003;162(4):587-97.
180. Hillary RF, FitzGerald U. A lifetime of stress: ATF6 in development and homeostasis. Journal of biomedical science. 2018;25(1):1-10.
181. Yoshida H, Okada T, Haze K, Yanagi H, Yura T, Negishi M, et al. ATF6 activated by proteolysis binds in the presence of NF-Y (CBF) directly to the cis-acting element responsible for the mammalian unfolded protein response. Molecular and cellular biology. 2000;20(18):6755-67.
182. Haze K, Yoshida H, Yanagi H, Yura T, Mori K. Mammalian transcription factor ATF6 is synthesized as a transmembrane protein and activated by proteolysis in response to endoplasmic reticulum stress. Molecular biology of the cell. 1999;10(11):3787-99.
183. Ye J, Rawson RB, Komuro R, Chen X, Davé UP, Prywes R, et al. ER stress induces cleavage of membrane-bound ATF6 by the same proteases that process SREBPs. Molecular cell. 2000;6(6):1355-64.
184. Glembotski CC, Arrieta A, Blackwood EA, Stauffer WT. ATF6 as a Nodal Regulator of Proteostasis in the Heart. Frontiers in physiology. 2020;11:267.
185. Thuerauf DJ, Morrison LE, Hoover H, Glembotski CC. Coordination of ATF6-mediated transcription and ATF6 degradation by a domain that is shared with the viral transcription factor, VP16. Journal of Biological Chemistry. 2002;277(23):20734-9.
186. Iwawaki T, Akai R, Yamanaka S, Kohno K. Function of IRE1 alpha in the placenta is essential for placental development and embryonic viability. Proceedings of the National Academy of Sciences. 2009;106(39):16657-62.
187. Tsuru A, Fujimoto N, Takahashi S, Saito M, Nakamura D, Iwano M, et al. Negative feedback by IRE1β optimizes mucin production in goblet cells. Proceedings of the National Academy of Sciences. 2013;110(8):2864-9.

188. Chen Y, Brandizzi F. IRE1: ER stress sensor and cell fate executor. Trends in cell biology. 2013;23(11):547-55.
189. Korennykh AV, Egea PF, Korostelev AA, Finer-Moore J, Zhang C, Shokat KM, et al. The unfolded protein response signals through high-order assembly of Ire1. Nature. 2009;457(7230):687-93.
190. Huang S, Xing Y, Liu Y. Emerging roles for the ER stress sensor IRE1α in metabolic regulation and disease. Journal of Biological Chemistry. 2019;294(49):18726-41.
191. Riaz TA, Junjappa RP, Handigund M, Ferdous J, Kim H-R, Chae H-J. Role of endoplasmic reticulum stress sensor ire1α in cellular physiology, calcium, ROS signaling, and metaflammation. Cells. 2020;9(5):1160.
192. Kanda S, Yanagitani K, Yokota Y, Esaki Y, Kohno K. Autonomous translational pausing is required for XBP1u mRNA recruitment to the ER via the SRP pathway. Proceedings of the National Academy of Sciences. 2016;113(40):E5886-E95.
193. Yanagitani K, Kimata Y, Kadokura H, Kohno K. Translational pausing ensures membrane targeting and cytoplasmic splicing of XBP1u mRNA. Science. 2011;331(6017):586-9.
194. Sidrauski C, Walter P. The transmembrane kinase Ire1p is a site-specific endonuclease that initiates mRNA splicing in the unfolded protein response. Cell. 1997;90(6):1031-9.
195. Yoshida H, Matsui T, Yamamoto A, Okada T, Mori K. XBP1 mRNA is induced by ATF6 and spliced by IRE1 in response to ER stress to produce a highly active transcription factor. Cell. 2001;107(7):881-91.
196. Calfon M, Zeng H, Urano F, Till JH, Hubbard SR, Harding HP, et al. IRE1 couples endoplasmic reticulum load to secretory capacity by processing the XBP-1 mRNA. Nature. 2002;415(6867):92-6.
197. Filipowicz W. Making ends meet: a role of RNA ligase RTCB in unfolded protein response. The EMBO journal. 2014;33(24):2887-9.
198. Iwakoshi NN, Lee AH, Glimcher LH. The X-box binding protein-1 transcription factor is required for plasma cell differentiation and the unfolded protein response. Immunological reviews. 2003;194(1):29-38.
199. Reimold AM, Iwakoshi NN, Manis J, Vallabhajosyula P, Szomolanyi-Tsuda E, Gravallese EM, et al. Plasma cell differentiation requires the transcription factor XBP-1. Nature. 2001;412(6844):300-7.
200. Sriburi R, Jackowski S, Mori K, Brewer JW. XBP1 a link between the unfolded protein response, lipid biosynthesis, and biogenesis of the endoplasmic reticulum. The Journal of cell biology. 2004;167(1):35-41.
201. Park SW, Herrema H, Salazar M, Cakir I, Cabi S, Sahin FB, et al. BRD7 regulates XBP1s' activity and glucose homeostasis through its interaction with the regulatory subunits of PI3K. Cell metabolism. 2014;20(1):73-84.
202. Tao R, Chen H, Gao C, Xue P, Yang F, Han J-DJ, et al. Xbp1-mediated histone H4 deacetylation contributes to DNA double-strand break repair in yeast. Cell research. 2011;21(11):1619-33.
203. Wu J, Kaufman R. From acute ER stress to physiological roles of the unfolded protein response. Cell Death & Differentiation. 2006;13(3):374-84.

204. Hollien J, Lin JH, Li H, Stevens N, Walter P, Weissman JS. Regulated Ire1-dependent decay of messenger RNAs in mammalian cells. Journal of Cell Biology. 2009;186(3):323-31.
205. Han D, Lerner AG, Vande Walle L, Upton JP, Xu W, Hagen A, et al. IRE1alpha kinase activation modes control alternate endoribonuclease outputs to determine divergent cell fates. Cell. 2009;138(3):562-75.
206. Oikawa D, Tokuda M, Hosoda A, Iwawaki T. Identification of a consensus element recognized and cleaved by IRE1α. Nucleic acids research. 2010;38(18):6265-73.
207. Upton J-P, Wang L, Han D, Wang ES, Huskey NE, Lim L, et al. IRE1α cleaves select microRNAs during ER stress to derepress translation of proapoptotic Caspase-2. Science. 2012;338(6108):818-22.
208. Vakifahmetoglu-Norberg H, Zhivotovsky B. The unpredictable caspase-2: what can it do? Trends in cell biology. 2010;20(3):150-9.
209. Menu P, Mayor A, Zhou R, Tardivel A, Ichijo H, Mori K, et al. ER stress activates the NLRP3 inflammasome via an UPR-independent pathway. Cell death & disease. 2012;3(1):e261-e.
210. Verfaillie T, Salazar M, Velasco G, Agostinis P. Linking ER stress to autophagy: potential implications for cancer therapy. International journal of cell biology. 2010;2010.
211. Pattingre S, Tassa A, Qu X, Garuti R, Liang XH, Mizushima N, et al. Bcl-2 antiapoptotic proteins inhibit Beclin 1-dependent autophagy. Cell. 2005;122(6):927-39.
212. Lee A-H, Iwakoshi NN, Glimcher LH. XBP-1 regulates a subset of endoplasmic reticulum resident chaperone genes in the unfolded protein response. Molecular and cellular biology. 2003;23(21):7448-59.
213. Acosta-Alvear D, Zhou Y, Blais A, Tsikitis M, Lents NH, Arias C, et al. XBP1 controls diverse cell type-and condition-specific transcriptional regulatory networks. Molecular cell. 2007;27(1):53-66.
214. Walter F, Schmid J, Dussmann H, Concannon CG, Prehn JH. Imaging of single cell responses to ER stress indicates that the relative dynamics of IRE1/XBP1 and PERK/ATF4 signalling rather than a switch between signalling branches determine cell survival. Cell Death Differ. 2015;22(9):1502-16.
215. Lee K, Tirasophon W, Shen X, Michalak M, Prywes R, Okada T, et al. IRE1-mediated unconventional mRNA splicing and S2P-mediated ATF6 cleavage merge to regulate XBP1 in signaling the unfolded protein response. Genes & development. 2002;16(4):452-66.
216. Yamamoto K, Sato T, Matsui T, Sato M, Okada T, Yoshida H, et al. Transcriptional induction of mammalian ER quality control proteins is mediated by single or combined action of ATF6α and XBP1. Developmental cell. 2007;13(3):365-76.
217. Lin JH, Li H, Yasumura D, Cohen HR, Zhang C, Panning B, et al. IRE1 signaling affects cell fate during the unfolded protein response. science. 2007;318(5852):944-9.
218. Lin JH, Li H, Zhang Y, Ron D, Walter P. Divergent effects of PERK and IRE1 signaling on cell viability. PloS one. 2009;4(1):e4170.
219. Novoa I, Zeng H, Harding HP, Ron D. Feedback inhibition of the unfolded protein response by GADD34-mediated dephosphorylation of eIF2α. The Journal of cell biology. 2001;153(5):1011-22.

220. Woehlbier U, Hetz C. Modulating stress responses by the UPRosome: a matter of life and death. Trends in biochemical sciences. 2011;36(6):329-37.
221. Danial NN, Korsmeyer SJ. Cell death: critical control points. Cell. 2004;116(2):205-19.
222. McCullough KD, Martindale JL, Klotz L-O, Aw T-Y, Holbrook NJ. Gadd153 sensitizes cells to endoplasmic reticulum stress by down-regulating Bcl2 and perturbing the cellular redox state. Molecular and cellular biology. 2001;21(4):1249-59.
223. Marciniak SJ, Yun CY, Oyadomari S, Novoa I, Zhang Y, Jungreis R, et al. CHOP induces death by promoting protein synthesis and oxidation in the stressed endoplasmic reticulum. Genes & development. 2004;18(24):3066-77.
224. Ming J, Ruan S, Wang M, Ye D, Fan N, Meng Q, et al. A novel chemical, STF-083010, reverses tamoxifen-related drug resistance in breast cancer by inhibiting IRE1/XBP1. Oncotarget. 2015;6(38):40692.
225. Logue SE, McGrath EP, Cleary P, Greene S, Mnich K, Almanza A, et al. Inhibition of IRE1 RNase activity modulates the tumor cell secretome and enhances response to chemotherapy. Nature communications. 2018;9(1):1-14.
226. Chen X, Iliopoulos D, Zhang Q, Tang Q, Greenblatt MB, Hatziapostolou M, et al. XBP1 promotes triple-negative breast cancer by controlling the HIF1α pathway. Nature. 2014;508(7494):103-7.
227. Idowu MO, Kmieciak M, Dumur C, Burton RS, Grimes MM, Powers CN, et al. CD44+/CD24−/low cancer stem/progenitor cells are more abundant in triple-negative invasive breast carcinoma phenotype and are associated with poor outcome. Human pathology. 2012;43(3):364-73.
228. Lin Y, Zhong Y, Guan H, Zhang X, Sun Q. CD44+/CD24-phenotype contributes to malignant relapse following surgical resection and chemotherapy in patients with invasive ductal carcinoma. Journal of experimental & clinical cancer research. 2012;31(1):1-9.
229. Creighton CJ, Li X, Landis M, Dixon JM, Neumeister VM, Sjolund A, et al. Residual breast cancers after conventional therapy display mesenchymal as well as tumor-initiating features. Proceedings of the National Academy of Sciences. 2009;106(33):13820-5.
230. Hervé M-A, Buteau-Lozano H, Vassy R, Bieche I, Velasco G, Pla M, et al. Overexpression of vascular endothelial growth factor 189 in breast cancer cells leads to delayed tumor uptake with dilated intratumoral vessels. The American journal of pathology. 2008;172(1):167-78.
231. Linderholm B, Hellborg H, Johansson U, Elmberger G, Skoog L, Lehtiö J, et al. Significantly higher levels of vascular endothelial growth factor (VEGF) and shorter survival times for patients with primary operable triple-negative breast cancer. Annals of oncology. 2009;20(10):1639-46.
232. Ribatti D, Nico B, Ruggieri S, Tamma R, Simone G, Mangia A. Angiogenesis and antiangiogenesis in triple-negative breast cancer. Translational Oncology. 2016;9(5):453-7.
233. Harnoss JM, Le Thomas A, Reichelt M, Guttman O, Wu TD, Marsters SA, et al. IRE1α Disruption in Triple-Negative Breast Cancer Cooperates with Antiangiogenic Therapy by Reversing ER Stress Adaptation and Remodeling the Tumor Microenvironment. Cancer research. 2020;80(11):2368-79.

234. Ghosh R, Lipson KL, Sargent KE, Mercurio AM, Hunt JS, Ron D, et al. Transcriptional regulation of VEGF-A by the unfolded protein response pathway. PloS one. 2010;5(3):e9575.
235. Zhao N, Cao J, Xu L, Tang Q, Dobrolecki LE, Lv X, et al. Pharmacological targeting of MYC-regulated IRE1/XBP1 pathway suppresses MYC-driven breast cancer. The Journal of clinical investigation. 2018;128(4):1283-99.
236. McGrath EP, Logue SE, Mnich K, Deegan S, Jäger R, Gorman AM, et al. The Unfolded Protein Response in Breast Cancer. Cancers (Basel). 2018;10(10).
237. Sanches M, Duffy NM, Talukdar M, Thevakumaran N, Chiovitti D, Canny MD, et al. Structure and mechanism of action of the hydroxy–aryl–aldehyde class of IRE1 endoribonuclease inhibitors. Nature communications. 2014;5(1):1-16.
238. Cross BC, Bond PJ, Sadowski PG, Jha BK, Zak J, Goodman JM, et al. The molecular basis for selective inhibition of unconventional mRNA splicing by an IRE1-binding small molecule. Proceedings of the National Academy of Sciences. 2012;109(15):E869-E78.
239. Papandreou I, Denko NC, Olson M, Van Melckebeke H, Lust S, Tam A, et al. Identification of an Ire1alpha endonuclease specific inhibitor with cytotoxic activity against human multiple myeloma. Blood. 2011;117(4):1311-4.
240. Volkmann K, Lucas JL, Vuga D, Wang X, Brumm D, Stiles C, et al. Potent and selective inhibitors of the inositol-requiring enzyme 1 endoribonuclease. Journal of Biological Chemistry. 2011;286(14):12743-55.
241. Siwecka N, Rozpędek-Kamińska W, Wawrzynkiewicz A, Pytel D, Diehl JA, Majsterek I. The Structure, Activation and Signaling of IRE1 and Its Role in Determining Cell Fate. Biomedicines. 2021;9(2):156.
242. Serres S, Soto MS, Hamilton A, McAteer MA, Carbonell WS, Robson MD, et al. Molecular MRI enables early and sensitive detection of brain metastases. Proceedings of the National Academy of Sciences. 2012;109(17):6674-9.
243. Rivenbark AG, O'Connor SM, Coleman WB. Molecular and cellular heterogeneity in breast cancer: challenges for personalized medicine. The American journal of pathology. 2013;183(4):1113-24.
244. Palmieri D, Bronder JL, Herring JM, Yoneda T, Weil RJ, Stark AM, et al. Her-2 overexpression increases the metastatic outgrowth of breast cancer cells in the brain. Cancer research. 2007;67(9):4190-8.
245. Ashby MC, Tepikin AV, editors. ER calcium and the functions of intracellular organelles. Seminars in cell & developmental biology; 2001: Elsevier.
246. Torres M, Encina G, Soto C, Hetz C. Abnormal calcium homeostasis and protein folding stress at the ER: A common factor in familial and infectious prion disorders. Communicative & integrative biology. 2011;4(3):258-61.
247. Mehrabadi AR, Korolainen MA, Odero G, Miller DW, Kauppinen TM. Poly (ADP-ribose) polymerase-1 regulates microglia mediated decrease of endothelial tight junction integrity. Neurochemistry international. 2017;108:266-71.
248. Goel HL, Mercurio AM. VEGF targets the tumour cell. Nature Reviews Cancer. 2013;13(12):871-82.
249. Masjedi A, Hashemi V, Hojjat-Farsangi M, Ghalamfarsa G, Azizi G, Yousefi M, et al. The significant role of interleukin-6 and its signaling pathway in the

immunopathogenesis and treatment of breast cancer. Biomedicine & Pharmacotherapy. 2018;108:1415-24.
250. Jaskulska A, Janecka AE, Gach-Janczak K. Thapsigargin—From Traditional Medicine to Anticancer Drug. International Journal of Molecular Sciences. 2021;22(1):4.
251. Chen X, Cubillos-Ruiz JR. Endoplasmic reticulum stress signals in the tumour and its microenvironment. Nature Reviews Cancer. 2020:1-18.
252. Costa-Mattioli M, Walter P. The integrated stress response: From mechanism to disease. Science. 2020;368(6489).
253. Laksitorini MD, Yathindranath V, Xiong W, Parkinson FE, Thliveris JA, Miller DW. Impact of Wnt/β-catenin signaling on ethanol-induced changes in brain endothelial cell permeability. Journal of Neurochemistry. 2021;157(4):1118-37.
254. Persidsky Y, Ramirez SH, Haorah J, Kanmogne GD. Blood–brain barrier: structural components and function under physiologic and pathologic conditions. Journal of Neuroimmune Pharmacology. 2006;1(3):223-36.
255. Stamatovic SM, Johnson AM, Keep RF, Andjelkovic AV. Junctional proteins of the blood-brain barrier: new insights into function and dysfunction. Tissue barriers. 2016;4(1):e1154641.
256. Nitta T, Hata M, Gotoh S, Seo Y, Sasaki H, Hashimoto N, et al. Size-selective loosening of the blood-brain barrier in claudin-5–deficient mice. The Journal of cell biology. 2003;161(3):653-60.
257. Tawara K, Scott H, Emathinger J, Ide A, Fox R, Greiner D, et al. Co-expression of VEGF and IL-6 family cytokines is associated with decreased survival in HER2 negative breast cancer patients: subtype-specific IL-6 family cytokine-mediated VEGF secretion. Translational oncology. 2019;12(2):245-55.
258. Dent S. The role of VEGF in triple-negative breast cancer: where do we go from here? Annals of oncology. 2009;20(10):1615-7.
259. Zhu X, Zhou W. The emerging regulation of VEGFR-2 in triple-negative breast cancer. Frontiers in endocrinology. 2015;6:159.
260. Abcouwer SF, Marjon PL, Loper RK, Vander Jagt DL. Response of VEGF expression to amino acid deprivation and inducers of endoplasmic reticulum stress. Investigative ophthalmology & visual science. 2002;43(8):2791-8.
261. Hyder SM, Liang Y, Wu J, Welbern V. Regulation of thrombospondin-1 by natural and synthetic progestins in human breast cancer cells. Endocrine-related cancer. 2009;16(3):809.
262. Fontana A, Filleur S, Guglielmi J, Frappart L, Bruno-Bossio G, Boissier S, et al. Human breast tumors override the antiangiogenic effect of stromal thrombospondin-1 in vivo. International journal of cancer. 2005;116(5):686-91.
263. John AS, Rothman VL, Tuszynski GP. Thrombospondin-1 (TSP-1) stimulates expression of integrin 6 in human breast carcinoma cells: a downstream modulator of TSP-1-induced cellular adhesion. Journal of oncology. 2010;2010.
264. Lynch JM, Maillet M, Vanhoutte D, Schloemer A, Sargent MA, Blair NS, et al. A thrombospondin-dependent pathway for a protective ER stress response. Cell. 2012;149(6):1257-68.
265. Kazerounian S, Yee KO, Lawler J. Thrombospondins in cancer. Cell Mol Life Sci. 2008;65(5):700-12.

266. Ghajar CM, Peinado H, Mori H, Matei IR, Evason KJ, Brazier H, et al. The perivascular niche regulates breast tumour dormancy. Nature cell biology. 2013;15(7):807-17.
267. Dethlefsen C, Højfeldt G, Hojman P. The role of intratumoral and systemic IL-6 in breast cancer. Breast cancer research and treatment. 2013;138(3):657-64.
268. Singh A, Purohit A, Duncan L, Mokbel K, Ghilchik M, Reed M. Control of aromatase activity in breast tumours: the role of the immune system. The Journal of steroid biochemistry and molecular biology. 1997;61(3-6):185-92.
269. Salgado R, Junius S, Benoy I, Van Dam P, Vermeulen P, Van Marck E, et al. Circulating interleukin-6 predicts survival in patients with metastatic breast cancer. International journal of cancer. 2003;103(5):642-6.
270. Zhang G-J, Adachi I. Serum interleukin-6 levels correlate to tumor progression and prognosis in metastatic breast carcinoma. Anticancer research. 1999;19(2):1427-32.
271. Abana CO, Bingham BS, Cho JH, Graves AJ, Koyama T, Pilarski RT, et al. IL-6 variant is associated with metastasis in breast cancer patients. PLoS One. 2017;12(7):e0181725.
272. Sanchez CL, Sims SG, Nowery JD, Meares GP. Endoplasmic reticulum stress differentially modulates the IL-6 family of cytokines in murine astrocytes and macrophages. Scientific reports. 2019;9(1):1-12.